KRISS

Korea Research Institute of Standards and Science

CCQM-P190

Thickness Measurement of nm HfO$_2$ Films

A Pilot Study for the Consultative Committee on
Amount of Substance

Kyung Joong Kim
Division of Industrial Metrology
Korea Research Institute of Standards and Science,
267 Gajeong-ro, Yuseong-gu, Daejeon 34113, Republic of Korea

September, 2020

CONTENTS

ANNEX

Thickness Measurement of nm HfO$_2$ Films

K. J. Kim[1], A Kim[1], C. S. Kim[1], S. W. Song[1], H. Ruh[1],W. E. S. Unger[2], J. Radnik[2], J. Mata-Salazar[3], J. M. Juarez-Garcia[3], O. Cortazar-Martinez[4], A. Herrera-Gomez[4], P. E. Hansen[5], J. S. Madsen[5], C. A. Senna[6], B. S. Archanjo[6], J. C. Damasceno[6], C. A. Achete[6], H. Wang[7], M. Wang[7], D. Windover[8], E. Steel[8], A. Kurokawa[9], T. Fujimoto[9], Y. Azuma[9], S. Terauchi[9], L. Zhang[9], W. A. Jordaan[10], S. J. Spencer[11], A. G. Shard[11], L. Koenders[12], M. Krumrey[12], I. Busch[12], C. Jeynes[13]

[1]KRISS (Daejeon, Korea), [2]BAM (Berlin, Germany), [3]CENAM (Queretaro, Mexico), [4]CINVESTAV (Queretaro, Mexico), [5]DFM (Hørsholm, Danmark), [6]INMETRO (Rio De Janeiro, Brasil) [7]NIM (Beijing, China), [8]NIST (Gaithersburg, USA), [9]NMIJ (Tsukuba, Japan), [10]NMISA, (Pretoria, South Africa), [11]NPL (Teddington, UK), [12]PTB (Braunschweig and Berlin, Germany), [13]University of Surrey Ion Beam Centre (Guildford, UK)

*Electronic mail: kjkim@kriss.re.kr

A pilot study for the thickness measurement of HfO$_2$ films was performed by Surface Analysis Working Group (SAWG) of Consultative Committee for Amount of Substance (CCQM). The aim of this pilot study is to ensure the equivalency in the measurement capability of national metrology institutes for the thicknesses measurement of HfO$_2$ films.

In this pilot study, the thicknesses of six HfO$_2$ films with the nominal thickness range from 1 nm to 4 nm were measured by X-ray Photoelectron Spectroscopy (XPS), X-ray Reflectometry (XRR), X-ray Fluorescence Analysis (XRF), Transmission Electron Spectroscopy (TEM), Spectroscopic Ellipsometry (SE) and Rutherford Backscattering Spectrometry (RBS).

The reference thicknesses were determined by mutual calibration of a zero offset method (Medium Energy Ion Scattering Spectroscopy (MEIS) of KRISS) and a length unit traceable method (the average thicknesses of three XRR data except the thinnest film). These reference thicknesses are traceable to length unit because they are based on the traceability of XRR.

It should be noted that the amount of substance of HfO$_2$ expressed in the usual units of mass per unit area was obtained directly by RBS and indirectly through a further analysis (by NIST) of the XRR data, demonstrating that these films were markedly less dense than bulk.

For the thickness measurement by XPS, the effective attenuation length of Hf 4f electrons has been determined. In the cases of XRR and TEM, the offset values can be determined from the linear fitting between the reference thicknesses and the individual data by XRR and TEM. The amount of substance of HfO$_2$, expressed as thickness of HfO$_2$ films (in both linear and areal density units), was found to be a good subject for a CCQM key comparison.

1. INTRODUCTION

The thickness measurement of gate dielectric materials with a thickness of less than 1 nm is one of the most important measurement issues for the continual scaling down of semiconductor devices. HfO_2 is a dielectric material that can be used as an alternative to SiO_2. Therefore, a traceable thickness measurement of ultrathin HfO_2 films by physical or chemical methods is required for the advanced semiconductor industries.

The thickness measurement of nanoscale SiO_2 films on Si substrates was the first subject of international comparison of surface analysis by the Surface Analysis Working Group (SAWG) of the Consultative Committee for Amount of Substance (CCQM) in 2004. [1] As a result, the traceability for the thickness measurements of ultra-thin SiO_2 thin films on Si(100) and Si(111) substrates was established from the first key comparison (K-32) of SAWG.[2]

Thickness measurement results by various measurement methods were compared in the pilot study (P-38) for the thickness measurements of nm SiO_2 films. The results were linearly fitted with the nominal thicknesses. Large offset values were found in the thickness values measured by means of physical methods such as Spectroscopic Ellipsometry (SE), X-ray Reflectometry (XRR) and Transmission Electron Spectroscopy (TEM) and Medium Energy Ion Scattering Spectrometry (MEIS). The offset values were found to be attributed to surface contamination and the difficulty in the determination of the locations of the interfaces and surfaces. The offset value of MEIS was large because the thickness by MEIS was determined from the peak width of the amorphous SiO_2 layer in the MEIS spectra with the double aligned channeling geometry.

However, the offset value of X-ray Photoelectron Spectroscopy (XPS) measured from the reference geometry was close to zero. This is theoretically reasonable because the thickness of the SiO_2 layer depends on the chemical amount of oxide intensity derived from the SiO_2 layer. The linearity of XPS thickness in the sub-nm SiO_2 films has been also proven.[3,4] However, for the

[1] M. P. Seah, S. J. Spencer, F. Bensebaa, I. Vickridge, H. Danzebrink, M. Krumrey, T. Gross, W. Oesterle, E. Wendler, B. Rheinländer, Y. Azuma, I. Kojima, N. Suzuki, M. Suzuki, S. Tanuma, D. W. Moon, H. J. Lee, H. M. Cho, H. Y. Chen, A. T. S. Wee, T. Osipowicz, J. S. Pan, W. A. Jordaan, R. Hauert, U. Klotz, C. van der Marel, M. Verheijen, Y. Tarnminga, C. Jeynes, P. Bailey, S. Biswas, U. Falke, N. V. Nguyen, D. Chandler-Horowitz, J. R. Ehrstein, D. Muller and J. A. Dura, Critical review of the current status of thickness measurements for ultrathin SiO_2 on Si Part V. Results of a CCQM pilot study, Surf. Interface Anal., 36, 1269 (2004)

[2] M. P. Seah, CCQM-K32 key comparison and P84 pilot study: Amount of silicon oxide as a thickness of SiO_2 on Si, Metrologia 45 (2008) Tech. Suppl. 08013.

[3] K. J. Kim, K. T. Park, and J. W. Lee, Thickness measurement of SiO_2 films thinner than 1 nm by X-ray photoelectron spectroscopy, Thin Solid Films 500, 356 (2006)

[4] K. J. Kim and M. P. Seah, Ultra-thin SiO_2 on Si VIII. Accuracy of method, linearity and attenuation lengths for

thickness measurement by XPS, the effective attenuation length (EAL) of photoelectrons should be precisely determined at the given experimental conditions because it depends on the specified geometry of the spectrometer and the setting parameters due to the effects of elastic scattering. [5,6]

For Rutherford Backscattering Spectrometry (RBS) the offset value was also close to zero: this is reasonable for the same reason as for XPS: the number of Hf counts is (for a thin layer) strictly proportional to the areal density of Hf atoms (given properly normalized data). The absolute traceability of RBS has been unequivocally demonstrated recently, although these present measurements are not fully traceable (discussed below).[7]

A mutual calibration method was suggested to determine the effective attenuation length of photoelectrons in the thickness measurement of oxide films. In this method, XPS with zero offset value acts as a zero offset method and TEM or XRR act as length unit traceable methods where the thickness in length units is directly obtained. As the results, the mutual calibration method can be a traceable method that determines the thickness of nanoscale oxide films. The mutual calibration method was successively applied for the thickness measurement of hetero-oxide films with an interfacial oxide layer.

XPS, RBS and MEIS, on the other hand, have measurements of thickness in units of Quantity of Material (QoM). RBS is absolutely traceable in principle and has been used recently as such for measurements of the Ga photoionization cross-sections.[8] Note that the material density (hard to measure for thin films) is the ratio of the QoM and the linear thickness.

In this study, the results of the CCQM P-190 pilot study on the thickness measurement of hetero-oxide HfO_2 films are reported. The thickness of HfO_2 films on Si substrates was measured by XRR, TEM, and SE (in length units), and by RBS (in QoM units). XPS and MEIS are sensitive to QoM but are usually calibrated in length units, as they are here.

XPS, Surf. Interface Anal. 39, 512 (2007)

5 K. J. Kim, Y. S. Kim, J. S. Jang, J. W. Kim and K. W. Kim, A mutual calibration method to certify the thickness of nanometre oxide films, Metrologia 45, 507 (2008)

6 K. J. Kim, J. S. Jang, J-H. Lee, Y.-J. Jee and C.-S. Jun, Determination of the Absolute Thickness of Ultrathin Al_2O_3 Overlayers on Si (100) Substrate, Anal. Chem. 81, 8519 (2009)

7 C. Jeynes, RBS as a new primary direct reference method for measuring quantity of material, Nucl. Instrum. Methods B 406, 30 (2017)

8 Rainer Unterumsberger, Philipp Hönicke, Julien L. Colaux Chris Jeynes, Malte Wansleben, Matthias Müller and Burkhard Beckhoff, Accurate experimental determination of gallium K- and L3-shell XRF fundamental parameters, J. Anal. At. Spectrom. 33, 1003 (2018)

2. PREPARATION OF THE SAMPLES

A series of $HfO_2/SiO_2/Si(100)$ films were fabricated for the certification of thickness by mutual calibration with a length unit traceable method and an offset traceable method. Six HfO_2 films with the nominal thicknesses of 1.0, 1.5, 2.0, 2.5, 3.0, and 4.0 nm were grown on the polished side of Si (100) substrates by atomic layer deposition (ALD). Before the growth of the HfO_2 films, 2 nm SiO_2 layer was grown on the Si (100) substrates by thermal oxidation to prevent the diffusion of oxygen atoms from the HfO_2 films to Si (100) substrate as shown in Figure 2-1. The wafers were cut into small specimens with the size of 10 mm x 10 mm.

The density of the HfO_2 layer produced by ALD may differ from the bulk density. The density is the parameter relating the layer thickness to the quantity of material (QoM) per unit area. The participants of the following key comparison are encouraged to provide, in addition to the layer thickness, the layer density or the mass deposition for every sample.
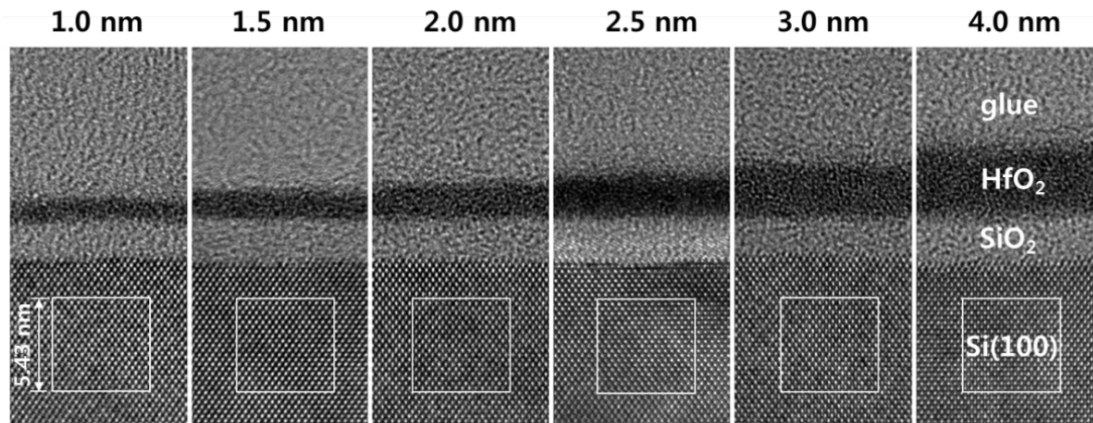

Figure 2-1. TEM images of the specimens used in P-190. The thickness of SiO_2 layers are 2 nm and the nominal thicknesses of the HfO_2 layers are (a) 1.0 nm, (b) 1.5 nm, (c) 2.0 nm, (d) 2.5 nm, (e) 3.0 nm and (f) 4.0 nm

The sample cleaning was recommended to remove surface contaminants originated from dicing or sample handling. The contaminants on the HfO_2 samples were dip in reagent grade acetone, followed by sonicating the samples for at least 5 min. To further remove the contaminants, dipping the samples in isopropyl alcohol, sonicating the samples for at least 5 min and rinsing the samples by sonicating in deionized water was recommended. The samples should not be dried during each solvent exchange step. In the case of 2.0 nm HfO_2 film, the thickness difference before and after this cleaning was about 0.01 nm. For the further removal of the surface contaminants, the cleaning procedure in the protocol of K-32 is recommended.

3. OUTLINE OF THE PILOT STUDY

A. Objective

The objective of the CCQM P-190 pilot study is to determine the thickness of HfO_2 films on Si substrates and to establish the traceability in the thickness measurement of nm HfO_2 films for the subsequent key comparison. There was no limitation in choosing the analytical techniques for the measurement of film thickness.

B. Timetable

In April 2017, the thickness measurement of HfO_2 films was suggested as a new subject for the pilot study in CCQM SAWG. The film thicknesses of the HfO_2 films were determined by mutual calibration method using TEM and XPS analysis. The protocol and the test specimens have been delivered to the participants by the end of June 2017. The results of the pilot study were gathered by the end of November 2017 and reported at the CCQM meeting in April 2018.

C. Participation

10 NMIs and 1 DI and two other institutions participated in CCQM P-190 pilot study as shown in Table 3-1.

Table 3-1. Participants in P-190.

No.	Organisation	Country	Participants
1	BAM	Germany	W. E. S. Unger, J. Radnik
2	CENAM	Mexico	J.H. Mata-Salazar, J.M. Juarez-Garcia
3	CINVESTAV	Mexico	O. Cortazar-Martinez, A. Herrera-Gomez
4	INMETRO	Brasil	C. A. Senna, B. S. Archanjo, J. C. Damasceno, C. A. Achete
5	DFM	Danmark	P. E. Hansen, J. S. Madsen
6	KRISS	Korea	K. J. Kim, A Kim, C. S. Kim, S. W. Song, H. Ruh
7	NIM	China	H. Wang, M. Wang
8	NIST	USA	D. Windover, E. Steel
9	NMIJ	Japan	A. Kurokawa, T. Fujimoto, Y. Azuma, S. Terauchi, L. Zhang
10	NMISA	South Africa	W. A. Jordaan
11	NPL	UK	S. Spencer, A. Shard
12	PTB	Germany	L. Koenders, M. Krumrey, I. Busch
13	U. of Surrey	UK	C. Jeynes

4. DETERMINATION OF REFERENCE THICKNESS

A. Goal of Pilot Study

In this pilot study, the measured thicknesses (T_m) of six HfO$_2$ films by various methods (XPS, TEM, XRR, SE and XRF) were fitted with a straight line to the reference thickness (T_{ref}) to determine the gradient m as a scaling constant and the constant c as the zero-thickness offset from the following relation,

$$T_m = mT_{ref} + c \qquad\qquad (Eq.4\text{-}1)$$

The goal of this pilot study is to compare the slope m and offset c and to investigate the true thickness of the HfO$_2$ films by calibration of the slope and offset values.

B. Determination of Reference Thicknesses

For the meaningful comparison of the slope m and offset c of the reported film thicknesses, the reference thicknesses of the HfO$_2$ films should be traceably determined. Mutual calibration with a length-unit traceable method (LTM) and a zero offset method (ZOM) was suggested as the traceable method to determine the reference thickness.

MEIS data shown in Figure 4-1 were agreed to be used as the ZOM data in the web meeting 2020 and the subsequent discussions because the thicknesses by XPS were found to be highly affected by the surface contamination layer on the reference samples in this pilot study. In MEIS analysis, the thickness of the HfO$_2$ films can be determined from the measured number of constituent Hf atoms within a unit area and the number density of the bulk HfO$_2$. However, the fraction of scattered ions reaching the detector is related to the scattering cross section of the constituent atoms. In the thickness measurement of an HfO$_2$ thin film grown on crystalline Si substrate, the signal intensity of the substrate can be a basis for thickness measurement because the number density of crystalline Si is constant. Figure 4-1 shows the MEIS spectra of Si (100) substrate (magenta) without film and HfO$_2$/SiO$_2$/Si (100) film (blue).[9] The fact that the intensities of the Si substrate are identical in the substrate without film and in the ultra-thin HfO$_2$/SiO$_2$/Si (100) films is the basis for the thickness measurement. For this reason, the relative intensity ratio $R_{MEIS} = I_B/I_A$) of film material (B) to substrate (A) is proportional to the amount of hafnium, and therefore to the thickness (T_{MEIS}) of the HfO$_2$ layer.

---

[9] K. J. Kim, T. G. Kim, J. H. Kwon, H. Ruh, K. Park and W. J. Min, Traceable thickness measurement of ultrathin HfO$_2$ films by medium-energy ion scattering spectroscopy, Metrologia 57 (2020) 025001.
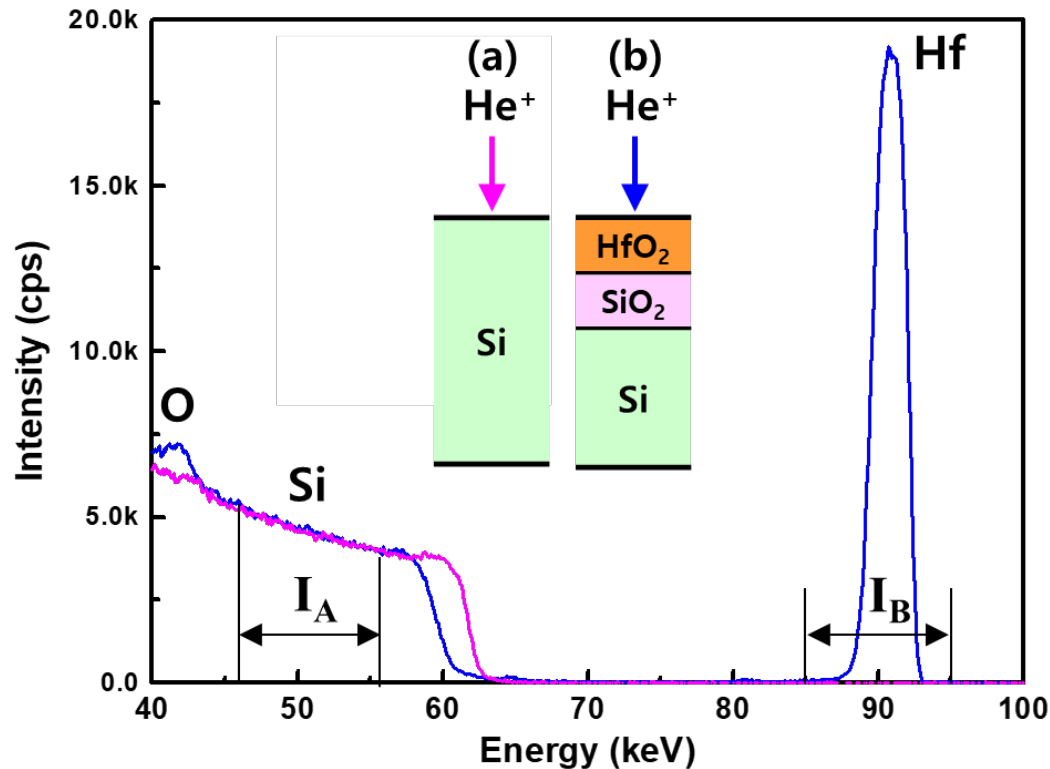
Figure 4-1. MEIS spectra of (a) Si (100) substrate without film (magenta) and (b) HfO$_2$ (3.47 nm) /SiO$_2$/Si (100) film (blue).

The proportionality factor can be determined from the slope, derived from mutual calibration by MEIS as ZOM and XRR as a LTM. The intensities of the crystalline Si substrate (I_A) were determined to be in the energy range from 46 keV to 56 keV from the MEIS spectra shown in Figure 4-1. The intensities of Hf in the six HfO$_2$ films (I_B) were also determined to be in the energy range from 85 keV to 95 keV. Table 4-1 shows the MEIS intensities of the substrate (I_A) and of the HfO$_2$/SiO$_2$/Si (100) films (I_B), and their ratios ($R = I_B/I_A$) determined from the three MEIS spectra.

XRR and TEM are the representative LTMs because they are based on the X-ray wavelength and the lattice constant of crystalline Si substrate, respectively. However, the reported XRR data ($T_{ave,XRR}$) shown in Table 4-2 were chosen as the length-unit traceable thicknesses because the film thicknesses by HR-TEM were scattered in a wide thickness range and could not be used to obtain the reference values. In the web meeting 2020 and the subsequent discussions, it was decided to exclude the thicknesses of the thinnest film in the calculation of the average XRR thicknesses because they are too thin to measure the precise thickness by XRR.

Table 4-1. MEIS intensity ratios ($R=I_B/I_A$) determined from three MEIS spectra

Measurement		1	2	3	4	5	6
1	I_A	456,211	456,813	457,875	458,174	459,707	462,033
	I_B	111,006	175,448	239,460	303,839	369,497	500,151
	$R=I_B/I_A$	0.2433	0.3841	0.5230	0.6632	0.8038	1.0825
2	I_A	456,968	455,821	457,874	458,486	458,420	461,614
	I_B	111,259	175,679	238,932	303,589	368,062	500,280
	$R=I_B/I_A$	0.2435	0.3854	0.5218	0.6622	0.8029	1.0838
3	I_A	457,262	456,454	458,058	457,814	459,414	461,386
	I_B	111,185	176,238	238,702	303,155	367,120	502,713
	$R=I_B/I_A$	0.2432	0.3861	0.5211	0.6622	0.7991	1.0896
Average of R		0.2433	**0.3852**	**0.5220**	**0.6625**	**0.8019**	1.0853
Stdev of R		0.0002	0.0010	0.0009	0.0006	0.0025	0.0038
u of R		0.0001	**0.0006**	**0.0005**	**0.0003**	**0.0014**	0.0022

Table 4-2. The average thickness of the HfO$_2$ films from four XRR data.

Laboratory	Measured Thickness (nm)					
	1	2	3	4	5	6
KRISS	0.98	1.38	1.77	2.18	2.60	3.49
NIST	0.81	**1.36**	**1.81**	**2.24**	**2.71**	3.51
NMIJ	0.95	**1.41**	1.78	2.26	2.73	3.61
PTB	-	**-**	1.83	2.23	2.73	3.56
Average (nm)	**0.880**	**1.385**	**1.807**	**2.243**	**2.723**	**3.560**
Stdev (nm)	0.099	0.035	0.025	0.015	0.012	0.050
u (nm)	0.070	**0.025**	**0.015**	**0.009**	**0.007**	0.035

It was decided also to exclude the thicknesses of the thickest film in the calculation of the average thicknesses because they are too thick to measure the precise thickness by XPS and MEIS. The XRR data of KRISS was excluded because the slope and offset value are inconsistent with the average XRR data.

C. Reference Thicknesses and Uncertainties by Mutual Calibration (MC)

In the same series of HfO$_2$ films, the measured XRR thicknesses (T_{XRR}) and the MEIS intensity ratio (R_{MEIS}) for mutual calibration are represented by a linear regression equation and the slope and the intercept are calculated by Eq.4-2.

$$T_{XRR} = mR_{MEIS} + c \qquad \text{(Eq.4-2)}$$

The thicknesses of the individual samples measured by XRR ($T_{i,XRR}$) and MEIS ($T_{i,MEIS}$) are calibrated by Eq.4-3 and Eq.4-4 because the slope (m) obtained by XRR and the intercept (c) obtained by MEIS are traceable to length unit.

$$T_{c,i,XRR} = T_{i,XRR} - c \qquad \text{(Eq.4-3)}$$

$$T_{c,i,MEIS} = mR_{i,MEIS} \qquad \text{(Eq.4-4)}$$

The certified thicknesses ($T_{c,i}$) of the individual samples are calculated by Eq.4-5 from the arithmetic mean of the individual calibrated thicknesses ($T_{c,i,XRR}, T_{c,i,MEIS}$) from Eq.4-3 and Eq.4-4.

$$T_{c,i} = \frac{1}{2}(T_{c,i,MEIS} + T_{c,i,XRR}) \qquad \text{(Eq.4-5)}$$

In this process, the measurement uncertainty of the certified value is calculated by the following steps.

(1) Definition of measurand ($T_{c,i}$) and input quantities in model equation

The model equation to obtain the measurement uncertainty is given by Eq.4-2, which is obtained by substitution of the equations calibrated by the intercept (Eq.4-3) and slope (Eq.4-4) to Eq.4-5,

$$T_{c,i} = \frac{1}{2}(mR_{i,MEIS} + T_{i,XRR} - c) \qquad \text{(Eq.4-6)}$$

Here, m and c are the slope and intercept of the linear regression line, respectively. $R_{i,MEIS}$ and $T_{i,XRR}$ are the MEIS intensity ratio and the thicknesses of the ith sample measured by XRR, respectively.

(2) Finding standard uncertainties of the input quantities

The standard uncertainty and correlation coefficient for the slope (m) and intercept (c) are calculated by regression equations as shown in Annex E.

For the ith sample, the standard uncertainties for the results by MEIS and XRR are determined from the individual measurement procedures by considering their uncertainties with the types of A and B. As shown in the Eq.4-6, the arithmetic mean value is determined from the measured values for one sample by two methods.

When the arithmetic mean value of the different measurement results for the same sample is used as a model equation for uncertainty evaluation, the result may be under-estimated if the correlation coefficient is not considered. Therefore, the correlation coefficient of two different input quantities is set to 1 as a conservative approach.

(3) Calculation of combined standard uncertainty of measurand ($T_{c,i}$)

If there is a correlation between the input quantities, the combined standard uncertainty of measurand can be determined by Eq.4-8 from a general function with a correlation between the input quantities, Eq.4-7,

$$y = f\ (x_1, x_2, \cdots, x_N) \tag{Eq.4-7}$$

$$u_c^2(y) = \sum_{i=1}^{N}\left(\frac{\partial f}{\partial x_i}\right)^2 u^2(x_i) + 2\sum_{i=1}^{N-1}\sum_{j=i+1}^{N}\left(\frac{\partial f}{\partial x_i}\right)\left(\frac{\partial f}{\partial x_j}\right)u(x_i)u(x_j)r(x_i, x_j) \tag{Eq.4-8}$$

By this method, the equation to determine the combined standard uncertainty ($u_c(T_{ci})$) for the measurand ($T_{c,i}$) is derived to be Eq.4-9.

$$u_c^2(T_{c,i}) = \left(\frac{R_{i,MEIS}}{2}\right)^2 u^2(m) + \left(\frac{m}{2}\right)^2 u^2(R_{i,MEIS})$$
$$+ \left(\frac{1}{2}\right)^2 u^2(T_{i,XRR}) + \left(\frac{-1}{2}\right)^2 u^2(c)$$
$$+ 2\left(\frac{R_{i,MEIS}}{2}\right)\left(\frac{-1}{2}\right)u(m)u(c)r(m,c)$$
$$+ 2\left(\frac{m}{2}\right)\left(\frac{1}{2}\right)u(R_{i,MEIS})u(T_{i,XRR})r(R_{i,MEIS}, T_{i,XRR}) \tag{Eq.4-9}$$

(4) Calculation of expanded uncertainty

The expanded uncertainty is calculated from the coverage factor by considering the confidence level and the estimated probability distribution. The expanded uncertainty for the measurand in the general model equation (Eq.4-6) is determined by Eq.4-10.

$$U = k \cdot u_c(y) \tag{Eq.4-10}$$

From the same manner, the expanded uncertainty of the measurand ($T_{c,i}$) can be expressed by Eq.4-11.

$$U = k \cdot u_c\left(T_{c,i}\right) \tag{Eq.4-11}$$

The coverage factor (k) is determined according to the distribution form of the measurand (T_{ci}). The distribution form of the measurand is determined according to the magnitude of the uncertainties and degrees of freedom for the results by MEIS or XRR and for those of the intercept and slope. Here, the coverage factor is chosen from t-distribution corresponding to the smallest degrees of freedom and 95 % level of confidence among the two kinds of input quantities.

In the 1st order linear regression equation, if the standard uncertainties of the intercept and slope are relatively large and the number of comparison samples is n, the final degrees of freedom of the measurand are n-2.

The combined standard uncertainty and the expanded uncertainty were calculated by a simulation program developed by Dr. Jin Chun Woo of KRISS.[10] It was developed to apply for the thickness measurement by mutual calibration using a linear regression equation. In this program, if the input cells are filled with the measured thicknesses, the standard uncertainties and the number of the samples, the film thicknesses, the slope and the offset values, the combined standard uncertainties and the expanded uncertainties for the individual samples are calculated.

In the determination of the reference thicknesses, the number of samples (n) is 4 and the degrees of freedom of the measurand are 2 (= n-2). Figure 4-2 and 4-3 show the images of the Inputting zone and Result zone of the program for the measurement of the reference thicknesses by mutual calibration from T_{XRR} and R_{MEIS} as the $T_{i,LTM}$ and $T_{i,ZOM}$, respectively.

Inputting Zone ;   **Fill the blue cells for this calculation !!**

1. Enter the order of linear regression :   1
2. Enter the no. of regression data(n) :   4
3. Enter n regression data pairs at following cells :

Standard No.	$T_{i,ZOM}$ value, x_i	$T_{i,ZOM}$ combined standard uncertainty, $u(x_i)$	$T_{i,LTM}$ value, y_i	$T_{i,LTM}$ combined standard uncertainty, $u(y_i)$
1	0.3852	0.0006	1.385	0.025
2	0.522	0.0005	1.807	0.015
3	0.6625	0.0003	2.243	0.009
4	0.8019	0.0014	2.723	0.007

Figure 4-2. Inputting zone of the program for the thickness measurement by mutual calibration by T_{XRR} and R_{MEIS} as the $T_{i,LTM}$ and $T_{i,ZOM}$, respectively.

---

[10] Jin Chun Woo and Kyung Jung Kim, "Uncertainty; Thickness measurement of nm oxide films by mutual calibration," http://uncertainty.co.kr/

Result Zone ;   Find the results from white cells!!

A. Coefficients of the regression line :

Order	0	1
Coefficient(a_i)	1.421E-01	3.200E+00
$u(a_i)$	3.740E-02	6.101E-02

B. Correlation factor

Correlation factor, $r(a_1, a_0)$	-9.673E-01

C. Degrees of freedom

2

Regression Curve (plot of T_{TEM} (y) vs T_{MEIS} (x))

D. Certified value and uncertainty

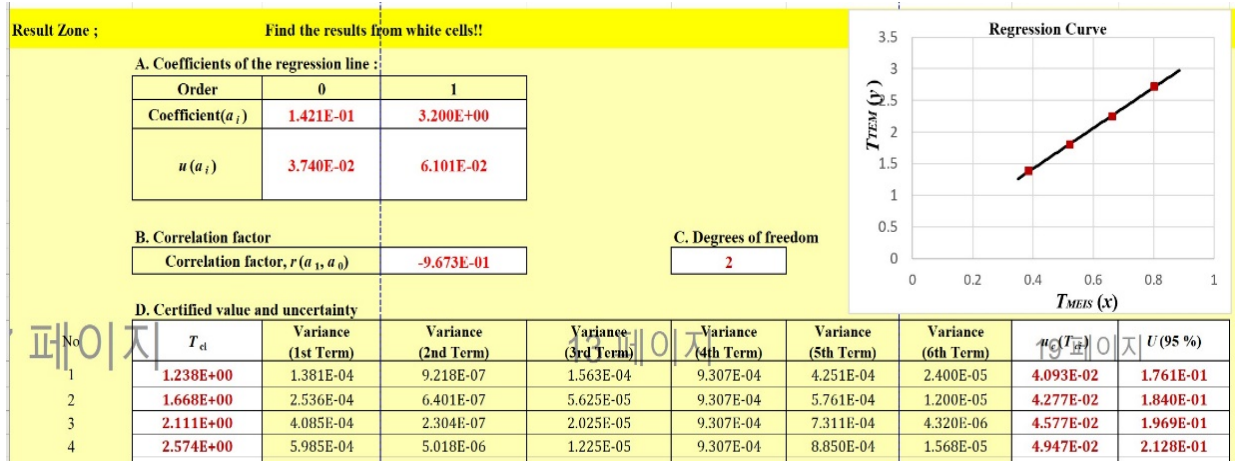| No	T_{cl}	Variance (1st Term)	Variance (2nd Term)	Variance (3rd Term)	Variance (4th Term)	Variance (5th Term)	Variance (6th Term)	$u_c(T_{cl})$	U (95 %)
1	1.238E+00	1.381E-04	9.218E-07	1.563E-04	9.307E-04	4.251E-04	2.400E-05	4.093E-02	1.761E-01
2	1.668E+00	2.536E-04	6.401E-07	5.625E-05	9.307E-04	5.761E-04	1.200E-05	4.277E-02	1.840E-01
3	2.111E+00	4.085E-04	2.304E-07	2.025E-05	9.307E-04	7.311E-04	4.320E-06	4.577E-02	1.969E-01
4	2.574E+00	5.985E-04	5.018E-06	1.225E-05	9.307E-04	8.850E-04	1.568E-05	4.947E-02	2.128E-01

Figure 4-3. Result zone of the program for the measurement of reference thickness by mutual calibration from T_{XRR} and R_{MEIS} as the $T_{i,LTM}$ and $T_{i,ZOM}$, respectively.

Table 4-3. The reference thicknesses and uncertainties of the HfO$_2$ films by mutual calibration method.

Thickness	Reference Thickness and Uncertainty (nm)					
	1	2	3	4	5	6
T_{ref}	-	1.24	1.67	2.11	2.57	-
u_{ref}	-	0.041	0.043	0.046	0.049	-
U_{ref}	-	0.176	0.184	0.197	0.213	-

As a result, the reference thicknesses and their uncertainties of the HfO$_2$ films determined by mutual calibration method are described in Table 4-3.

5. RESULTS AND DISCUSSIONS

A. X-ray Photoelectron Spectroscopy (XPS)

The method to determine the thickness of nm HfO$_2$ film on Si (100) substrate thickness by XPS has been published. In XPS, the thickness of HfO$_2$ film is determined by the following equation.

$$T_{HfO2} = L\cos\theta\ln(\frac{R_{exp}}{R_0} + 1)$$ (Eq.5-1)

Where L is the effective attenuation length (EAL) of photoelectrons ejected from the overlayer

HfO$_2$ film, θ is the emission angle of an electron from the surface normal, R_{exp} is the intensity ratio of thin HfO$_2$ film to the substrate, and R_0 is the intensity ratio of pure HfO$_2$ film to the substrate.

$$R_0 = \frac{I_{ove}^{\infty}}{I_{sub}^{\infty}} \qquad \text{(Eq.5-2)}$$

R_0 is obtained from the pure HfO$_2$ and SiO$_2$ samples, where the pure samples were composed of 50 nm thick films on Si (100) substrate. R_0 is the ratio of the Hf $4f$ (I_{ove}^{∞}) to Si $2p$ (I_{sub}^{∞}) peak intensities measured from the pure HfO$_2$ and SiO$_2$ samples. R_{exp} is the ratio of Hf $4f$ (I_{ove}^{exp}) to Si $2p$ (I_{sub}^{exp}) peak intensity in the XPS spectra of the HfO$_2$ films as shown in Figure 5-1,

$$R_{exp} = \frac{I_{ove}^{exp}}{I_{sub}^{exp}} \qquad \text{(Eq.5-3)}$$

$$I_{sub}^{exp} = I_{SiO2}^{exp} + I_{Si}^{exp} \times \left(\frac{I_{SiO2}^{\infty}}{I_{Si}^{\infty}}\right) \qquad \text{(Eq.5-4)}$$

$$I_{SiO2}^{exp} = I_{SiO2} + 0.75 \times I_{Si2O3} + 0.5 \times I_{SiO} + 0.25 \times I_{Si2O} \qquad \text{(Eq.5-5)}$$

$$I_{Si}^{exp} = I_{Si} + 0.75 \times I_{Si2O} + 0.5 \times I_{SiO} + 0.25 \times I_{Si2O3} \qquad \text{(Eq.5-6)}$$

I_{sub}^{exp} is calculated from the combination of the interfacial SiO$_2$ and the substrate Si components. It is important to combine the two components effectively to determine the thickness by Eq.4-4 because the SiO$_2$ layer is also regarded as a component of the substrate. The two substrate components I_{SiO2}^{exp} and I_{Si}^{exp} can be evaluated by Eq.5-4 and 5-5, respectively. In Eq.4-4, the EAL of photoelectron, L, is an important parameter to determine the film thickness. The L value can be determined by the mutual calibration of a series of films with different thicknesses. Eight laboratories were involved in the thickness measurement of HfO$_2$ films by XPS.

Eight laboratories participated in this pilot study as shown in Table 5-1. Most of the laboratories used monochromatic Al Kα line (1486.6 eV) as the x-ray sources except NIM using Mg Kα line (1253.6 eV)
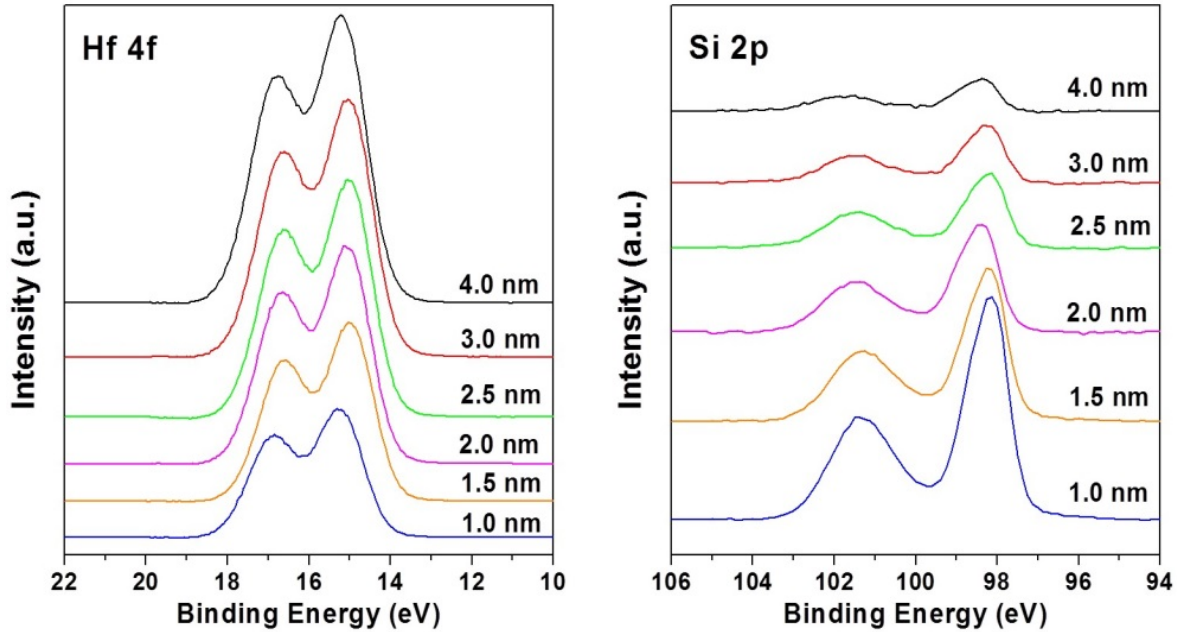
Figure 5-1. XPS spectra of the Si 2*p* and Hf 4*f* peaks of the HfO$_2$ films on Si (100) substrate as function of thickness

EAL is an important parameter to determine the film thickness. However, the EAL values were determined by different methods from the participating laboratories. The EAL value of BAM (1.840 nm) was determined by referencing the thickness T$_{ove}$ obtained for the 4, 6 and 8 nm thick HfO$_2$ film with XPS to the thickness obtained for the same samples with X-ray reflectometry investigations performed by the PTB.

Table 5-1. XPS instruments involved in CCQM P-190

Laboratory	Maker	Model	X-ray source
BAM	Kratos Analytical	AXIS Ultra DLD	mono-Al Kα
CENAM	ThermoFisher Scientific	ARXPS	mono-Al Kα
KRISS	Ulvac-PHI	VersaProbe II	mono-Al Kα
NIM	ThermoFisher Scientific	Escalab 250 Xi	Mg Kα
NIST	Kratos Analytical	Axis Ultra DLD	mono-Al Kα
NMIJ	Ulvac-PHI	ESCA5800	mono-Al Kα
NMISA	Ulvac-PHI	Quantum 2000	mono-Al Kα
NPL	Kratos Analytical	Axis Ultra DLD	mono-Al Kα

Table 5-2. Experimental parameters of XPS in CCQM P-190

Laboratory	EAL, L (nm)	Electron Emission Angle, θ (°)	R_0
BAM	1.840	0	4.210
CENAM	-	5, 15, 25, 35, 45, 55	-
KRISS	1.939	45	4.251
NIM	1.781	10	4.309
NIST	2.155	0	4.749
NMIJ	2.020	34	4.470
NMISA	2.180	45	4.733
NPL	2.100	34	4.410
Average	2.002	-	4.447
Standard deviation	0.155	-	0.219
Relative standard deviation %	7.740	-	4.931

The EAL value of KRISS (1.939 nm) was determined from mutual calibration with the thicknesses by XPS and TEM. The EAL value of NIM (1.781) was experimentally determined from a series of $HfO_2/SiO_2/Si(100)$ films with the certified thicknesses ranging from 1 nm to 4 nm of the HfO_2 films. The EAL value of NMIJ (1.840 nm) was determined from the basis of thickness by XRR. NIST value was decided by using the relationship $L_{SLA} = \lambda_i$ cited in Jablonski and Powell [11] and $L_{ave} = \lambda_i(1 - 0.735\omega)$ by Powell and Jablonski[12].

In NPL, EALs were estimated using the formula S3.[13] The author reports an 8% root mean square scatter in the results from known materials and this is taken as the relative standard error. The relevant attenuation lengths are: $L_{Hf4f} = 2.10 \pm 0.17$ nm and $L_{Si2p} = 2.00 \pm 0.16$ nm. The EAL value of NMISA was determined by calculating the average value over the expected thickness range specified by the NIST SRD82 database.

The average of the reported EAL values is 2.002 nm and the relative standard deviation (RSD) is 7.7%. The reason for the large RSD value is that most values were evaluated with different methods. The development of a common method to determine the EAL value is required.

[11] A. Jablonski and C.J. Powell, Practical expressions for the mean escape depth, the information depth, and the effective attenuation length in Auger-electron spectroscopy and x-ray photoelectron spectroscopy, J. Vac. Sci. Technol. A 27, 253 (2009)

[12] C.J. Powell, A. Jablonski, Surface sensitivity of X-ray photoelectron spectroscopy, Nucl. Instrum. Methods Phys. Res. Sect. A 601, 54 (2009)

[13] M. P. Seah, Simple universal curve for the energy-dependent electron attenuation length for all materials, Surf. Interface Anal. 44, 1353 (2012)

R_0 is also very important to determine the film thickness. It is experimentally obtained from the ratio of the Hf $4f$ (I_{ove}^∞) to Si $2p$ (I_{sub}^∞) peak intensities measured from the pure HfO_2 and SiO_2 films grown on Si (100) substrate. It shows a wide distribution with a large relative standard deviation of 4.9%. A critical reason of this result is that the surface contamination of the HfO_2 films by hydrocarbon during the cleaning procedure with isopropyl alcohol is much more severe than that of the SiO_2 films.

As reported by NPL, the thickness of the contaminated surface carbon layer (d_C) on two reference samples (thick HfO_2 and SiO_2) was estimated using the following equation[14].

$$d_c = -L_{C1s} \cos\theta \ln(1 - \frac{I_{C1s}}{I_{C1s}^\infty}) \qquad \text{(Eq.5-7)}$$

Where L_{C1s} is the effective electron attenuation length for contaminated carbon 1s electrons and I_{C1s}^∞ is XPS intensity of pure bulk contaminant. L_{C1s} was estimated using the following equation[15].

$$L_{C1s}(\text{E; average organic}) = 0.00837E^{0.842} \qquad \text{(Eq.5-8)}$$

where E is the kinetic energy of electrons in electron volts. The effect of IPA soaking time on the carbon removal for HfO_2 and SiO_2 samples is shown in Figure 5-2. For the SiO_2 reference sample, the thickness of the contaminated carbon layer decreases from 0.564 nm to 0.107 nm as the soaking time of the sample in isopropyl alcohol (IPA) increases from 0 hour to 24 hours. On the other hand, the contaminated carbon layer on a HfO_2 reference sample only reduced from 1.307 nm to 0.698 nm after overnight IPA soaking. After the overnight soaking, the carbon layer for HfO_2 samples was 7 times thicker than that for SiO_2 samples, which severely affects the R_0 values. It is consistent with the previous results.[16] As a result, the investigation of a new cleaning process of HfO_2 films with different chemical solvent is required to minimize the uncertainty of the R_0value by balancing the amount of surface contaminations for SiO_2 and HfO_2 films. The R_0value is recommended to be corrected because it affects the slope and the offset value. The correction of the R_o value from the

[14]"Evaluation of a simple correction for the hydrocarbon contamination layer in quantitative surface analysis by XPS", J. Elec. Spec. 148, 21 (2005); "Ultrathin SiO_2 on Si. I. Quantifying and removing carbonaceous contamination", J. Vac. Sci. Technol. A 21, 345 (2003)

[15]"Attenuation lengths in organic materials" Surf. Interface Anal. 43, 744 (2011).

[16]"Adsorption of Moisture and Organic Contaminants on Hafnium Oxide, Zirconium Oxide, and Silicon Oxide Gate Dielectrics" J. Electrochem. Soc. 150, F186 (2003).

effect of the attenuation through the contamination layer is recommended as a method to reduce the effect of the contamination layer as reported by NPL.
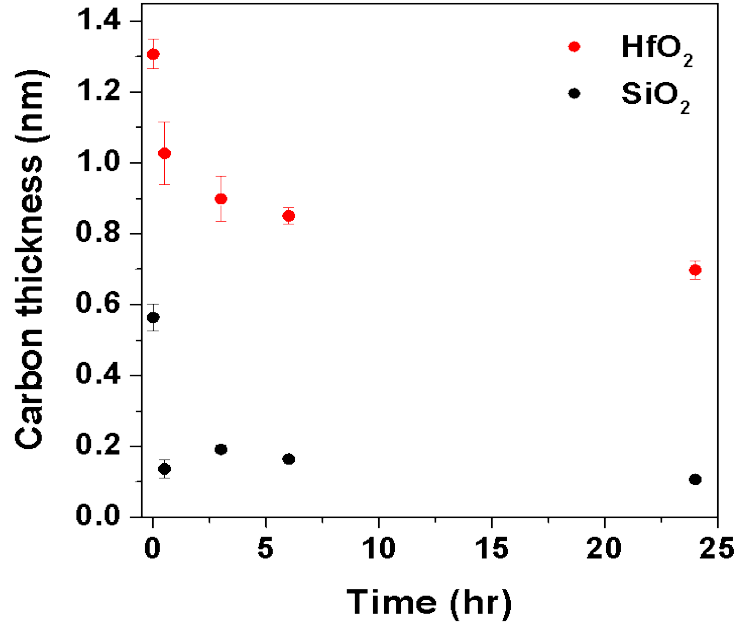

Figure 5-2. Effect of IPA soaking time on the carbon removal for HfO_2 and SiO_2 samples

The measured intensities of the reference HfO_2 and SiO_2 films were corrected for attenuation through the carbon layer using the following equation,

$$I_\infty = I \exp\left(\frac{d_C}{L\cos\theta}\right)$$ (Eq.5-9)

where I_∞ is the estimated reference intensity, I is the measured intensity and L is the estimated effective attenuation length for electrons with the kinetic energy of the elemental peak in the carbon overlayer. Using the correction factor in equation (13), and estimates of ~10% error in L and ~20% error in d_C, the Hf 4f intensity from pure HfO_2 was found to be a factor 1.33 ± 0.06 larger than the measured intensity. For the Si and SiO_2 samples the correction factor was 1.09 ± 0.01. The oxide thickness on the reference Si sample was found to be 0.78 nm. However the samples with HfO_2 layers have a larger oxide thickness of ~1.45 nm with some correlation to the HfO_2 thickness. By combining the relevant equations (analogous to equation 13) the substrate intensity for samples 1 to 6 was estimated to be ~3% lower than that of the Si reference sample. From these considerations, the reference intensity ratio, $R_o = I_\infty$ (Hf 4f in HfO_2)/ I_∞(Si 2p in substrate) was determined to be

R_o = 4.41 ± 0.27 for this instrument and settings.

Eight laboratories participated in this pilot study by XPS as shown in Table 5-3. The slope and offset values were calculated from the mutual calibration of the reported thicknesses in y-axis and the reference thicknesses in x-axis. The XPS data without CENAM shows the distribution of m values from 1.045 to 1.198 and c values from -0.150 nm to 0.059 nm. The average values of m and c are 1.124 and -0.032 nm. The average offset value of -0.032 nm is not significant in the context of the range of offsets from participants and is less than the standard uncertainties of the reference thicknesses. It is worth noting that the average offset is strongly influenced by the results of BAM and NIST, the two participants who used normal incidence emission where there is a risk of photoelectron diffraction affecting the silicon intensities.. The difference of the slope m value from the unit value is related to both the effective attenuation length (L_{HfO_2}) and the experimental parameter R_o.

For the precise thickness measurement of HfO_2 films close to the real value by XPS, the calibration of EAL value (L) by the reference thicknesses described in Table 5-4 is recommended. The correct determination of R_o value by minimization of the surface carbon layer or correction of R_o value from the effect of contamination layer is also recommended. Because of the correlation between R_o and EAL and the significant uncertainty and bias in R_o from different levels of carbon contamination on the reference samples, an accurate value for the EAL of electrons in HfO_2 films cannot be found in this pilot study. A revised procedure for XPS data analysis is required and this is set out in Appendix F.

Table 5-3. CCQM P-190 results by XPS.

Laboratory	Reference and Measured Thickness (nm)						Slope m	Offset c (nm)
		1.24	1.67	2.11	2.57			
BAM	0.72	1.14	1.60	2.06	2.53	3.51	1.045	-0.150
CENAM	0.87	1.15	1.54	1.73	2.37	2.56	0.871	0.045
KRISS	0.94	1.46	2.02	2.53	3.01	3.78	1.164	0.046
NIM	0.98	1.53	2.07	2.61	3.12	4.07	1.198	0.059
NIST	0.82	1.30	1.77	2.30	2.79	3.81	1.129	-0.101
NMIJ	0.83	1.33	1.85	2.32	2.78	3.64	1.087	0.007
NMISA	0.79	1.27	1.85	2.31	2.72	3.81	1.084	-0.020
NPL	0.85	1.37	1.86	2.37	2.91	3.81	1.158	-0.070
Average (nm)	0.85	1.34	1.86	2.36	2.84	3.78	1.124	-0.032

Stdev (nm)	0.09	0.13	0.16	0.18	0.19	0.17	0.05	0.08
RSD (%)	10.53	9.48	8.43	7.48	6.83	4.55	4.80	-

In the thickness measurement of HfO$_2$ films by XPS using Eq.5-1, the EAL value (L), the electron emission angle (θ), the intensity ratio (R_{exp}) of HfO$_2$ films to the substrate, and the intensity ratio (R_0) of pure HfO$_2$ film to the substrate are the main parameters.

Therefore, the uncertainty (U) in the thickness measurement by XPS can be determined by the combined standard uncertainty (u_c) and the coverage factor (k) at 95% confidence level from the following equation,

$$U = ku_c$$
$$u_c{}^2 = u_{R_0}{}^2 + u_{R_{exp}}{}^2 + u_\theta{}^2 + u_L{}^2$$

where u_{R_0} and $u_{R_{exp}}$ are the standard uncertainties in the determination of R_0 and R_{exp}, respectively. u_{R_0} and $u_{R_{exp}}$ are Type A uncertainties which can be directly determined by repetitive experiments. u_θ is the standard uncertainty in the setting of the electron emission angle, which is related with the specification of the spectrometer in the setting of the electron emission angle. u_L is the standard uncertainty in the determination of the electron EAL. Evaluation of u_L is somewhat complicated because the EAL values were determined by various methods.

For the precise determination of the EAL and R$_0$ values, the thicknesses were measured again by XPS at the reference geometry (RG) and using corrections for carbon overlayer attenuation by NPL, NIM and KRISS from a short round robin test as shown in Table 5-4. The re-determined EAL value at RG shows a narrow range variation from 1.809 to 1.858. The standard uncertainties of the revised EAL and R$_0$ values at RG were highly improved to 0.013 nm and 0.038, respectively. As a result, in the case of thickness measurement by XPS at the reference geometry, the EAL value of 1.834 nm and R$_0$ value of 4.377 are recommended with the relative standard uncertainties of 0.013 nm and 0.038, respectively. It should be noted that the transmission of the XPS instrument may affect the value of R$_0$ and the recommended value is for calibrated instrument Al Kα instruments at the reference geometry.

A subset of the results reported in Table 5-3 can be adjusted using these recommended values and Eq.5-1. The results from CENAM did not use this equation and cannot be recalculated and NIM used a lower energy X-ray source for which these recommended values are not appropriate. The adjusted values are provided in Table 5-4. The use of consensus values for EAL and R$_0$ have a small effect on the scatter in the results. The large offset of the results from BAM persist and the

slopes of the KRISS and NMISA results are anomalous. This suggests that analysis using the reference geometry is important to obtain consistent results.

Table 5-4. Re-measured EAL value at the reference geometry

Laboratory	Reported EAL (nm)	R_0 value	Slope in mutual calibration with reference thickness in x-axis	Revised EAL (nm)
KRISS	1.826	4.452	0.984	1.856
NIM	1.825	4.397	1.009	1.809
NMIJ	2.020	4.390	1.087	1.858
NPL	2.100	4.270	1.158	1.813
Average	1.943	4.377	1.060	1.834
Standard deviation	0.139	0.077	0.079	0.027
Standard uncertainty	0.070	0.038	0.039	0.013

Table 5-5. CCQM P-190 results by XPS.

Laboratory	Reference and Measured Thickness (nm)						Slope m	Offset c (nm)
		1.24	1.67	2.11	2.57			
BAM	0.69	1.10	1.55	2.01	2.47	3.44	1.026	-0.165
KRISS	0.87	1.36	1.88	2.36	2.81	3.54	1.094	0.027
NIST	0.75	1.18	1.59	2.06	2.48	3.37	0.991	-0.053
NMIJ	0.77	1.22	1.70	2.13	2.55	3.33	0.993	0.016
NMISA	0.71	1.13	1.63	2.02	2.37	3.30	0.932	0.019
NPL	0.76	1.21	1.64	2.08	2.55	3.32	1.002	-0.032
Average (nm)	0.76	1.20	1.67	2.11	2.54	3.38	1.006	-0.031
Stdev (nm)	0.06	0.09	0.12	0.13	0.15	0.09	0.053	0.037
RSD (%)	8.25	7.50	7.00	6.21	5.87	2.68	5.27	-

B. X-ray Reflectometry (XRR)

XRR (X-ray reflectometry) is one of the powerful techniques such as TEM (transmission electron microscopy), SE (spectroscopic ellipsometry), and XPS (X-ray photoelectron spectroscopy) for the determination of t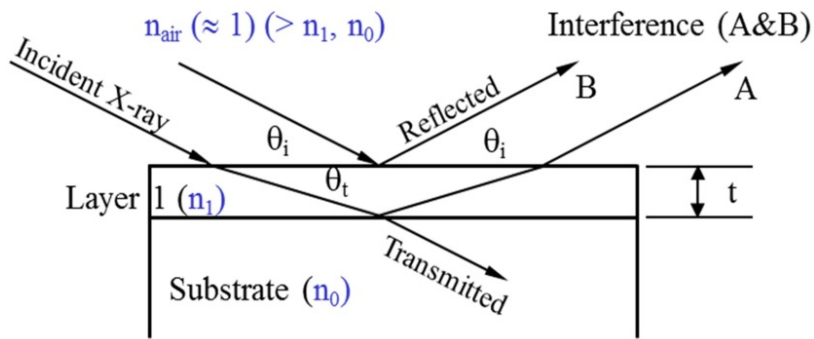he thickness of thin-films. X-rays incident to the surface of a thin-film on a substrate at a glancing angle are reflected simultaneously at the surface and the 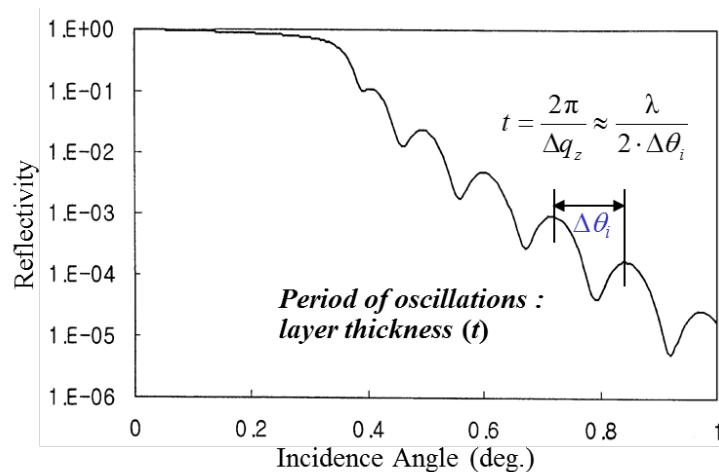interface and the reflected X-rays interfere with each other due to the path difference they traveled. The interference produces thickness fringes, i.e., oscillations, Figure 5-4, and the oscillations are superposed in the reflectivity curve. The period of the oscillations, therefore, has a relationship with the thickness of the film.

Figure 5-3. X-rays incident at a glancing angle are reflected simultaneously at the surface and the interface, and the reflected X-rays interfere with each other.

$$t = \frac{2\pi}{\Delta q_z} \approx \frac{\lambda}{2 \cdot \Delta\theta_i}$$

Period of oscillations :
layer thickness (t)

Figure 5-4. A typical reflectivity curve as a function of incidence angle which shows thickness fringes produced by the interference due to the reflected X-rays A and B in Figure 5-3.

XRR is applicable to almost all kinds of thin-films that have different electron densities from those of substrates, and the measurable range of thickness is from ~ 1 nm up to ~ 1 μm. Thickness of a film, *t*, is expressed as the following equation

$$t = \frac{2\pi}{\Delta q_z} \approx \frac{\lambda}{2 \cdot \Delta\theta_i}$$

where Δq_z is a difference of wavevector transfer, $\Delta\theta_i$ is a period of oscilliations of thickness fringes and λ is wavelength of X-rays. Since the thickness depends on the wavelength and the angle, the traceability of the thickness of a thin film determined by XRR can be maintained through the calibration of the wavelength and the angle.

Four laboratories were participated in this pilot study by XRR as shown in Table 5-6. The XRR shows the distribution of m values from 0.919 to 1.011 and c values from 0.111 nm to 0.239 nm as shown in Table 5-7. Excluding the KRISS data, the average values of m and c are 1.005 and 0.133 nm. The true thicknesses of the HfO_2 films can be determined by calibrate the offset values. The average slope of 1.005 is very close to an ideal value, which means that XRR can act as a length unit traceable method in mutual calibration.

Table 5-6. XRR instruments involved in CCQM P-190

Laboratory	Maker	Model	X-ray source
KRISS	Bruker	D8 discover	Cu X-ray
NIST	Rigaku	SmartLab XRD	Cu X-ray
NMIJ	Rigaku	Traceable X-ray Reflectometer	Cu X-ray
PTB	Panalytical	Empyrian	Cu X-ray

Table 5-7. CCQM P-190 results by XRR

Laboratory	Reference and Measured Thickness (nm)						Slope m	Offset c (nm)
		1.24	1.67	2.11	2.57			
KRISS	0.98	1.38	1.77	2.18	2.60	3.49	0.919	0.239
NIST	0.81	1.36	1.81	2.24	2.71	3.51	1.011	0.111
NMIJ	0.95	1.41	1.78	2.26	2.73	3.61	1.003	0.142
PTB	-	-	1.83	2.23	2.73	3.56	1.001	0.145
Average (nm)	0.88	1.39	1.81	2.24	2.72	3.56	1.005	0.133
Stdev (nm)	0.10	0.04	0.03	0.02	0.01	0.05	0.005	0.019
RSD (%)	11.25	2.55	1.39	0.68	0.42	1.40	0.53	14.19

C. Transmission Electron Microscopy (TEM)

High-resolution TEM is a length-unit traceable thickness measurement method because the scale is based on the lattice constant. Especially, in the thin films grown on Si (100) wafers, the crystalline lattice planes of Si can be directly used as an internal standard to measure the absolute film thickness. The lattice distance between the Si (110) planes in the cross-sectional TEM image is 0.543 nm as shown in Figure 5-5.
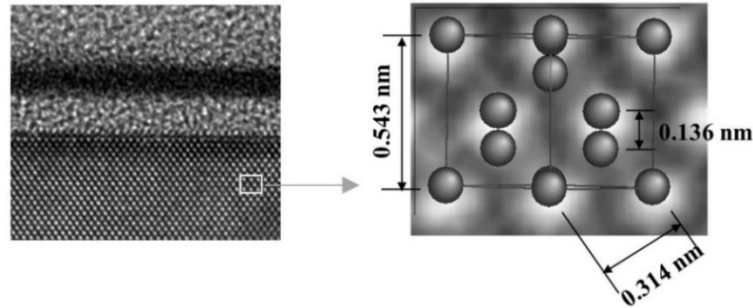

Figure 5-5. Lattice constant of Si(100) substrate.

The HR-TEM image of a $HfO_2/SiO_2/Si(100)$ film can be simply converted to intensity line profile image from the average contrast of the region of interest (ROI) as shown in Figure 5-6. For the precise measurement, the aspect ratio of the lattice line should be maximized by aligning the lines to be parallel to the lattice direction parallel to the interface and film surface.

The locations of the interface and the surface to measure the film thickness can be determined by two methods. The first method is average contrast method. In this method, the location of the SiO_2/HfO_2 interface can be determined from the point of half contrast between the average contrast of the SiO_2 (I_{SiO_2}) and HfO_2 (I_{HfO_2}) layers, $(I_{SiO_2}+I_{HfO_2})/2$.
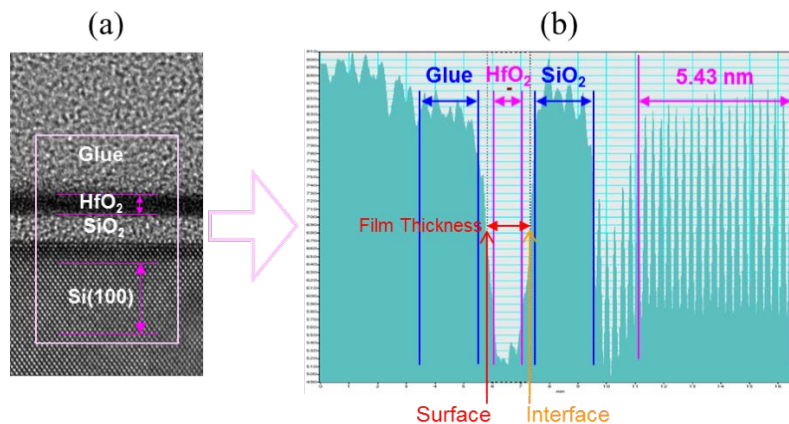

Figure 5-6. High resolution TEM image (a) and intensity profile image (b) of a HfO_2 (1.5 nm)/SiO_2(2.0 nm)/Si(100) film.

As the same manner, the location of the film surface can be determined from the point of half contrast between the average contrast of HfO_2 (I_{HfO_2}) and glue (I_{glue}) layers by ($I_{HfO_2}+I_{glue}$)/2. The film thickness can be measured from the distance between the SiO_2/HfO_2 interface and the surface of the HfO_2 layer. The thickness of the HfO_2 layer can be simply determined from the ratio of line widths of the HfO_2 layer and the 10 Si (110) lattices corresponding to 5.43 nm.

The second method is differentiation method. In this method, the locations of the SiO_2/HfO_2 interface and the surface of HfO_2 film can be also determined from the inflection points in the differentiated intensity profile as shown in Figure 5-7.[17] At first, in the standard, an intensity profile (b) is acquired in the ROI of HR-TEM image by integrating the individual intensity profiles, which can be measured along the line in the direction perpendicular to the interface, in the direction along the interface (white arrow in (a)). At second, moving-averaged processing is applied to the intensity profile to reduce the noise on the slope which corresponds to the interface region of the intensity profile. The range $2 \leq n \leq 7$ is recommended to be suitable as the number of points to involve in the calculation of the moving-averaged processing. After then, the moving-averaged intensity profile is differentiated by differential processing. (c)
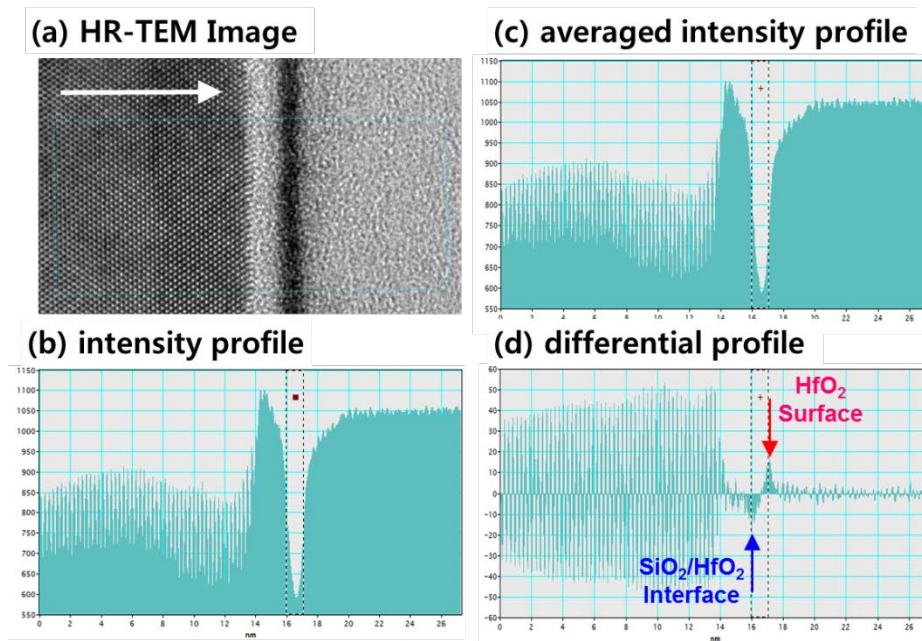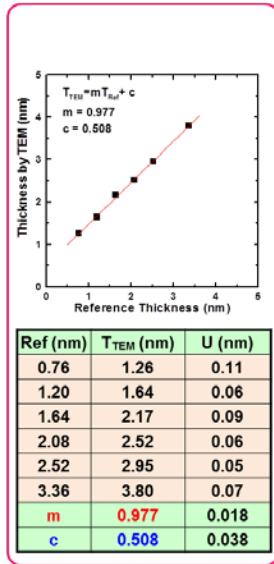

Figure 5-7. High resolution TEM image (a), intensity profile image (b), intensity profile image after moving-averaged processing (c) and averaged intensity profile after differential processing (d)

---

[17] ISO-20263 "Microbeam analysis — Analytical electron microscopy — Method for the determination of interface position in the cross-sectional image of the layered materials"

(a) average contrast method

$T_{TEM} = mT_{Ref} + c$
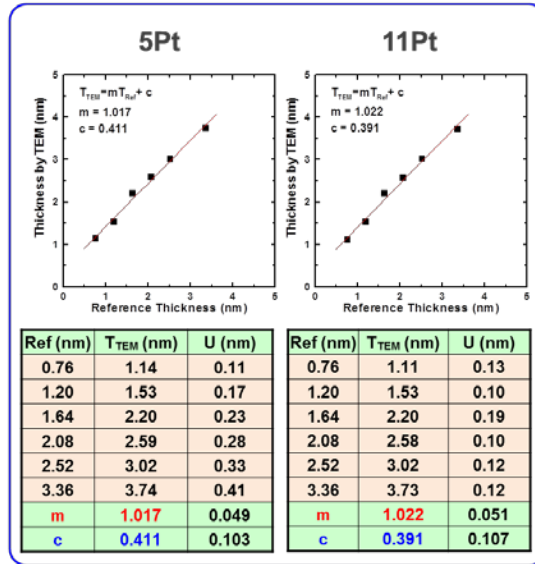$m = 0.977$
$c = 0.508$

(b) differentiation method

5Pt

$T_{TEM} = mT_{Ref} + c$
$m = 1.017$
$c = 0.411$

11Pt

$T_{TEM} = mT_{Ref} + c$
$m = 1.022$
$c = 0.391$

Ref (nm)	T_{TEM} (nm)	U (nm)
0.76	1.26	0.11
1.20	1.64	0.06
1.64	2.17	0.09
2.08	2.52	0.06
2.52	2.95	0.05
3.36	3.80	0.07
m	0.977	0.018
c	0.508	0.038

Ref (nm)	T_{TEM} (nm)	U (nm)
0.76	1.14	0.11
1.20	1.53	0.17
1.64	2.20	0.23
2.08	2.59	0.28
2.52	3.02	0.33
3.36	3.74	0.41
m	1.017	0.049
c	0.411	0.103

Ref (nm)	T_{TEM} (nm)	U (nm)
0.76	1.11	0.13
1.20	1.53	0.10
1.64	2.20	0.19
2.08	2.58	0.10
2.52	3.02	0.12
3.36	3.73	0.12
m	1.022	0.051
c	0.391	0.107

Figure 5-8. Film thicknesses of KRISS TEM determined by the two methods, average contrast method (a) and differentiation method using 5-, and 11-point moving average.(b)

The locations of the SiO_2/HfO_2 interface and the surface of HfO_2 film are defined as the positions in the horizontal axis of the differential curve corresponding to the minimal and maximal peaks, respectively. (d)

Figure 5-8 shows the thicknesses determined from the two methods for the data of KRISS. The thicknesses determined by the differentiation method are slightly thinner than those by the average contrast method. The important point is that the linearity of the thickness by the average contrast method is more linear to the reference thickness than that by the differentiation method. Another point is that the slope (m) of the thickness by the average contrast method (0.977) is smaller than that by the differentiation method (1.017).

In this type of TEM measurement, the combined standard uncertainty u_c is calculated from the equation $u_c^2 = u_m^2 + u_r^2 + u_l^2$. The first term ($u_m$) is the standard uncertainty in the measurement of film thickness. The second term is the standard uncertainty (u_r) in the measurement of line width of the periodic Si (110) lattice planes. The third term is the standard uncertainty (u_l) of the variation of the Si (110) lattice constant.

Four laboratories measured the film thickness by TEM as shown in Table 5-8. The results show wide distributions of slope from 0.707 to 1.168 and offset from 0.25 nm to 1.13 nm as shown in Table 5-9. The reason of this wide distribution is the absence of a well-defined protocol for the measurement of film thickness by TEM.

Table 5-8. TEM instruments involved in CCQM P-190

Laboratory	Maker	Model	V_{ACC} (kV)	Method to determine thickness
KRISS	FEI	Tecnai G2 F30	300	average contrast
NMIJ	JEOL	JEM-3000F	300	differentiation
NIST	FEI	Titan 80-300	300	STEM, average contrast
INMETRO	FEI	Titan 80-300	300	differentiation

KRISS determined the film thickness by the average contrast method. TEM thickness of NMIJ was determined by the differentiation method. The integrated intensity profile was smoothed by the 11-point moving average and differentiated. The maximum and minimum positions of the differentiated profile were defined as the interface positions and the film thickness was evaluated with a scale given by (200) spacing of Si, 0.2715 nm. In the case of NIST, film thicknesses were determined from scanning TEM (STEM) images. The center of the HfO_2 layer was determined by finding the position of the maximum intensity value in the profile. The baseline intensity is also determined from the mean of the intensity in the SiO_2 substrate region. From the baseline intensity and the peak intensity estimated by calculating the mean value surrounding the maximum pixel, the points in both the SiO_2/HfO_2 interface and the surface of the HfO_2 layer where the intensity equals 20 % and 80 % of the peak intensity value were determined. The locations of the interface and surface were defined as the mid-points between the 20 % and 80 % intensity onset points. In the case of INMETRO, the film thickness was determined by the differentiation method.

From these results, in this stage, TEM is difficult to be used as a length unit traceable method in mutual calibration. A precisely revised protocol including HR-TEM image, sampling method, the measurement procedure for the determination of film thickness is required. And an international round robin test by the revised protocol is also recommended.

Table 5-9. CCQM P-190 results by TEM

Laboratory	Reference and Measured Thickness (nm)						Slope m	Offset c (nm)
		1.24	1.67	2.11	2.57			
KRISS	1.25	1.60	2.11	2.57	3.03	3.76	1.072	0.294
NIST	1.72	1.95	2.20	2.70	2.88	3.52	0.742	1.025
NMIJ	1.20	1.60	2.10	2.60	3.00	4.20	1.060	0.314
INMETRO	1.30	1.66	2.15	2.94	3.33	4.22	1.308	0.038
Average (nm)	1.37	1.70	2.14	2.70	3.06	3.93	1.046	0.418
Stdev (nm)	0.24	0.17	0.05	0.17	0.19	0.34	0.232	0.424
RSD (%)	17.44	9.83	2.12	6.21	6.25	8.75	22.222	-

D. Spectroscopic Ellipsometry (SE)

Ellipsometry is one of the most important methods for the thickness measurement of thin oxide films used in the industries of semiconductor and display because it is fast, economic and very precise. However, although the thickness measurement of SiO_2 films by ellipsometry is very reproducible, the offset value was found to be larger than 1 nm in the CCQM pilot study P-38. Therefore the thickness measurement of the oxide films thinner than 1 nm is very restricted and the surface contamination layer should be clearly removed.

Three laboratories were participated in this pilot study by ellipsometry as shown in Table 5-10 and 5-11. DFM, NPL and CENAM has reported the surface contamination differently. Conformity can be achieved between the reported values by adding 0.3 nm to the thickness and offset values reported by DFM in Table 5-10.

Table 5-10. SE instruments involved in CCQM P-190

Laboratory	Maker	Model	Source
CENAM	HORIBA	LT M200AGMS	Xe high pressure
DFM	home build generalized ellipsometer		LDLS light source
NPL	Woollam	M-2000 DI	192 nm ~ 1700 nm

Table 5-11. CCQM P-190 results by SE

Laboratory	Reference and Measured Thickness (nm)						Slope m	Offset c (nm)
		1.24	1.67	2.11	2.57			
CENAM	1.65	1.80	2.25	2.90	3.10	4.20	1.025	0.568
DFM	1.57	2.00	2.65	3.01	3.56	4.31	1.137	0.648
NPL	1.85	2.38	2.82	3.31	3.76	4.55	1.045	1.085
Average (nm)	1.59	1.96	2.47	2.97	3.37	4.25	1.069	0.767
Stdev (nm)	0.29	0.37	0.30	0.31	0.34	0.27	0.060	0.278
RSD (%)	18.53	18.73	12.31	10.31	10.21	6.44	5.588	-

E. X-ray Reflectometry combined with X-ray Fluorescence Analysis (XRR/XRF)

Film thickness is also can be measured by XRF (X-ray fluorescence analysis) because the emission of characteristic X-rays from the oxide layer is depending on the thickness of the film. Only PTB measured the thickness by a combination of XRF and XRR. The thickness of the thicker

layers was determined by X-ray reflectometry (XRR)[18],[19]. Monochromatic X-rays impinging on the surface at grazing incidence are reflected at the layer surface and at the layer-substrate-interface. Both components exhibit a path difference and interfere. By varying the incidence angle, oscillations in the reflectance are observed. Maxima (or minima in case of a phase shift) occur if the path difference is a multiple of the wavelength. From the known wavelength and the observed periodicity, the layer thickness can be determined. For the thinner layers, X-ray fluorescence analysis (XRF) has been used and was calibrated with XRR results.[20] Here, the ratio of the intensity of the Hf Lα line to the intensity of the Si Kα line has been calibrated using the XRR result for the thickest layer with a nominal thickness of 8 nm.

Before the measurements, the samples were cleaned according to the procedure proposed in the protocol. The sample was installed horizontally (reflecting side up) in a UHV-reflectometer[21] which was operated at the four-crystal monochromator (FCM) beamline[22] in the PTB laboratory at the synchrotron radiation facility BESSY II in Berlin. The beam size was about 0.5 mm (horizontal) x 0.3 mm (vertical). The sample was adjusted by means of the linear translations in such a way that, for the calibration, the beam impacts the center of the coated area.

Measurement

For XRR, the photon energy was set to 8048 eV and for some samples as well to 10000 eV. The grazing incidence angle θ was increased stepwise from 0° to about 3° (on some samples up to about 5°), a photodiode always followed the reflected beam (θ/2θ scan). At each position, the photocurrent was normalized to the current of the thin photodiode operated in transmission in the incoming beam. For XRF, the incident photon energy was set to 10800 eV, the grazing incidence angle was set to 10° and the detection angle for the energy-dispersive silicon drift detector (SDD) to 35°. A background correction has been applied for the spectra.

---

[18] M. Krumrey, M. Hoffmann, G. Ulm, K. Hasche, and P. Thomsen-Schmidt. Thickness determination for SiO2 films on Si with X-ray reflectometry at the Si K edge. Thin Solid Films **459**, 241 (2004)

[19] M. Krumrey, G. Gleber, F. Scholze, and J. Wernecke. Synchrotron radiation-based X-ray reflection and scattering techniques for dimen-sional nanometrology. Meas. Sci. Technol. **22**, 094032 (2011)

[20] P. M. Dietrich, D. Treu, H. Kalbe, M. Krumrey, T. Gross, K. Marti and W.E.S. Unger. Experimental determination of the effective attenuation length of Palladium 3d pho-toelectrons in a magnetron sputtered Pd nanolayer Surf. Interface Anal. 49, 464 (2017)

[21] D. Fuchs, M. Krumrey, F. Scholze and G. Ulm, High precision soft x-ray reflectometer, Rev. Sci. Instrum. **66**, 2248 (1995)

[22] M. Krumrey and G. Ulm, High accuracy detector calibration at the PTB four-crystal monochromator beam-line Nucl, Instr. and Meth. A 467, 1175 (2001)

Results

As shown in Figure 5-9, two different methods were used to obtain the HfO_2 layer thickness from the oscillations observed in XRR: complete modeling using the optical constants of the involved materials, leading to d_{XRR_fit} [23], and linear regression from a plot of the angle of the minima (sine, squared) against their order number (squared)[24], leading to d_{XRR_min}.

Very good fit results were obtained from the modeling by including the SiO_2 layer below and an additional contamination layer on top of the HfO_2 layer. However, the resulting HfO_2 layer thickness was identical (deviations $<1\%$) without the additional layers, because - in contrast to SiO_2 layers[25] - the density of the relevant layer is much higher than the density of the adjacent materials.
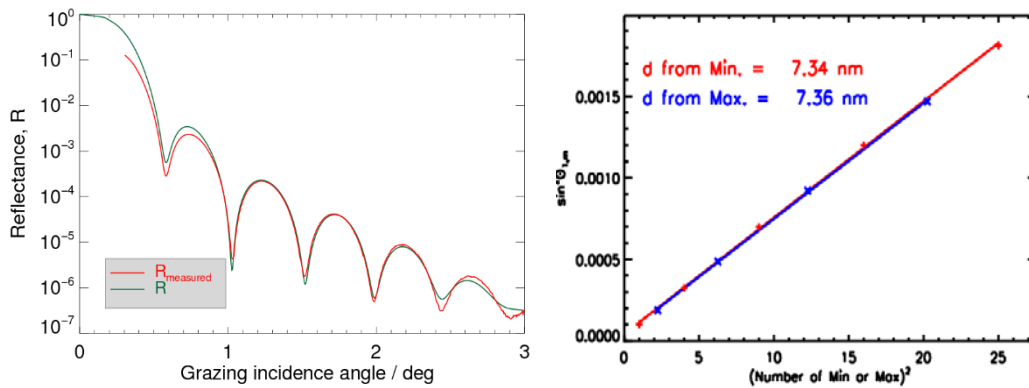
Figure 5-9. Measured and fitted reflectance of the layer with a nominal thickness of 8 nm (left), and linear regression from a plot of the angle of the minima and maxima (sine, squared) against their order number (squared) from this measurement (right)

The values d_{XRR_mean} are the mean values from both XRR evaluation methods, while the values d_{XRF} are the results from the XRF measurements as shown in Figure 5-10, calibrated with the XRR results from the thickest layer with $d_{nom} = 8$ nm. The final thickness values d are provided with their associated uncertainties U_d. Table 5-12 shows the obtained film thicknesses by XRR and XRF from PTB.

---

[23] D. Windt IMD—Software for modeling the optical properties of multilayer films. Computers in Physics 12, 360 (1998)

[24] U. Pietsch, V. Holy and T. Baumbach High-Resolution X-ray scattering – From thin films to lateral nanostructures Springer, New York (2004)

[25] C. Soo Kim, H.-G. Jeon, Y. Jung, M. Choi, B. Ob, and K.-H. Kim. Observation of surface contamination layer by X-ray reflectometry (XRR) analyses Surf. Interface Anal. 49, 522 (2017)
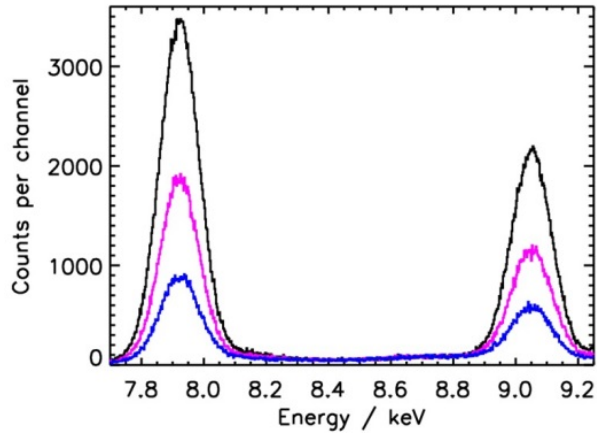
Figure 5-10. Measured fluorescence intensities of Hf Lα and Hf Lβ₁ radiation for the layers with nominal thicknesses of 8 nm, 4 nm and 2 nm, respectively, at an excitation energy of 10800 eV

Table 5-12. Film thicknesses measured by XRR and XRF from PTB

d_{nom} (nm)	d_{XRR_fit} (nm)	d_{XRR_min} (nm)	d_{XRR_mean} (nm)	d_{XRF} (nm)	d (nm)	U_d (nm)
8.00	7.27	7.35	7.31		7.31	0.14
6.00	5.41	5.46	5.44	5.44	5.44	0.08
4.00	3.58	3.59	3.58	3.62	3.60	0.07
3.00	2.66	2.76	2.71	2.70	2.71	0.10
2.00				1.78	1.78	0.07
1.00				1.00	1.00	

The values in *italics* are only indicative.

The uncertainty stated is the expanded measurement uncertainty obtained by multiplying the standard measurement uncertainty by the coverage factor $k = 2$. The measurement uncertainty encompasses: the uncertainty contributed by the wavelength or photon energy of the radiation, the angular accuracy of the reflectometer and the data evaluation based on the methods described above.

Table 5-13. CCQM P-190 results by XRF.

Laboratory	Reference and Measured Thickness (nm)						Slope m	Offset c (nm)
		1.24	1.67	2.11	2.57			
PTB	1.00	-	1.78	-	2.71	3.60	1.033	0.064

F. Rutherford Backscattering Spectrometry (RBS)

RBS is capable of high absolute (traceable) accuracy because the measurement model (VIM §2.48) is both very well defined and very simple, and, crucially, because the interaction (nuclear scattering) cross-section is known analytically. The classical scattering formula derived by Rutherford in 1912 is an approximation assuming zero nuclear size and bare nuclei (no electron screening). The former assumption leads to negligible error for 1.5 MeV ^{4}He scattering on ^{16}O (and all heavier) nuclei, and the screening correction is small for RBS and can be calculated *ab-initio* with low extra uncertainty for the final calculated cross-section. Very simple detectors are used with effectively 100% detection efficiency. These issues are all covered authoritatively by Jeynes *et al.*[26]

MEIS, with exactly the same physics but a much lower energy beam, does not have such high traceable accuracy as RBS because the low energy particle detector is much more complicated, and because the screening correction is no longer small. These and other effects result in much larger combined uncertainties.

The film thickness was measured by RBS from University of Surrey. A set of 6 samples arrived on 17th May 2016 and were analyzed in July 2016 using 1.5 MeV ^{4}He and two silicon diode detectors at about 150° and 170° backscattering angle. All the parameters were calibrated in the same run under the Calibration and Measurement Capability accredited to ISO 17025.

Certificate #0013 (calibration date 14th July 2016) specifies a standard combined uncertainty for the implanted dose of the standard (working reference) sample of 1.1%, with parameters measured as follows (standard combined uncertainties are given) :

Beam Energy: 1528 ± 1 keV; GVM factor: 1.00545 ± 0.00056

Detector A: $173.9 \pm 0.17°$; 350 TFU dead layer; 1.6814 ± 0.0024 keV/ch gain; 40.0 ± 1.1 keV offset

Detector B: $148.4 \pm 0.12°$; 390 TFU dead layer; 1.6110 ± 0.0024 keV/ch gain; 49.5 ± 0.2 keV offset

The calibration was completed according to the protocol in Colaux & Jeynes.[27]

The measurements were reported 24th May 2017 (Job#4389). They were made both in the normal (100) direction, and in the (110) direction (45° incidence, ~45° exit to the B detector, ~75° exit to the B detector) to give greater sensitivity to the thin films with no added angular uncertainty.

---

[26] C. Jeynes, N. P. Barradas and E. Szilágyi, Accurate determination of quantity of material in thin films by Rutherford backscattering spectrometry, Anal. Chem. 84, 6061 (2012)

[27] J.L. Colaux, C. Jeynes, Accurate electronics calibration for particle backscattering spectrometry, Anal. Methods 7, 3096 (2015)
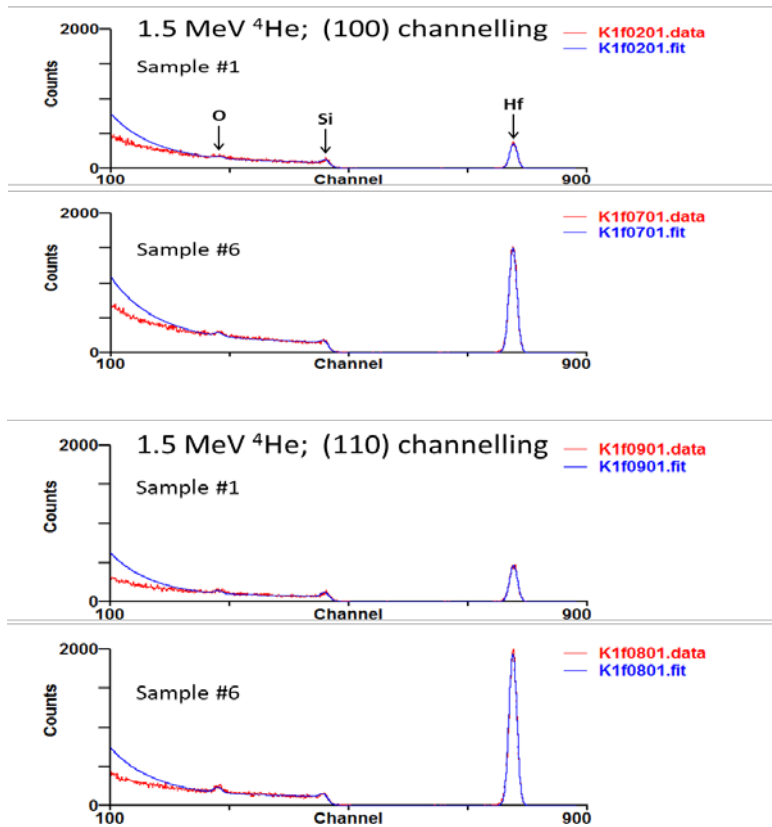
Figure 5-11. (100) and (110) channeling (normal and 45° beam incidence), detector A

Channeling also greatly reduces the Si substrate background to the O signal, allowing the silica layer to be measured as well. Figure 5-11 shows the thinnest and thickest films using detector A. The O signal includes O in the silica and O in the hafnia. The "Si" signal includes some non-channeling signal from the substrate, and the overlap with the substrate channeling signal, which can be seen on a log scale: see Figure 5-12, which also shows the presence of some contamination which is consistent with 0.013 nm Zn at the HfO_2/SiO_2 interface.
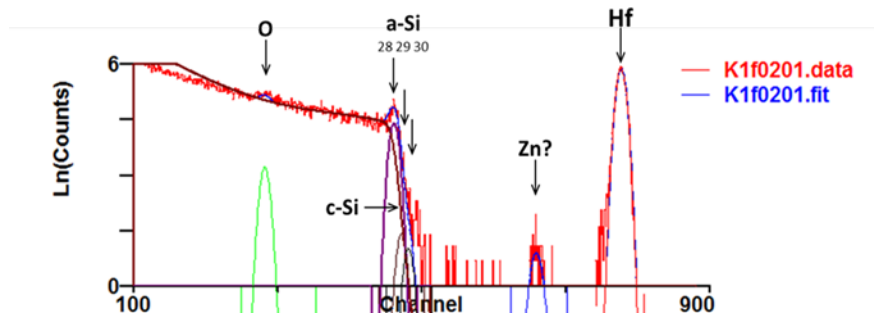
Figure 5-12. (100) channeling on sample #1 (log scale)

This signal is a constant for all the spectra, with standard deviation of 15% for the whole dataset.

The non-channeled Si component can be distinguished from the channeled component. Note also that the Si isotopes are also fitted accurately.

Figure 5-12 also shows an extra signal at the foot of the Si signal (consistent with the presence of P) and another extra signal at the tail of the Hf signal. This latter, together with the fact that the Hf signal *shape* is not well fitted (the signal appears to have better energy resolution than the fit) suggests signal broadening due to thickness non-uniformity (the spot size is about 1 mm). This conclusion is supported by similar observation on the Si signal, but has not been fitted in this work.

A detailed analysis was undertaken, but it is not yet fully traceable and the apparent thickness non-uniformity is not quantified. Two detectors were used throughout. Two sets of measurements were made channeling in different directions (100) and (110). Multiple replicates were also made. However, this analysis depends on normalization through the charge, and the charge collection was intermittently cross-checked against an inserted Faraday cup. An internal calibration was also made by obtaining "non-channeled" spectra of the thickest hafnia films: in this case the Hf quantity of material can be obtained from the certified measurement[28] of the energy loss factor of Si for these beam conditions, which is an *intrinsic measurement standard* (VIM §5.10).

Table 5-14 shows the result. The fits are done imposing a 2 nm silica interlayer. This value cannot be extracted from these data with any precision, but it is known with a low uncertainty from other measurements, so we add it as a prior to the analysis. Also, the stoichiometry of both oxides (the hafnia and the silica) is treated as a prior. Again, there is substantial external evidence for these assumptions. Therefore Table 5-14 tells us two things related to the internal consistency of the dataset. First, it splits the O signal between the two oxides (given that the fit takes the silica thickness as a prior), and then the Hf content determines how much of the a-Si is in the surface silica, and hence the silica thickness. The average thickness must be 2 nm (the prior). But the RSD (0.9%) is very low. It does not have to be that low. The reason that it is *not zero* is related to the counting statistics on the Hf signal, but the reason that it is *low* is related to the general linearity (and internal consistency) of the dataset.

What is remarkable, secondly, is that the interface a-Si layer thickness turns out to be very well determined. This layer (between the silica and the substrate) is freely determined by this analysis, not being affected by the priors. If the measurements were poor this layer thickness (1.4 nm) would

---

28 J.L. Colaux, C. Jeynes, Accurate electronics calibration for particle backscattering spectrometry, Anal. Methods 6, 120 (2014)

be essentially undetermined, being a residue of small signals. But it is determined with an RSD of only 8%, that is, 0.1 nm.

Table 5-14. Results averaged over all measurements normalised to "a" set

Spectrum	Hf	O	a-Si	HfO₂	SiO₂	a-Si	Nominal HfO₂	
postfix	TFU	TFU	TFU	nm	nm	nm	nm	ratio
K1	1.86	12.46	11.30	0.67	1.98	1.38	1.1	0.612
K2	2.99	14.75	11.87	1.08	1.99	1.50	1.6	0.674
K3	4.01	16.83	11.86	1.45	2.00	1.50	2.1	0.690
K4	4.86	18.58	10.37	1.75	2.01	1.20	2.7	0.650
K5	5.93	20.74	11.33	2.14	2.01	1.39	3.1	0.691
K6	7.82	24.59	11.13	2.83	2.03	1.35	4.0	0.706
Average					2.00	1.39		0.67
Relative Standard Deviation					0.86%	8.0%		5.1%

"TFU" ≡ "thin film units" ≡ 10^{15} atoms/cm². To obtain nm the following densities were assumed: for HfO₂, 9.68 g/cc; for SiO₂, 2.2 g/cc; for Si, 2.32 g/cc

The actual origin of this "a-Si" layer is to do with the channeling behavior of the beam: that is, when the directed beam enters the single crystal the portion of it that strikes the top layers of the atom strings must be scattered. Only the remnant can go unscattered down the crystal channels. The value itself (1.4 nm) is quite hard to model and of no interest in this analysis, but was observed previously in a comparable analysis.[ref.1]

The last RSD, 5%, refers to to ratio of the measured to the reference hafnia thickness. Since the reference values supplied in 2016 with the samples have now been modified, the ratio itself (0.67) is of no interest. And of course, the reference values have their own uncertainties, so that the RSD of this dataset also includes the reference uncertainty (1%, see above). Therefore, the present measurement precision (VIM §2.15) is determined by Table 5-14 at 4.9%. This is effectively an ANOVA analysis, which quantitatively represents the internal consistency of the dataset.

Uncertainty Analysis

Table 5-15 shows the combined standard uncertainty of this dataset, 6.3%, which is dominated (as expected) by the measurement precision (4.9%). This main component is determined by an ANOVA analysis of the self-consistency of the (extensive) dataset. The detailed (bottom-up) analysis of the uncertainty of this complex dataset is intricate, so that the ANOVA analysis (top-down) is more satisfactory. But the bottom-up uncertainties sketched in the Report (Job#4389) is

consistent with the top-down conclusion. The various items listed are treated as independent. This could be largely justified by a more detailed discussion: but we emphasize here that this uncertainty estimate is still a conservative one. The absolute value determined is traceable, and sufficient data were collected to obtain independent checks on the main elements of the measurement model. The approach used is fully justified in the literature (Jeynes *et al*, 2012; Colaux & Jeynes, 2015, refs.26,27).

Table 5-15. Uncertainty Analysis for RBS data

Source of uncertainty	type	Standard uncertainty	Comment
Counting statistics	A	0.9%	ANOVA, from Table 5-14, measured silica thickness
Measurement precision	A	4.9%	ANOVA, from Table 5-14, measured/reference ratio
Absolute parameters accuracy	A	1.1%	From ISO 17025 Certificate #0013
Systematic bias (charge)	A	2.9%	From Table 5-14 of Report (Job#4389; charge measurement)
Systematic bias (solid angle)	B	2%	From §5.38 of Report (Job#4389; double scattering uncertainty)
Systematic bias (detA/detB)	A	1.1%	From Table 5-14 of Report (Job#4389; charge measurement)
Combined Standard Uncertainty		6.3%	

Note that "measurement precision" allows for reference uncertainty of 1%

Table 5-16 shows MEIS and RBS data directly compared, together with the reference values. The MEIS raw data are in arbitrary (relative) units; the RBS data are in TFU (thin film units: 10^{15} atoms/cm^2), and the reference values are in nm. Converting TFU to areal density (g/cm^2) it is obvious that the RBS values and the (mutually calibrated) reference values are independent measurements which can be combined to give direct measurements of film density (g/cm^3).

Table 5-17 shows MEIS data expressed as nm (using the mutual calibration with XRR), together with the RBS data also expressed as nm using the density 8.23 g/cm^3 derived from comparison with the reference values. Linear regression allowing a zero offset gives 1.6% uncertainty for the slope and 39% uncertainty for the offset. Given that the value for c is near-zero, and that the regression uncertainty is of the same order, and that no offset is expected (for the same reason that no offset is expected for MEIS), we can set c=0. Then the uncertainty on the gradient reduces to 1.1%, confirming that the data are consistent with zero offset.

Table 5-16. Film density by RBS. MEIS intensities are taken from Table 4-1. RBS values of Hf content (in TFU) are taken from Table 5-14. TFU ≡ "thin film units" ≡ 10^{15} atoms/cm^2. Bulk HfO$_2$ density (last column) taken as 9.68 g/cm^3. Reference thickness values are taken from Table 4-3.

#	MEIS Intensity	RBS Hf TFU	RBS/ MEIS	Reference nm	RBS/ Ref	HfO$_2$ μg/cm^2	Density g/cc	% bulk
1		1.86				0.65		
2	0.3852	2.99	7.76	1.24	2.41	1.05	8.43	87.1%
3	0.5220	4.01	7.68	1.67	2.40	1.40	8.39	86.7%
4	0.6625	4.86	7.34	2.11	2.30	1.70	8.05	83.2%
5	0.8019	5.93	7.39	2.57	2.31	2.07	8.06	83.3%
6		7.82				2.73		
Average			2.74		2.36		8.23	
Standard Deviation			0.21		0.06		0.20	
Relative Standard Deviation (%)			2.8		2.5		2.5	

Table 5-17. MEIS and RBS data (in nm) with the slope of their linear regression against the reference. The MEIS data are relative and calibrated against reference #2. The RBS data are absolute and converted from TFU to length units through the average density obtained from the reference values (see Table 5-16). The standard errors of the linear regression (assuming zero offset) are given. This Table is calculated using 3 sig.fig. The MEIS data are more precise than this so that the "SE of slope" given in the Table is due essentially to rounding errors.

Laboratory	Reference and Measured Thickness (nm)						Slope m	SE of slope	RSD (%)
		1.24	1.67	2.11	2.57				
MEIS		1.24	1.68	2.13	2.58		1.0061	0.0019	0.19
RBS	0.79	1.27	1.70	2.06	2.52	3.32	0.9906	0.0111	1.12

6. SUMMARY OF RESULTS

Figure 6-1 (a) shows the summary plot of m and c for the reported individual data from XPS (■), XRR(●), TEM(◇), SE(△), XRR/XRF(■) and RBS (▼). Figure 6-1 (b) shows the plot for the average values of m and c for XPS, XRR, TEM, SE, XRF, and RBS, respectively.

The individual XPS data (blue circle) shows the distribution of m values from 1.045 to 1.198 and c values from -0.150 nm to 0.059 nm. The average values of m and c are 1.124 and -0.032 nm. The average offset value of -0.032 nm means that XPS has some problem as a zero offset method.

The individual XRR data (pink circle) shows the distribution of m values in a narrow range from 0.919 to 1.011 and c values from 0.111 nm to 0.239 nm. Four laboratories were participated in this pilot study by XRR as shown in Table 5-7. Excluding the KRISS data, the average values

of m and c are 1.005 and 0.133 nm. XRR is theoretically traceable to length unit because the measured film thickness is based on the wavelength of x-ray source. As a result, the true thicknesses of the HfO_2 films can be determined by XRR by the calibration of the offset values.
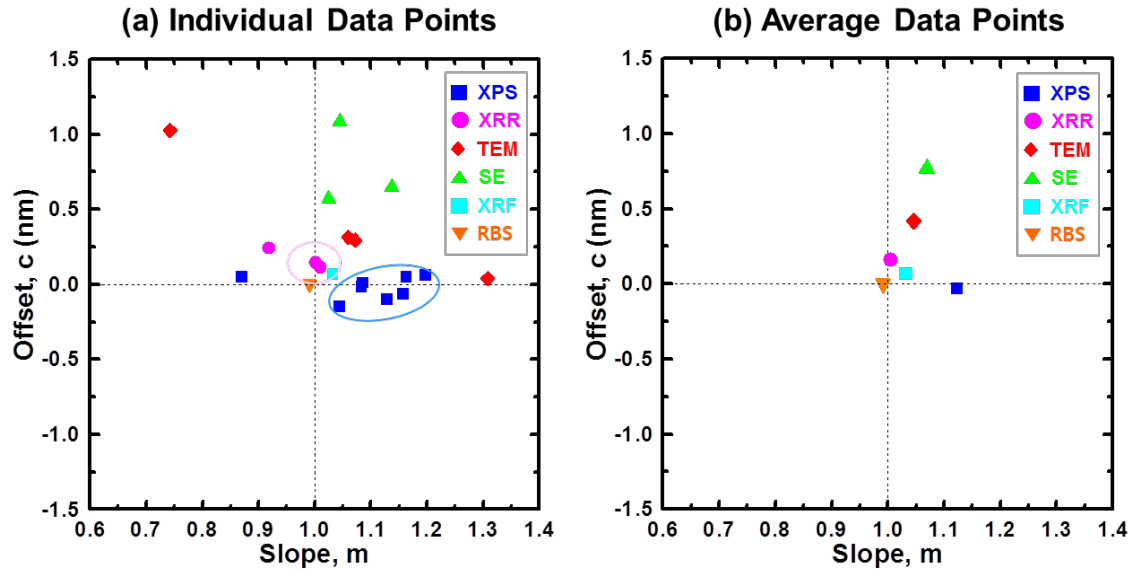

Figure 6-1. Summary plot of *m* and *c* for (a) the reported individual data and (b) average value of XPS, XRR, TEM, SE, XRF and RBS.

The individual TEM data shows a very scattered distribution of m values in the wide range of 0.742 ~ 1.308 and c values of 0.038 nm ~ 1.025 nm. The average values of m and c are 1.046 and 0.418 nm, respectively. Although TEM is traceable to the length scale, the correct and precise measurement of film thickness is restricted to the difficulties in the determination of interface and surface locations and sample preparation is complicated. The true thicknesses of the HfO_2 films can be determined by TEM by the calibration of the offset values.

Table 5-11 shows three data points by spectroscopic ellipsometry. The individual slope values of 1.025, 1.045 and 1.137 are not similar. The offset values of 0.568 nm, 0.648 nm and 1.085 nm are also largely different. Although the surface contamination was reported as a reason of the large offset value in the thickness measurement of nm SiO_2 films by ellipsometry, the reason of the large difference in the offset value of spectroscopic ellipsomery data should be precisely investigated.

There is a data set obtained by a combination of XRR and XRF. The values of the slope and the offset are 1.033 and 0.064 nm, respectively. Like MEIS and RBS (and for very similar reasons) XRF is also expected to be a zero-offset method.

The results summarized so far have all reported film thickness measurements in length units (nm). These measurements do not themselves determine the Quantity of Material (QoM) present (in units of atoms/cm^2). Traceable QoM measurements made by RBS yield film densities when combined with linear thickness measurements (reported in Table 5-16), and direct density measurements by XRR are reported in Table B-9. These independent methods agree that the density of these hafnia films are about 80 % of the expected bulk value. Their numerical agreement is also good considering the uncertainties. At present there is no evidence for a measurable variation of the film density with film thickness. The markedly reduced density must also affect the interpretation of the XPS results.

7. CONCLUSIONS

In this pilot study, the thicknesses of thin HfO$_2$ films were measured by various methods. The reference thicknesses of the films were determined by mutual calibration from the MEIS intensity ratios and the reported thicknesses by XRR (page 8~13). Recently, after the pilot study, it was successfully proved that the MEIS intensity ratios can act as a perfect zero offset method in the thickness measurement of ultra-thin HfO$_2$ films.[29]

In the case of XRR, the average thicknesses by three NMIs (PTB, NMIJ and NIST) were chosen as the length-unit traceable thickness data for the mutual calibration (it was decided to exclude KRISS data in the calculation of the average thickness). The reference thicknesses are demonstrably traceable (if the KRISS data can properly be ignored), and there is therefore a basis for confirming the feasibility of thickness measurement of nm HfO$_2$ films by these combined measurement methods.

From the various thickness measurements of the thin HfO$_2$ films, MEIS and TEM are free from the effect of surface contamination. The effect of surface contamination is also not serious in XRR and XRF.

Although the effective EAL and R$_0$ values were determined to be 1.834 nm and 4.377 with the relative standard uncertainties of 0.013 nm and 0.038, at the reference geometry. These values are appropriate for calibrated, monochromated Al Kα with a geometry close to the magic angle

---

[29] K. J. Kim, T. G. Kim, J. -H. Kwon, H. Ruh, K. Park, and W. J. Min, Traceable thickness measurement of ultra-thin HfO$_2$ films by medium energy ion scattering spectroscopy, Metrologia 57, 025001 (2020).

between incoming X-rays and outgoing photoelectrons. For instruments which do not meet these criteria, the value of R_0 should be found independently.

The R_0 value is highly affected by surface contamination on the reference samples. However, the reference intensities could be measured by XPS using a suitable procedure to account for variations in carbon contamination on reference samples. It should be noted that the reference intensity is dependent upon the silicon oxide layer thickness and this should also be accounted for.

The best solution for the thickness measurement by XPS is the perfect removal of the surface contamination layer and the correction of the effect of the surface contamination layer, which is not easy. The XPS thickness measurement procedure suggested by NPL is recommended (Annex F). The thickness calculation equation was derived again from the basic XPS equations by Dr. Alberto Herrera Gómez of Mexico. The re-calculated thicknesses by the re-determined thickness calculation equation showed a small offset value of 0.02 nm in the linear regression fitting against the reference thicknesses as shown in Annex G.

The thickness (in areal density units) measured by RBS combines with these linear thickness measurements to give the film density, which also given independently by XRR. Combined XRR/RBS data shows that these HfO_2 films have only about 80% of the bulk density.

Annex A. Experimental details of XPS data

(1) KRISS

X-ray photoelectron spectroscopy (XPS) measurements were performed by using Ulvac-PHI VersaProbe II XPS system. Spectra were taken by using monochromatic Al Kα X-rays (1486.6 eV) with 100 µm X-ray beam size (25 W power). Photoelectrons were collected with a 45° emission angle from the surface normal. Si 2p spectra were obtained with a pass energy of 46.95 eV and a step energy of 0.10 eV. For the Hf 4f, the pass energy and step energy were set to be 23.50 eV and 0.05 eV, respectively. All the measurements were performed without charge compensation. Five different spots were measured from each sample. Spectra were fitted by using Casa XPS software.

All samples were cleaned by dipping in reagent grade acetone, followed by sonicating the sample for 10 min. Then, all samples were transferred to isopropyl alcohol (IPA) bath without drying the acetone. After sonicating the samples in IPA for 10 min, the samples were thoroughly rinsed with deionized (DI) water (18 MΩ). The Si chip was further cleaned to remove a native oxide layer. The chip was dipped in 6:1 buffered oxide etchant (BOE) for 1 min (6:1 BOE; 6:1 volume ratio of 40% NH_4F in water to 49% HF in water), followed by rinsing with DI water.

In order to obtain the signal intensities, Si 2p and Hf 4f peaks were fitted by using Casa XPS software. A Shirley background was used. Both Si 2p and Hf 4f peaks were fitted using Gaussian Lorentzian sum function. For the Si 2p peak fitting, six peak method was used (ISO 14701), where Si 2p spectra were fitted with doublet Si(0), Si(I), Si(II), Si(III), and Si(IV) peaks. The peak position of Si(I), Si(II), and Si(III) peaks were constrained with the shift of 0.95 eV, 1.75 eV, and 2.48 eV, respectively. On the other hand, the Si(IV) peak was not constrained. The binding energy difference between the Si(0) doublet peaks was 0.6 eV, and the intensity ratio was fixed to 0.5. The FWHM upper limit of Si(II), Si(III), and Si(IV) was 1.5 eV, while the limit of Si(I) was 1.7 eV. For the Hf 4f spectra, the intensity ratio was fixed to 0.75.

Considering the Eqn. (4) to determine the average thickness of HfO_2 films, the uncertainty of this project comes from mainly three components which are L, θ, and intensity average. Additional uncertainty (u_{eq}) coming from the equations was considered. The combined standard uncertainty was calculated by using Kragten's spreadsheet method. The expanded uncertainty was determined according to the Guide to Expression of Uncertainty in Measurement (GUM). Uncertainty source and values are listed in Table A-1.

Table A-1. Uncertainty sources in the thickness measurement of HfO_2 films by XPS of KRISS.

Source of uncertainty	Type	Standard uncertainty
intensity averages (u_{R_0})	A	0.77%
intensity averages ($u_{R_{exp}}$)	A	sample dependent (0.22 to 1.00%)
L	B	4.07%
electron emission angle (θ)	B	$\pm 2°$ (4.44%)
equation validity	B	± 0.025 nm

The determination of L results in the largest contribution to uncertainty which is the range from 45.44% to 55.65% of the contribution. In the mutual calibration method to determine the L, the linearity in the XPS-TEM thickness plot contributes to the uncertainty of L (± 0.079 nm). The uncertainty source of the second largest contribution is the emission angle (θ) ranging from 34.52% to 42.27%. This contribution results from the roughness of samples, sample mounting, and sample holders. Based on our experience, the largest uncertainty for the emission angle is $2°$. The uncertainty of intensity averages measured from thin HfO_2 films and pure samples comes from the homogeneity across the sample surface and the XPS instrumentation conditions. Since the uncertainty coming from peak fitting showed negligible contribution, it was not considered.

Table A-2. KRISS data for the thickness measurement of HfO_2 films by XPS with input parameters, and the expanded uncertainty at 95% confidence level (k=2).

Parameter	Reference and Measured Thickness (nm)					
	0.76	1.20	1.64	2.08	2.52	3.36
Effective attenuation length, L	1.939 ± 0.079 nm					
Electron emission angle, θ	$45° \pm 2°$					
R_0	$1.956 \pm 0.770\%$					
R_{exp}	1.942	3.720	6.597	10.424	15.560	28.793
$u_{R_{exp}}$ (%)	± 0.220	± 0.476	± 0.219	± 0.261	± 0.621	± 1.005
Thickness (nm)	0.944	1.461	2.023	2.530	3.006	3.777
U of thickness (nm)	0.114	0.166	0.225	0.279	0.330	0.413

The thickness measurement of HfO_2 films by XPS were determined by Eqn. (4). The input parameters, the calculated thickness and the expanded uncertainty at 95% confidence level (k=2) are shown in Table A-2. The L value of (1.939 ± 0.079) nm was determined from mutual calibration by XPS and TEM. The emission angle of electron (θ) was fixed to be $45^o ± 2^o$ and the R_0 value was measured to be 1.956 ± 0.770%. The reason of the low R_0 value was that the different pass energies of 47.0 eV and 23.5 eV were used for the analysis of Si 2p and Hf 4f spectra, respectively. The re-measured R_0 value using the same pass energy of 47.0 eV was 4.251.

(2) BAM

The X-ray photoelectron spectra were obtained with a KRATOS Axis Ultra DLD with monochromatic Al Kα radiation with an energy of 1486.6 eV. A spot size of 300 x 700 µm² and an energy of 150 W were used. The spectra were collected in normal emission, a pass energy of 10 eV was used. The step size was set to 0.1 eV, the dwell time to 0.5 s. The measurements were performed in hybrid mode without any charge compensation. The Si $2p$ and Hf $4f$ spectra were measured with three sweeps seven times.

For removing contaminants the HfO_2 samples were dipped in reagent grace acetone, followed by sonicating for 5 min. Subsequently, the samples were dipped in isopropyl alcohol and then sonicated. Finally, the samples were sonicated in deionized water. The Si wafer was etched in a buffered NH_4F/HF solution to remove the native Si oxide layer.

Peak fitting was performed with Unifit (Universal Spectrum Processing, Analysis and Presentation Software) Version 2017, Revision R (Unifit Scientific Software GmbH, Leipzig, Germany). A Tougaard Background was used. The peaks were fitted using a Gaussian-Lorentzian sum function peak shape model. Five doublet peaks were used for fitting the Si $2p$ spectrum: doublets for elemental Si, Si_2O, SiO, and Si_2O with constrained shifts of 0.95 eV, 1.75 eV, and 2.48 eV to higher binding energies regarding elemental Si[30,31] and a doublet for SiO_2 with a non-constrained binding energy shift. The binding energy differences between the Si $2p_{3/2}$ and Si $2p_{1/2}$ 0.6 eV were for each doublet, the intensity ratio was fixed to 0.5, the FWHM and the Lorentzian-Gaussian mixing were the same for both peaks of each doublet. For the Hf $4f$ doublet, the FWHM

[30] F. J. Himpsel, F. R. McFeely, A. Taleb-Ibrahimi, J. A. Yarmoff, Phys. Rev. B 38, 6084 (1988)

[31] J. W. Keister, J. E. Rowe, J. J. Kolodziej, H. Niimi, H.-S. Tao, T. E. Madey, G. Lucovsky, J. Vac. Sci. Technolog. A 17, 1250 (1999)

and the Lorentzian-Gaussian mixing were fixed to be the same for each peak of the doublets. Regarding Eq. 5-1 for determining the film thickness, the main components for the measurements uncertainty are originated from L (the effective attenuation length), the emission angle θ and the intensities. The combined standard uncertainty and the expanded uncertainty was determined according to the "Guide of Uncertainty of Measurements".

The effective attenuation length was determined by comparing the values obtained with XPS as described above with the results of X-ray reflectometry which was performed by the PTB (Physikalisch - Technische Bundesanstalt). The measurements were done at three samples with a nominal HfO_2 film thickness of 4, 6 and 8 nm with the mutual calibration method. The linear regression of the XPS-XRR results leads to value for L of 1.84 ± 0.31 nm. With this uncertainty value, L is by far the main contribution to uncertainty budget. Table A-3 summarizes the different contributions to this budget. It must be mentioned, that the uncertainty for the intensities averages $u_{R_{exp}}$ increases with the film thickness.

Table A-3. Uncertainty sources in the thickness measurement of HfO_2 films by XPS of BAM.

Source of uncertainty	Type	Standard uncertainty
intensity averages (u_{R_0})	A	3.1 %
intensity averages ($u_{R_{exp}}$)	A	Sample dependent (3.4 to 6.8 %)
L	B	16.8 %
electron emission angle (θ)	B	$\pm 2°$ (4.4 %)

Table A-4. BAM data for the thickness measurement of HfO_2 films by XPS with input parameters, and the expanded uncertainty at 95% confidence level (k=2).

Parameter	Reference and Measured Thickness (nm)					
	0.76	1.20	1.64	2.08	2.52	3.36
Effective attenuation length, L	1.84 ± 0.31 nm					
Electron emission angle, θ	$0° \pm 2°$					
R_0	4.21 ± 0.13					
R_{exp}	2.07	3.75	6.01	9.48	13.09	25.68
$u_{R_{exp}}$ (%)	± 3.7	± 3.7	± 3.4	± 4.7	± 5.3	± 6.7
Thickness (nm)	0.74	1.17	1.63	2.17	2.60	3.61
U of thickness (nm)	0.26	0.42	0.58	0.80	0.94	1.36

The thickness measurement of HfO_2 films by XPS was determined by Eq.4-4. The input parameters, the calculated thickness and the expanded uncertainty at 95% confidence level (k=2) are shown in Table A-4. The L value of 1.84 ± 0.31 nm was determined from mutual calibration by XPS and XRR. The XRR results obtained by PTB at the samples with a nominal HfO_2 thickness of 4, 6 and 8 nm were used. The emission angle of an electron (θ) was fixed to be $0^o \pm 2^o$ and the

R_0 value was measured to be 4.21 ± 3.1 %.

(3) NIM

X-ray photoelectron spectroscopy (XPS) measurements were performed by using Thermo Fisher Scientific Escalab 250Xi XPS system. Spectra were taken by using Mg Kα X-rays (1253.6 eV) with 500 µm X-ray beam size (200 W power). Photoelectrons were collected with a 10° emission angle from the surface normal. Si $2p$, Hf $4f$ spectra were obtained with a pass energy of 20 eV and a step energy of 0.05 eV. Six different spots were measured from each sample with charge compensation.

In order to obtain the signal intensities, Si $2p$ and Hf $4f$ peaks were fitted by using Advantage software provided by the Maker. Background was removed using smart method modified from Shirley method. In case of $HfO_2/SiO_2/Si(100)$ samples, six peak method was used (ISO 14701) for the Si $2p$ peak fitting, where Si $2p$ spectra were fitted with doublet Si(0), Si(I), Si(II), Si(III), and Si(IV) peaks. The peak position of Si(I), Si(II), and Si(III) peaks were constrained with the shift of 0.95 eV, 1.75 eV, and 2.48 eV, respectively. On the other hand, the Si(0) doublet peaks and Si(IV) peak were not constrained. In case of thick $HfO_2(50nm)/Si(100)$ and $SiO_2(50nm)/Si(100)$ samples, Hf $4f$ spectra and Si $2p$ spectra were fitted with one peak, while Si $2p$ spectra were fitted with doublet Si(0) and Si(III) peaks for Si wafer sample. At last, the intensities of SiO_2 and Si were calculated according to ISO 14701.

The thickness of HfO_2 films was determined according to the procedures described in the reference.[32] The value of R_0 (4.309) was experimentally determined from HfO_2(50 nm)/Si(100) and SiO_2(50 nm)/Si(100) films as received. The relative ratio (0.956) of the Si $2p$ peak intensities of SiO_2(50 nm)/Si(100) film and Si wafer as received was also experimentally measured. The value

---

[32] K. J. Kim, S. M. Lee, J. S. Jang, M. Moret, Thickness measurement of a thin hetero-oxide film with an interfacial oxide layer by X-ray photoelectron spectroscopy, Appl. Surf. Sci. 258, 3552 (2012)

of L (1.781) was experimentally determined from a series of $HfO_2/SiO_2/Si(100)$ films with the certified thicknesses ranging from 1 nm to 4 nm of the HfO_2 films. The XPS measurements were repeated six times for each sample.

The measurement uncertainty has mainly six contributing terms, viz. the counting statistics (μ_n), the setting of the angle of emission (μ_θ), the attenuation length (μ_{AL}), the angular averaging of the entrance solid angle of the spectrometer (μ_{LA}), the use of non-standard peak shapes or fitting algorithms in software (μ_F) and the non-use of satellite subtraction, spin-orbit subtraction, fitting of 6 peaks (μ_P). The counting statistics (μ_n) is equal to the relative standard deviation of six repeated measurements.

(4) NIST

XPS was employed to acquire spectra using an Axis Ultra DLD spectrometer from Kratos Analytical using monochromatic Al Kα X-rays (10 mA, 15 kV). Monochromatic X-rays were directed towards the surface at an angle of 60 degrees from the surface normal. Photoelectrons were collected along the surface normal from an area defined by the FOV1 lens and 110 micrometer aperture (spot size ≈ 190 micrometers diameter) and analyzed at a pass energy of 40 eV using a hemispherical analyzer. The Si $2p$ and Hf $4f$ regions were collected using total acquisition times of 1200 milliseconds per step and 0.100 eV steps.

Samples underwent preliminary analysis by XPS prior to undergoing the cleaning step suggested in step 5 of the Protocol for Measurements. The cleaning step was followed in accordance with the directions and then the samples were subsequently loaded into the vacuum chamber. The analysis chamber was maintained at a pressure of $2x10^{-9}$ torr throughout the duration of the data collection. Data was collected on the HfO_2 thin films and controls in two batches due to space constraints: the first set of samples included the 1.0 nm though 3.0 nm nominal film thicknesses (5 different specimens), and the second set of samples included the nominally 4.0 nm film and all 3 control specimens (4 different specimens). 6 spots were collected from each of the thin films while 3 were collected from the separate HfO_2, SIO_2 and Si controls. Efforts were made to ensure that the spots chosen were kept 2 mm to 3 mm away from the edges of the sample chips provided and at least 1 mm separated from one another.

Average Thickness of the HfO_2 films.

As close as possible, the methods for calculating HfO$_2$ film thickness were taken from previous research with deviations outlined below. The Hill equation was employed to calculate the HfO$_2$ film thickness (t_{film}) and is as follows:

$$t_{film} = L \, \cos\theta \, \ln\left(\frac{R_{exp}}{R_0} + 1\right) \quad \text{---------------------------------------(Eq.A-1)}$$

where L is the effective attenuation length for electrons ejected from the overlayer, θ is the angle between electron collection and the surface normal, and R$_0$ and R$_{exp}$ are the ratios of overlayer to substrate intensities (I_{over} and I_{sub}, respectively) for pure substances (∞) and experimental (exp) specimens. The equations are listed as follows:

$$R_0 = \frac{I_{over}^{\infty}}{I_{sub}^{\infty}} \quad \text{-- (Eq.A-2)}$$

$$R_{exp} = \frac{I_{over}^{exp}}{I_{sub}^{exp}} \quad \text{-- (Eq.A-3)}$$

I_{over}^{∞} was measured from the 50 nm thick HfO$_2$ film grown on a Si substrate after Ar$^+$ sputtering for 20 seconds, and I_{sub}^{∞} was measured from the 50 nm thick SiO$_2$ film grown on a Si substrate after Ar$^+$ sputtering for 20 seconds, as provided in the pilot study. I_{over}^{exp} was measured by directly measuring the rsf correct Hf 4f signal. I_{sub}^{exp} required additional work. The substrate consisted of a 2 nm SiO$_2$ film on a Si bulk chip. To account for all of the photoelectron intensity deriving from the two parts of the substrate, the following equations were employed to relate all intensity to SiO$_2$:

$$I_{sub}^{exp} = I_{SiO2}^{exp} + I_{Si}^{exp} * R_0^{\frac{SiO2}{Si}} \quad \text{--- (Eq.A-4)}$$

$R_0^{\frac{SiO2}{Si}}$ represented the ratio of intensities for a thick SiO$_2$ film (I_{sub}^{∞}) and a silicon wafer sputtered clean to remove the oxide film (I_{Si}^{∞}).

To obtain the necessary values for intensities, the acquired spectra were extracted from the vendor's software and analyzed using Casa XPS software. For all spots and all specimens, Hf 4f and Si 2p spectra were fit with a Shirley background. As previously stated, the signal intensity for the Hf 4f region was the rsf corrected area under the curve and for each spot on each thin film, this became the measure of I_{over}^{exp} or I_{over}^{∞} for the controls. To acquire the rsf corrected intensity for I_{sub}^{exp}, values for I_{SiO2}^{exp} and I_{Si}^{exp} first had to gleaned from the data which was achieved through peak fitting Si (IV), Si(III), Si(II), Si(I) and Si(0) features into the Si 2p envelope, following the procedure in Kim et al.

The one point of deviation involved determination of L for electrons ejected from the overlayer. While many samples were provided, a separate, thick control specimen designed to calculate an experimentally determined value of L was not provided. Therefore, it was decided to use the two following relationships cited in Jablonski and Powell[33]

$$L_{SLA} = \lambda_i \text{ ---(Eq.A-5)}$$

and by Powell and Jablonski[34]

$$L_{ave} = \lambda_i(1 - 0.735\omega) \text{ ---(Eq.A-6)}$$

Where

$$\omega = \lambda_i/(\lambda_i + \lambda_t) \text{ --- (Eq.A-7)}$$

which is the single scattering albedo, λ_i is representative of the inelastic mean free path and λ_t is representative of the transport mean free path. It is important to remember that Eq.A-6 calculates L_{SLA} following the straight-line approximation (SLA) which neglects the impacts of elastic scattering while Eq.A-7 accounts for this calculating in calculating L_{ave}. To obtain λ_i and λ_t for the electrons ejected from the HfO$_2$ overlayer, NIST SRD 82 was employed using 1383 eV for the Si 2p electron energy, while 9.68 g/cm^3 and 5.5 eV were employed for the density and band gap energy, respectively, of the HfO$_2$ film. The values for λ_i and λ_t were 2.155 and 6.313, respectively. As stipulated in the next section, λ_i is responsible for a significant type B error in our uncertainty. In close, L_{SLA} and L_{ave} yielded values of 2.155 nm and 1.752 nm, respectively. Lastly, we attempted some modelling with SESSA to generate L_{SESSA} values for comparison using equation 1 and found that the values were more comparable with L_{ave} than L_{SLA}.

Uncertainty

When considering uncertainty for this project, it was evaluated based on the three components of equation 1: L, $cos\ \theta$, and $\ln(\frac{R_{exp}}{R_0} + 1)$. As mentioned in the previous section and is demonstrated in Table A-5, calculations of L which incorporated λ_i result in the largest contribution to the error with an estimated uncertainty, or relative standard deviation (RSD), of 10 %[35]. In other words, based on $\lambda_i = 2.155$ nm the uncertainty would be ± 0.216 nm.

[33] A. Jablonski and C.J. Powell, Practical expressions for the mean escape depth, the information depth, and the effective attenuation length in Auger-electron spectroscopy and x-ray photoelectron spectroscopy, J. Vac. Sci. Technol. A 27, 253 (2009)

[34] C.J. Powell, A. Jablonski, Surface sensitivity of X-ray photoelectron spectroscopy, Nucl. Instrum. Methods Phys. Res. Sect. A 601, 54 (2009)

[35] C. J. Powell and M. P. Seah, Precision, accuracy, and uncertainty in quantitative surface analyses by Auger-electron

Table A-5. Uncertainty sources and types in thickness measurement of HfO_2 films by XPS of NIST

Source of uncertainty	Type	Value Represents?	Source/Reference	Actual value
intensity averages	A	Heterogeneity of the surface	Data	Specimen dependent
IMFP (λ)	B	Average error using approximation	Reference	10%
θ	B	Range of the tilt	experience	±2

With respect to $cos\ \theta$, θ can vary slightly due to variables such as mechanical problems of the stage, poorly mounted samples, and sample holders not held as rigidly as necessary which leads to a slight tilt. Based on professional experience, +/- 2° is about the largest difference observed to this point on our system. Therefore, $cos\ \theta$ would be represented by a value of 1 ± 0.000609.

Lastly, the error associated with $\ln(\frac{R_{exp}}{R_0} + 1)$ was purely derived from the standard deviations from the XPS measured intensities for Hf 4f, metallic Si 2p, and oxidized Si 2p and demonstrate the homogeneity across the surface of the material. While the list of errors measured will not be detailed in this report for each species, the typical list of errors were between 1.4 % and 4.3 % RSD, with the notable exception of the nominally 1.5 nm thick HfO_2 layer which was an average RSD of 5.5 %. Correspondingly, the RSDs associated with all $\ln(\frac{R_{exp}}{R_0} + 1)$ values were < 5.3 %.

Results

As mentionned above, we employed two methods for calculating the value of L, and therefore have two tables of values. We have provided both below.

Table A-6. Calculated thicknesses using the Hill equation and L values determined by (left) excluding and (right) including scattering.

No	L_{SLA} Average Thickness (nm)	L_{SLA} Standard Deviation (nm)	No	L_{ave} Average Thickness (nm)	L_{ave} Standard Deviation (nm)
1	0.823	0.088	1	0.669	0.074
2	1.301	0.147	2	1.058	0.122
3	1.773	0.183	3	1.441	0.153
4	2.295	0.234	4	1.865	0.195
5	2.792	0.282	5	2.270	0.235
6	3.810	0.386	6	3.098	0.322

spectroscopy and x-ray photoelectron spectroscopy, J. Vac. Sci. Technol. A 8, 735 (1990).

(5) NMIJ

Three sets of the samples were analyzed with different measurement methods. The film thickness of sample set-A was measured by XRR, and that of the set-B was measured by XPS. The set-C was measured by TEM.

Calculation of the thickness by XPS

The thickness of the thin films of HfO$_2$ (d_{HfO2}) was determined from the following equations:

$$d_{HfO_2} = L\,cos\theta \times \ln(\frac{I_{HfO_2}/I_{sub}}{R_0} + 1)$$

$$I_{sub} = I_{Si} + \frac{I_{SiO2}}{R_{0-SiO2}}$$

where L is the effective attenuation length (EAL) for Hf $4f$ electrons in HfO$_2$, θ is the angle of emission of electrons measured from the surface normal, I_{HfO2} is the intensity of the Hf $4f$ peak, R_0 is the ratio of the peak intensity of the pure bulk HfO$_2$ and the Si substrate, I_{Si} is the intensity of the Si contribution to the Si $2p$ peak, I_{SiO2}, I_{Si2O3}, I_{SiO}, and I_{Si2O}, are the intensities of the SiO$_2$, Si$_2$O$_3$, SiO, and Si$_2$O contribution to the Si $2p$ peak, respectively, and R_{0-SiO2}, $R_{0-Si2O3}$, R_{0-SiO}, and R_{0-Si2O} are the ratios of the peak intensities of the pure bulk SiO$_2$, Si$_2$O$_3$, SiO, Si$_2$O, and the Si substrate.

To determine the value of the R_0, we used relation

$$I_{sub} = \frac{1}{R_0}(I_{HfO2}{}^\infty - I_{HfO2})$$
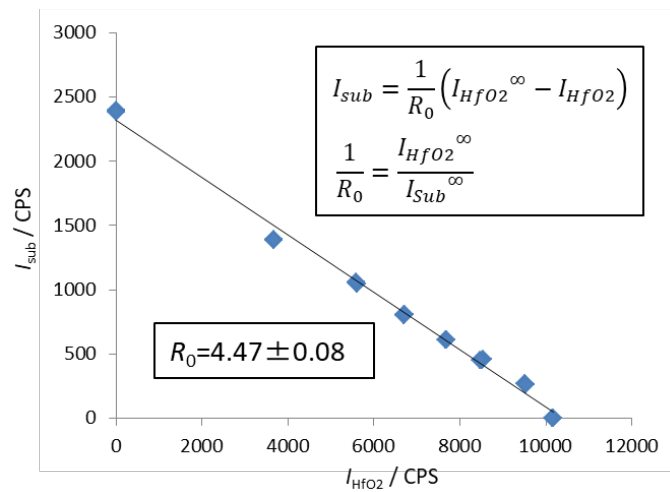
Figure A-1. The gradient of the plots of I_{sub} vs. I_{HfO2} for the sample set-A, the bulk sample of HfO$_2$ (film thickness of 50 nm) and the bulk sample of SiO$_2$ (film thickness of 50 nm).
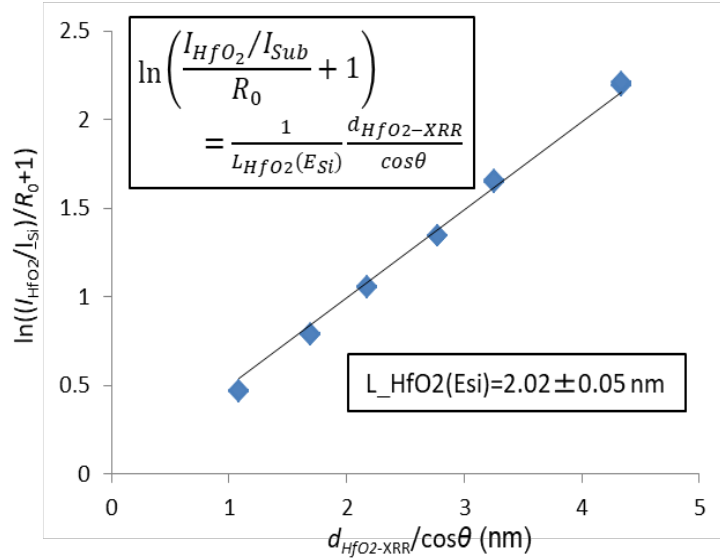
Figure A-2. The gradient of the plots of $\ln[I_{HfO2}/R_0 I_{sub}+1]$ vs. $d_{HfO2\text{-}XRR}/\cos\theta$ for the sample set-A for XRR measurement.

The value of R_0 was obtained from the gradient of the plots of I_{sub} vs. I_{HfO2} for the sample set-A and the bulk sample of HfO_2 (50 nm) and SiO_2 (50 nm).

To determine the value of the L, we used relation

$$\ln\left(\frac{I_{HfO_2}/I_{Sub}}{R_0}+1\right)=\frac{1}{L}\frac{d_{HfO2-XRR}}{\cos\theta}$$

where $d_{HfO2\text{-}XRR}$ is the thickness of HfO_2 thin films measured by XRR. The value of L was obtained from the gradient of the plots of $\ln[I_{HfO2}/R_0 I_{sub}+1]$ vs. $d_{HfO2\text{-}XRR}/\cos\theta$ for the sample set-A for XRR measurement.

Cleaning the samples

First, immerse the sample in high purity (99.5 %) acetone and then agitate ultrasonically for 5 minutes. Second, move the sample in high purity (99.9 %) isopropyl alcohol (IPA) and agitate ultrasonically for 5 minutes. Then renew the IPA and immerse the sample for more than 16 hours. After that, renew the IPA and agitate ultrasonically for 5 minutes. Then move the sample in pure water and agitate ultrasonically for 5 minutes. Finally renew the pure water and remove the liquid using a gas jet of dry nitrogen just before the measurement.

XPS measurements and data analysis

The XPS measurements were carried out with the XPS system of ULVAC-PHI ESCA5800

with monochromatized Al Kα X-rays. All of measurements were performed at the so-call reference geometry (at 34° from the surface normal in the azimuth at 22.5°). The film thickness of the set-B sample was measured by 6 times for each sample. The pass energy of 11.75 eV was used when analyzing the Si $2p$ and Hf $4f$ photoelectrons. The peak fittings were conducted by XPS peak fitting program XPSPEAK Version 4.1. The Shirley background was used. For Si $2p$ peaks, six-peak method was used (refer to ISO 14701).

Uncertainty

The uncertainty of the thickness of HfO$_2$ thin films derived from Equations (1) and (2) at the 95 % level of confidence was calculated from the following equation

$$u^2 = u_L{}^2 + u_{R0}{}^2 + u_\theta{}^2 + u_I{}^2$$

where u_L is the uncertainty in the EAL determined from the gradient of the plots of $\ln[I_{HfO2}/R_0 I_{sub}+1]$ vs. $d_{HfO2\text{-}XRR}/\cos\theta$, u_{R0} is the uncertainty in the R_0 obtained from the gradient of the plots of I_{sub} vs. I_{HfO2}, u_θ is the uncertainty in the θ, and u_I is the uncertainty in the intensities of the thin film of HfO$_2$ and substrate.

The contributions of u_L and u_{R0} were obtained from the results of L and R_0 estimated by the least-square method. Note that the uncertainties due to the thickness measurements by XRR were considered in the calculation of u_L. The u_θ was estimated from a contribution of $\pm 2°$, and the u_I was estimated from the standard deviation of measured intensities of six times for each sample.

Table A-7. NMIJ data for the thickness measurement of HfO$_2$ thin films by XPS.

Components	Sample No.					
	1	2	3	4	5	6
Evaluated Thickness (nm)	0.83	1.33	1.85	2.32	2.78	3.64
Uncertainty Source	Standard uncertainty					
EAL L (nm)	0.0206	0.0330	0.0457	0.0575	0.0687	0.0901
R_0 (nm)	0.0117	0.0165	0.0200	0.0225	0.0243	0.0266
Electron Emission Angle θ (nm)	0.0196	0.0314	0.0435	0.0547	0.0654	0.0857
Peak Intensity I (nm)	0.0039	0.0114	0.0058	0.0251	0.0335	0.0529
Combined Uncertainty (nm)	0.0310	0.0498	0.0664	0.0862	0.1035	0.1377
Expanded Uncertainty $k=2$ (nm)	0.06	0.10	0.13	0.17	0.21	0.28

Evaluated thickness and uncertainty budget

The XPS-measurement result of the sample set-B is shown in Table A-7. The budget sheet of the uncertainty is also shown in Table A-7. Expanded uncertainty was calculated using coverage factor (k) of 2, which gives a level of confidence of approximately 95%.

(6) NPL

X-ray photoelectron spectroscopy (XPS) measurements were performed using a Kratos Axis Ultra DLD XPS system. Spectra were taken using monochromatic Al Kα X-rays (1486.6 eV) from a 300 µm x 700 µm analysis area (75 W power). The samples were rotated through 22.5^o on the sample holder and the stage tilted to achieve a photoelectron take-off angle of 34° from the sample surface normal. This is described for a 100 surface orientated sample in ISO 14701:2011 Surface chemical analysis - X-ray photoelectron spectroscopy - Measurement of silicon oxide thickness. All samples were cleaned by sonicating in acetone for 10 min then transferred to isopropyl alcohol (IPA) without drying the acetone and sonicated for 10 min. The samples were then sonicated in ultra high purity water and soaked overnight in IPA. They were then sonicated in fresh IPA and dried with an argon jet. Si 2p and Hf 4f spectra were obtained with a pass energy of 40 eV and a step energy of 0.10 eV. All the measurements were performed without charge compensation. Spectra were acquired from three areas of each sample. Repeat spectra were then acquired from each of these areas.

Signal intensities from the Hf 4f and Si 2p high resolution spectra

CasaXPS was used for processing the data. Regions around the peaks were defined and the peak areas measured using Shirley backgrounds. However, for the three thickest HfO_2 films, linear backgrounds were used for the Si 2p due to the rise in background intensity towards the low binding energy. To enable raw intensities to be exported from CasaXPS the sensitivity factors were set to 1 and transmission function correction turned off.

Silicon dioxide thickness

Regions around the Si 2p peaks were defined, a Shirley background used and 6 components were fitted to the peaks as described in ISO/TC 201 Standard: ISO 14701:2011 – Surface chemical analysis – X-ray photoelectron spectroscopy—measurement of silicon oxide thickness.

Chemical composition from survey spectra

The files were converted from the Kratos format to .vms (ISO 14976:1998, VAMAS format) and Casa XPS used for processing the data. The latest transmission function processed with the NPL XPS Intensity calibration software was used to correct the intensity scale of the spectra. Regions around the appropriate peaks were defined. Tougaard backgrounds were used, apart from peaks were the background intensity rose towards lower binding energy, when a linear background was used instead. The average matrix sensitivity factors http://www.npl.co.uk/science-technology/surface-and-nanoanalysis/services/xps-and-aes-average-matrix-relative-sensitivity-factors, were used.[36]

Overlayer and substrate reference intensities

Carbon overlayer thicknesses, d_C, were estimated using compositions calculated from XPS and a method outlined.[37]

$$d_C = -L_{C1s} \cos \theta \ln(1 - X_C)$$

Where X_C is the equivalent homogeneous fraction of carbon calculated from XPS and L_{C1s} is the estimated effective attenuation length for electrons with KE of 1202 eV in organic materials. Inspection of the inelastic background at kinetic energies lower than the C 1s peak demonstrated that this element was present as an overlayer on all samples.

It was noted that carbon overlayer thicknesses for the hafnium oxide reference samples ($d_C \sim$ 1.0 nm) were larger than the silicon and silicon oxide reference samples ($d_C \sim$ 0.3 nm). The measured intensities of the reference samples were corrected for attenuation through this layer using equation 2.

$$I_\infty = I \exp \left(\frac{d_C}{L \cos \theta} \right)$$

Where I_∞ is the estimated reference intensity, I is the measured intensity and L is the estimated effective attenuation length for electrons with the kinetic energy of the elemental peak in the carbon overlayer. The value of L was found using equation 3.[38]

$$L = 0.00837 E^{0.842}$$

[36] M. P. Seah, I. S. Gilmore, S. J. Spencer, Quantitative XPS: I. Analysis of X-ray photoelectron intensities from elemental data in a digital photoelectron database, J. Electron. Spectrosc. Relat. Phenom. 120, 93 (2001)

[37] G. Smith, Evaluation of a simple correction for the hydrocarbon contamination layer in quantitative surface analysis by XPS, J. Elec. Spec. 148, 21 (2005)

[38] M. P. Seah, S. J. Spencer, Attenuation lengths in organic materials, Surf. Interface Anal. 43, 744 (2011)

Where E is the kinetic energy of electrons in electron volts. Using the correction factor in equation 2, and estimates of ~10% error in L and ~20% error in d_C, the Hf $4f$ intensity from pure HfO_2 was found to be a factor 1.33 ± 0.06 larger than the measured intensity. For the Si and SiO_2 samples the correction factor was 1.09 ± 0.01.

The reference intensity for Si $2p$ from the Si sample was a factor 1.22 larger than that of the SiO_2 sample. Here, the silicon oxide thickness is important and these were calculated from the Si $2p$ spectra using the method in ISO 14701:2011 "Surface chemical analysis -- X-ray photoelectron spectroscopy -- Measurement of silicon oxide thickness" which encapsulates the accurate method developed in CCQM P84 and used in CCQM K32. The oxide thickness on the reference Si sample was found to be 0.78 nm. However the samples with HfO_2 layers have a larger oxide thickness of ~1.45 nm with some correlation to the HfO_2 thickness. By combining the relevant equations (analogous to equation 2) the substrate intensity for samples 1 to 6 was estimated to be ~3% lower than that of the Si reference sample. From these considerations, the reference intensity ratio, $R = I_\infty$(Hf $4f$ in HfO_2)$/ I_\infty$(Si $2p$ in substrate) was determined to be $R = 4.41 \pm 0.27$ for this instrument and settings.

Electron effective attenuation lengths in HfO₂.

Electron attenuation lengths were estimated using the formula S3.[39] The author reports an 8% root mean square scatter in the results from known materials and this is taken as the relative standard error. The relevant attenuation lengths are: $L_{Hf4f} = 2.10 \pm 0.17$ nm and $L_{Si2p} = 2.00 \pm 0.16$ nm. Note that the error in the values are correlated and that the ratio of attenuation lengths $B = L_{Hf4f} / L_{Si2p} = 1.05 \pm 0.01$ has higher certainty because it relies only on the energy dependency of the electron effective attenuation length.

Calculation of thickness.

The HfO_2 thickness, d_{HfO2}, was calculated under the assumption of flat, uniform, unmixed layers of materials identical to the reference materials, by solving equation 4 for d_{HfO2}.

$$\frac{I_{Hf4f}}{R I_{Si2p}} = \frac{1 - \exp\left(\frac{-d_{HfO2}}{L_{Hf4f} \cos \theta}\right)}{\exp\left(\frac{-B d_{HfO2}}{L_{Hf4f} \cos \theta}\right)}$$

The samples had ~1 nm of carbon as an overlayer, which was not accounted for in the analysis

---

[39] M. P. Seah, Simple universal curve for the energy-dependent electron attenuation length for all materials, Surf. Interface Anal. 44, 1353 (2012)

because attenuation of both the substrate and overlayer intensities through this layer results in a negligible error. The potential error resulting from this overlayer was calculated also.

Uncertainty

Uncertainties in the various terms in Eq.5-1 are provided above, with the exception of the emission angle, θ, for which a standard uncertainty of 2° was used. The uncertainties were propagated through Eq.5-1 and Figure A-3 shows the relative contributions as a function of HfO$_2$ thickness. These are combined in quadrature to provide a standard uncertainty for the outputs of Eq.5-1. The uncertainty is dominated by that of the electron effective attenuation length. The relative standard uncertainty in thickness is ~10%.
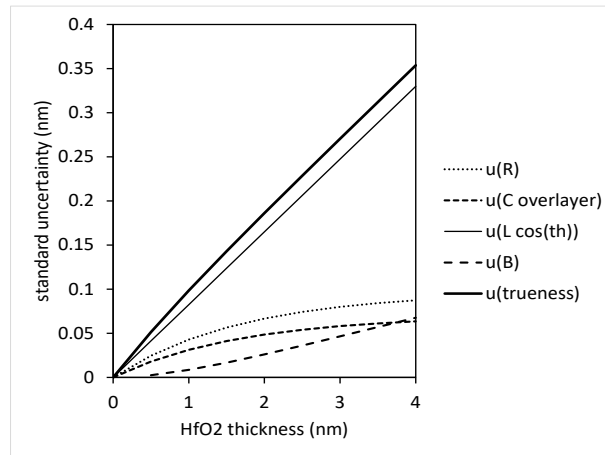
Figure A-3. contributions of uncertainties in Eqn. (4).

Repeat measurements (n = 6) demonstrated a relative standard deviation of ~1% in HfO$_2$ thickness using Eq.5-1. These uncertainties were combined in quadrature with those described above to generate the final uncertainties.

Table A-8. NPL data for the thickness measurement of HfO$_2$ films by XPS with input parameters and the expanded uncertainty at 95% confidence level (k=2).

Parameter	Reference Thickness (nm)					
	0.76	1.20	1.64	2.08	2.52	3.36
Effective Attenuation Length, L$_{Hf4f}$	2.10 ± 0.17 nm					
Electron Emission Angle, θ	$34° \pm 2°$					
B	1.05 ± 0.01					
R	4.41 ± 0.25					
Measured Thickness (nm)	0.85	1.37	1.86	2.37	2.91	3.81
U of Thickness (nm)	0.17	0.26	0.34	0.43	0.53	0.68

(7) CENAM (CINVESTAV)

All samples were analyzed by ARXPS at six different angles (85°, 75°, 65°, 55°, 45° and 35°). The description of the experimental setup can be found elsewhere[40]. The take-off angle dependence was analyzed employing the MultiLayer Model (MLM) to extract the structure of the film (thickness and composition of the constituting layers)[41]. The details of the analysis and the parameters employed can be found elsewhere[42]. The dependence of the signal intensity of species S (I_S) on the thickness (d_S) is the following[43]:

$$I_S(\alpha) = c\,\rho_S T_\alpha(\alpha) T_K(K_S) \frac{d\sigma_S}{d\Omega}(h\nu)\lambda_S(K_S)\sin\alpha \quad \times$$

$$\left[1 - \exp\left(-\frac{d_S}{\lambda_S \sin\alpha}\right)\right] \overset{\overset{\text{layers}}{\text{above S}}}{\underset{i}{\prod}} \exp\left(-\frac{d_i}{\lambda_{S,i}\sin\alpha}\right) \tag{Eq.A-8}$$

where ρ_S is the atomic density, $T_\alpha(\alpha)$ is the angular transmission function at angle α, $T_K(K_S)$ is the kinetic energy transmission function at electron kinetic energy K_S, $d\sigma_S/d\Omega(h\nu)$ is the photoelectric cross section at photon energy $h\nu$, $\lambda_S(K_S)$ is the effective attenuation length at kinetic energy K_S, $\{d_i\}$ are the thickness of the layers above species S, $\{\lambda_{S,i}\}$ are the EAL associated to the various layers, and c is an overall constant (the same for all species).

Since we are dealing with various species, Eq.A-8 represents a set of equations. In addition, when the measurements are done at various angles, the number of equations that Eq.A-8 represents increases. We considered five core levels (Hf 4*f*, Si 2*p* bulk, Si 2*p* oxide, C 1*s*, and Ba 3*d*) and six angles, giving a total of 30 simultaneous equations. The number of unknowns are four: the overall

---

[40] P.G. Mani-Gonzalez, M.O. Vazquez-Lepe, A. Herrera-Gomez, Aperture-time of oxygen-precursor for minimum silicon incorporation into the interface-layer in atomic layer deposition-grown HfO$_2$/Si nanofilms, J. Vac. Sci. Technol. A 33, 010602 (2015)

[41] A. Herrera-Gomez, F.S.S. Aguirre-Tostado, P.G.G. Mani-Gonzalez, M. Vazquez-Lepe, A. Sanchez-Martinez, O. Ceballos-Sanchez, R.M.M. Wallace, G. Conti, Y. Uritsky, Instrument-related geometrical factors affecting the intensity in XPS and ARXPS experiments, J. Electron Spectros. Relat. Phenomena. 184, 487 (2011).

[42] P.-G. Mani-Gonzalez, M.-O. Vazquez-Lepe, F. Espinosa-Magaña, A. Herrera-Gomez, Interface layer in hafnia/Si films as a function of ALD cycles, J. Vac. Sci. Technol. A 31, 010601 (2012)
D. Cabrera-German, G. Molar-Velázquez, G. Gomez-Sosa, W. de la Cruz, A. Herrera-Gomez, Detailed peak fitting analysis of the Zn 2p photoemission spectrum for metallic films and its initial oxidation stages, Surf. Interface Anal. 49, 1078 (2017)

[43] A. Herrera-Gomez, F.S. Aguirre-Tostado, P.G. Mani-Gonzalez, M. Vazquez-Lepe, A. Sanchez-Martinez, O. Ceballos-Sanchez, R.M. Wallace, G. Conti, Y. Uritsky, Instrument-related geometrical factors affecting the intensity in XPS and ARXPS experiments, J. Electron Spectros. Relat. Phenomena. 184, 487 (2011).

constant (c), the thickness of the carbon layer (d_c), the thickness of the hafnia layer (d_{Hf}), and the thickness of the silica layer (d_{Si}).   Since this is an over-determined equation system, the unknown parameters can be obtained through fitting in a very robust way.

The intercept, 0.267 nm, is close to the expected value of 0. However, the slope, 0.617, is relatively far from the expected value of 1.

Table A-9. Measured thickness and uncertainty of the HfO_2 films. The thickness of the silica layer is also shown.

Sample Number	Reference Thickness (nm)	Thickness hafnia layer (nm) uncertainty at 95% confidence	Thickness silica layer (nm)	Thickness carbon layer (nm)
1	0.76	0.87 ± 0.11	1.46	0.47
2	1.20	1.15 ± 0.14	1.72	0.47
3	1.64	1.54 ± 0.10	1.75	0.55
4	2.08	1.73 ± 0.20	2.44	0.43
5	2.52	2.37 ± 0.24	1.90	0.40
6	3.36	2.56 ± 0.25	1.89	0.44

(8) NMISA

Measurements were performed with a PHI Quantum 2000 Scanning XPS instrument using monochromatic Al Kα X-rays with a beam size of 100 µm at 25 W power and an electron emission angle of 45° from the surface normal. The samples were analysed as received, i.e. without any cleaning procedure performed. To ensure that measurement conditions remained constant, the spectra were acquired over the binding energy range of 0 to 200 eV which includes the Hf 4f and Si 2p peaks. A pass energy of 29.35 eV and a step size of 0.125 eV was used for all measurements. Peak fitting was done with Multipak using a Gaussian-Lorentzian mix. The Si 2p peak was fitted using the six peak method where the peak position of the Si(I), Si(II), and Si(III) peaks were constrained with the shift of 1.0 eV, 1.75 eV, and 2.50 eV, respectively and the Si(IV) peak unconstrained. The binding energy difference between the Si(0) doublet peaks was 0.55 eV. The FWHM ratio was constrained to 1:1 for all peaks except Si(IV). The value for L was determined by calculating the average value over the expected thickness range specified by the NIST SRD82 database. The value of R_0 determined experimentally. The results are shown in the table below.

Table A-10. NMISA data for the thickness measurement of HfO_2 films by XPS with input parameters, and the expanded uncertainty at 95% confidence level (k=2).

Parameter	Reference Thickness (nm)					
	0.76	1.20	1.64	2.08	2.52	3.36
Effective attenuation length, L	2.18					
Electron emission angle, θ	45					
R_0	4.733					
R_{exp}	3.16	6.02	10.93	16.40	22.86	51.11
$u_{R_{exp}}$ (%)	5	5	5	5	5	5
Measured Thickness (nm)	0.79	1.27	1.85	2.31	2.72	3.81
U of thickness (nm) **k = 2**	0.25	0.30	0.33	0.38	0.39	0.46

Annex B. Experimental details of XRR data

(1) KRISS

XRR measurements were performed using a commercial D8 discover by Bruker with Cu tube. The generated X-ray power was 1.6 kW. The incident X-ray line beam is parallelized by parabolic göbel mirror combined with incident slit of 0.1 mm. The reflected X-ray beam from sample is collected by a point scintillation detector with detector slit of 0.1 mm.

Surface contamination due to moisture and/or carbonaceous compounds may affect the thicknesses of samples. Therefore, it is very important to reduce the effect of surface contamination using proper surface cleaning procedure. HfO_2 sample is soaked in acetone solution for 1 week. Acetone is rinsed with alcohol rubbing surface of the sample to get rid of particles and acetone residue. Isopropyl alcohol (IPA) and deionized (DI) water are used for further rinsing. After rinsing, N_2 is blown to sample surface and baked at 60ºC for 15 minutes to remove remaining DI water.

For XRR measurement, cleaned samples are mounted on the center of goniometer horizontally. Proper detector angle and z-position of goniometer are determined for beam parallel condition. Incident X-ray angle and detector angle are moving together from 0° to 14° of 2 theta. Collected data are analyzed using a XRR analysis software LAPTOS by Bruker.

We build a simulation model as $HfO_2/SiO_2/Si$ since native oxide of Si should be considered and surface contamination is well removed by cleaning process. For the best fit, we simulated not only layer thickness but also density and roughness of reasonable values for the layers together.

The result of thickness measurements and the expanded uncertainties of 95% confidence level ($k=2$) are shown in Table B-1. Measurement uncertainty for the thickness using XRR contains uncertainty factors of the angle of the goniometer, the wavelength, repeated measurements and fitting together.

Table B-1. KRISS result with expanded uncertainty ($k=2$) by exploiting XRR.

Parameter	Nominal Thickness (nm)					
	1	1.5	2.0	2.5	3	4
Thickness (nm)	0.98	1.38	1.77	2.18	2.60	3.49
Expanded uncertainty (nm)	0.1	0.07	0.07	0.07	0.07	0.07

(2) NIST

To determine HfO$_X$ film thickness, we employed X-Ray Reflectivity (XRR) on each of 6 film stacks provided in the KRIST P-190 set. Each sample was measured with at least two measurements, with a minimum of 12 hours of collection time, per measurement. These extended collection times provide angular reflection ranges necessary for collecting reciprocal space interference information as to the film stack thickness and roughness, and with sufficient dynamic range statistics to reduce uncertainty in background from measurement over the measurement ranges.

Instrument

XRR measurements were performed using a commercial Rigaku[44] SmartLab X-ray diffraction instrument (Serial #: HD2731N). A Long, Fine Focus, Cu X-ray sealed tube source, operated at 40kV & 40mA excitation power, provided the incident X-ray radiation for the measurements (Tube Serial #: DK 401318). The divergent X-ray beam from the tube was 'parallelized' using a graded parabolic multilayer optic, model Rigaku CBO (Serial #: HD 037814) and energy filtered using a Ge (220) 2-bounce monochromator (Serial #: HD 02882). X-rays in reflection from the sample surfaces, were collected using a DTex Ultra Silicon Strip detector (Serial #: HD02634). Nominal slit configurations were 0.05 mm for both source slits, 0.2mm receiving side, and 0.4mm receiving scatter slit. Due to the small lateral dimensions of the XRR samples, a 2mm axial divergence slit was also used to limit incident X-rays to the sample lateral surface. No analyzer crystal was used. This slit configuration provides the greatest signal to noise XRR measurements when used on very flat, low roughness, films deposited on polished wafers. This somewhat "open receiving side" configuration will amplify any sample misalignments present, in the results. Measurements were performed over a range in 2θ of 0 to 0.174 rad and with a step resolution of Δ2θ = 87 µrad with 20s per point.

Instrument Uncertainty:

An X-ray diffractometer (reflectometer) measures the angles of the sample and detector relative to a 'somewhat' parallel X-ray source beam. In addition to measuring these angles, the instrument

---

44 Certain commercial equipment, instruments, or materials are identified in this paper in order to specify the experimental procedure adequately. Such identification is not intended to imply recommendation or endorsement by the National Institute of Standards and Technology, nor is it intended to imply that the materials or equipment identified are necessarily the best available for the purpose.

simultaneously records the intensity of the X-rays being either reflected or diffracted from a sample over a measured quantity of time. The typical X-ray measurement is therefore a set of paired angles and intensities over a range of discrete measurement points. These intensity and angle pairs are compared against model results from a highly constrained X-Ray Reflectivity first principles model of intensity variation with angle. Hence, instrument uncertainties can either manifest as errors in the parallel nature of the X-ray system, the wavelength determination of the X-rays being used, or in our measurement of angle(s) during data collection.

Both detector (2θ) and sample (ω) axes are optically encoded, providing local angular uncertainties for both angles, $\delta(2\theta)$ or $\delta(\omega)$, of less than 35 µrad. The Rigaku instrument realigns its X-ray optical pathway (mirrors, monochromators, sample slits, tube height, etc.) upon every remounting of the instrument components to maintain optimum instrument calibration. This configuration realignment was performed the starting day of the XRR measurements for this study. A Ge (220) reflection, symmetric cut, monochromator provides a measurement angular width of $\delta(2\theta) = 82$ µrad (caused by the dynamical diffraction peak width) and energy uncertainty of $\delta E/E = 2 \times 10^{-4}$ (intrinsic to the optic)[45]. Prior calibration using the Rigaku instrument have validated routine sample alignment to be better than $\delta(2\theta)$ of 88 µrad.

The energy uncertainty can be used directly within uncertainty estimations. The angular uncertainties can be applied to produce worst case +/- XRR measurement data shifts. We then analytically apply this angular shift to our aligned measured data and refine these extreme misalignment cases to provide parameter uncertainty estimates possible from instrument misalignment.

XRR Analysis

Data refinement was performed using the NIST/DANSE developed Relf1d package[46] within an Ubuntu 14.04.4 LTS environment and using a python (2.7.6), Numpy (1.8.2), Refl1d (0.7.7), and Bumps (0.7.5.6). Refl1d uses the Parratt formalism of treating each layer of a thin film stack as a separate slab of constant index of refraction, and different slabs will reflect and red refract X-rays using well understood, first-principles E&M equations (i.e. Snells Law).[47] The slab index of

[45] X-Ray Server URL: http://x-server.gmca.aps.anl.gov

[46] Kienzle, P.A., Krycka, J., Patel, N., & Sahin, I. (2011). Refl1D (Version 0.7.9a2) [Computer Software]. College Park, MD: University of Maryland. Retrieved November 30, 2016.

[47] L.G. Parratt, Surface Studies of Solids by Total Reflection of X-Rays. Phys. Rev. 95, 359 (1954)

refraction can be derived by knowing the incident X-ray energy and elemental composition to locate real (f1) and imaginary (f2) scattering coefficients from NIST tabulated scattering tables.[48] If layer composition stoichiometry is known, we can scale scattering parameters with electron density (and more informatively, mass density of the model layers).

For our layer stack, we have a strong contrast HfO_X layer on SiO_2 on Si. A unique nature of X-rays, is that the scattering coefficients of SiO_2 and Si is nearly identical around the Cu Kα energy region, allow us to ignore the SiO_2 layer in our model. This leaves us with only one deposited film layer, HfO_X. However, since our XRR measurements occur in air, we include a surface contamination layer in our modeling, with a majority C composition. To further simplify our model, we assumed a HfO_X layer stoichiometry to be that of HfO_2 and our layer density to be a ratio scaling to that of bulk hafnia (density of bulk HfO_2 = 9.68 g/cm^3). For our structural model, we allow the surface contamination layer to have an unknown density, thickness, and roughness, and, also allow the HfO_2 layer to vary in density, thickness, and roughness. Combined these parameters with a Si (SiO_2) interface roughness variable, we have a model containing 7 free parameters, allowed to vary over set ranges in a structural model. These constraint ranges are necessary to allow only unimodal parameter estimations during statistical parameter estimation via Monte Carlo methods. Allowed parameter estimations are provided as requested.

XRR Statistical sampling:

For model parameter estimation, we used the DiffeRential Evolution Adaptive Metropolis (DREAM) [49] algorithm within Relf1D. In our analysis, we sample at total of around 400,000 random steps, which takes around 4 hours [$2.5x10^8$ times faster than a traditional MC]. Figure B-1 shows the best fit XRR solution versus data for the nominal 4nm sample. This best fit case is where we start looking for uncertainties in the parameters.

XRR data scaling and likelihood:

XRR data is notoriously difficult to scale as data sets contain information in both the high intensity region near total critical reflection (first few hundred points in Figure B-1) and in the

---

48 https://physics.nist.gov/PhysRefData/FFast/html/form.html

49 Vrugt, J A., ter Braak, C.J.F., Diks, C.G.H., Robinson, B.A., Hyman, J.M., Higdon, D. Accelerating Markov chain Monte Carlo simulation by differential evolution with self-adaptive randomized subspace sampling. Int. J. Nonlin. Sci. Num. 10, 273 (2009)

oscillatory data near the background intensity levels (last few hundred points in Figure B-1) which are many orders of magnitude lower in intensity.
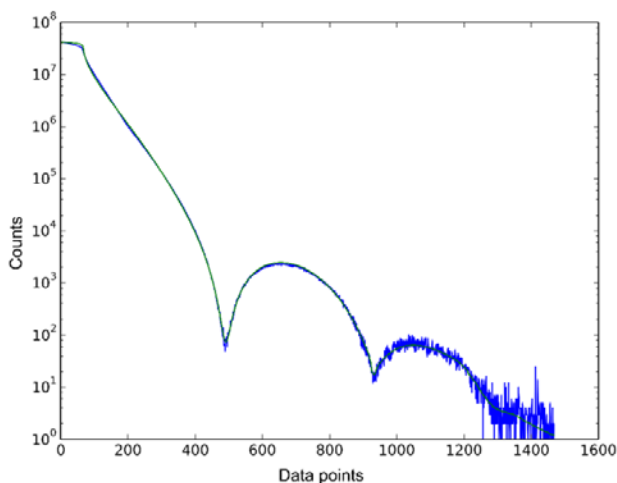

Figure B-1. XRR best fit example for the nominal 4 nm P-190 sample. The blue curve is data, the green is model. This best-case parameter estimates will correspond to the peak in the statistical uncertainty estimates, per parameter.

Both regions have value and correlation within the XRR first principles modeling and are often plotted in log scale to illustrate the multiscale nature of the information. We performed an extensive analysis of over 23 different scaling functions combined with L1 (model & data difference) and L2 (model and data difference squared) likelihood estimators. We chose the following residual function to be both robust and equal waiting in both XRR regimes for each of our data sets:

Formula 1: $\text{Residual(point)} = \text{abs}(\{\log_{10}[\text{model(point)}]^2 - \log_{10}[\text{data(point)}]^2\})$

Formula 1 was used as our likelihood function in our DREAM uncertainty estimations.

Instrument uncertainty:

We can use our uncertainty estimations in the instrument (detector) alignment, beam monochromator alignment, and sample alignment to estimate a min/max combined angular error of $\delta 2\theta = +/- 127\ \mu\text{rad}$ (using the NIST uncertainty machine).[50] We then apply this fixed +/- angle shift to our measured (aligned) XRR data and use these +/- offset measurements in two new DREAM Refl1d uncertainty estimates. In this way we can arrive at the direct impact of angular

---

50   https://uncertainty.nist.gov/

uncertainty on film thickness; an inference which is difficult to calculate empirically, due to parameter correlations within the highly constrained XRR model. The resulting best fit HfO_2 thickness from both the +/- DREAM estimates are then used as the instrument 95% confidence range. Each of these refinements have been run for the same 200,000 samples (2,000 steps x 100 chains + equivalent number of tuning steps.

Combined uncertainty

The parameter probability density functions for the aligned measurements provide us with 95% confidence intervals, which consider parameter correlations, and how well we can determine any given parameter from the known structure, data measurement range, and data quality. We combined this 95% confidence interval from parameter estimation with the +/- alignment contribution and the monochromater energy resolution into one combined uncertainty. To allow for the most conservative estimations, we assumed that in all cases the parameter confidence intervals were applied as a uniform distribution over the ranges. These three uncertainties represent the largest sources of error in thickness for this XRR measurement. We combine these uncertainties using the NIST Uncertainty Machine to find the uncertainty (U) contribution percentages for each uncertainty component, and the final values for thickness, u(thickness), and 95% (k=2) combined uncertainties.[51]

Table B-2. Table of the measured thickness of HfO_2 films

Reference Thickness (nm)	Measured Thickness (nm)	Expanded uncertainty at 95% confidence (nm)
0.76	0.81	[0.679 0.951]
1.20	1.36	[1.325, 1.398]
1.64	1.81	[1.793, 1.822]
2.08	2.24	[2.217, 2.264]
2.52	2.71	[2.687, 2.737]
3.36	3.51	[3.499, 3.527]

GUM[52] tables: Below are the combined uncertainties contributions for HfO_2 thickness in each sample. These are required for traceability.

---

51 https://uncertainty.nist.gov/

52 https://www.bipm.org/utils/common/documents/jcgm/JCGM_100_2008_E.pdf

Table B-3. Uncertainty estimation of thickness measurement for sample 1.

Component	HfO$_X$ Thickness (nm)	U contribution[53]
XRR analysis (scan #1) [Refl1D]	0.913 [0.736, 0.947] *	81.5%
XRR alignment (scan #1) [Refl1D] [δ2θ = +125 μrad]	[0.827, 0.949] **	18.4%
Monochromator ΔE	ΔE = 0.02% **	0.0002%
Total	0.8103	0.065 (nm) [0.679 0.951] *(k=2)*

*95% confidence interval from Refl1d (treated as uniform distribution)
** Range of best fit from +/- angular data refined using Refl1d (treated as uniform distribution)

Table B-4. Uncertainty estimation of thickness measurement for sample 2

Component	HfO$_X$ Thickness (nm)	U contribution
XRR analysis (scan #1) [Refl1D]	1.377 [1.326, 1.397] *	99.57%
XRR alignment (scan #1) [Refl1D] [δ2θ = +125 μrad]	[1.3748, 1.3795] **	0.42%
Monochromator ΔE	ΔE = 0.02% **	0.01%
Total	1.362 (nm)	0.0205 (nm) [1.325, 1.398] *(k=2)*

Table B-5. Uncertainty estimation of thickness measurement for sample 3

Component	HfO$_X$ Thickness (nm)	U contribution
XRR analysis (scan #1) [Refl1D]	1.8098 [1.796, 1.820] *	91%
XRR alignment (scan #1) [Refl1D] [δ2θ = +125 μrad]	[1.8053, 1.8127] **	8.7%
Monochromator ΔE	ΔE = 0.02% **	0.08%
Total	1.8072	0.00724 (nm) [1.793, 1.822] *(k=2)*

Table B-6. Uncertainty estimation of thickness measurement for sample 4

Component	HfO$_X$ Thickness (nm)	U contribution
XRR analysis (scan #1) [Refl1D]	2.2406 [2.223, 2.261]*	90.1%
XRR alignment (scan #1) [Refl1D] [δ2θ = +125 μrad]	[2.240, 2.252]**	9.9%
Monochromator ΔE	0.02%**	0.05%
Total	2.2406	0.0117 (nm) [2.217, 2.264] *(k=2)*

---

[53] https://uncertainty.nist.gov/NISTUncertaintyMachine-UserManual.pdf

Table B-7. Uncertainty estimation of thickness measurement for sample 5

Component	HfO$_X$ Thickness (nm)	U contribution
XRR analysis (scan #1) [Refl1D]	2.7143 [2.689, 2.731]*	92%
XRR alignment (scan #1) [Refl1D] [δ2θ = +125 μrad]	[2.710, 2.722]**	7.6%
Monochromator ΔE	ΔE = 0.02%**	0.062%
Total	2.712	0.0126 (nm) [2.687, 2.737] *(k=2)*

Table B-8. Uncertainty estimation of thickness measurement for sample 6

Component	HfO$_X$ Thickness (nm)	U contribution
XRR analysis (scan #1) [Refl1D]	3.511 [3.500, 3.522] *	73%
XRR alignment (scan #1) [Refl1D] [δ2θ = +125 μrad]	[3.506, 3.520] **	27%
Monochromator ΔE	ΔE = 0.02% **	0.29%
Total	3.513	0.0075 (nm) [3.499, 3.527] *(k=2)*

Density determination and uncertainty analysis: Of the 7 parameter which are constrained within our model, we also refined and provide uncertainty estimate for the density of the HfO$_2$ layer. In our modeling, we scaled density relative to a bulk value of 9.68 g/cm^3. Our model relies on accuracy in tabulated real and complex index of refraction, f1 and f2. For our model, which uses elements Si, O, C, and Hf, the tabulated values of f1 and f2 will have uncertainties of <2% for Cu radiation.[54] We can calculate a combined uncertainty for the hafnia density using the same DREAM analysis for aligned, and +/- misaligned measurements performed above in the thickness analysis. We need to now include an additional uncertainty component from our uncertainty in index of refraction. We again used, 95% confidence parameter estimates, and the best fit for the +/- misaligned cases, and assumed uniform distributions when applying the NIST uncertainty machine to calculate % contribution and (k=2) uncertainty estimates for combined uncertainty in hafnia density.

NOTE: In all cases, the density is less than 80% that of bulk HfO$_2$ density, which may have dramatic consequences on other measurement techniques.

---

[54] https://physics.nist.gov/PhysRefData/FFast/Text2000/sec06.html#tab2

Table B-9. Table of the measured density of HfO_2 films

Sample No.	Relative Density (scaled relative to 9.68 g/cm^3)	Expanded uncertainty at 95% confidence (nm)
1	0.763	[0.675, 0.857]
2	0.706	[0.679, 0.732]
3	0.735	[0.715, 0.756]
4	0.751	[0.731, 0.771]
5	0.762	[0.738, 0.785]
6	0.782	[0.759, 0.805]

(3) NMIJ

Description of the measurement methods and instruments used:

The XRR system had the X-ray source (18 kW) equipped with a Cu rotating anode. The X-ray beam is collected to form a parallel beam by a parabolic multilayer mirror. The beam is compressed and monochromated by a crystal mirror. Three types of crystal mirror are installed in this system. They can be selected in Ge(111) and Si(111) channel-cut crystal monochromator and Ge(220) 4-bounce monochromator combined with incident slits. The reflected X-ray was detected by a Si avalanche photodiode (APD). The Ge (111) channel-cut crystal as an analyser crystal and the reception slit with collimation mode were selected to derive a large signal dynamic range more than 10^8 with an appropriate resolution.

The standard used and the source of traceability to the SI units:

The value of X-ray wavelength recommended by CODATA was used, and the scanning angle of the XRR instruments was verified by the Japanese national angle standard.

Measurement procedure and data analysis:

1. The film thickness of the set-A sample was measured.
2. Sample setting: The sample was fixed on the sample holder by a vacuum chuck.
3. Sample alignment: Before measurements, the direct X-ray beam half cut alignment and the reflected X-ray beam half cut alignment were carried out under the analyser collimation mode. (The measurements were performed under the slit collimation mode.)
4. Measurement area: 5 mm × 15 mm around the centre of the sample.
5. Measurement condition: The sample was set in N_2 gas flow environment to avoid surface contamination during the measurement.

6. Measurements: The five measurements were performed for each sample.

7. Data analysis: The data analyses were performed by fitting a simulated XRR profile to the measured one. The values of the structural parameters for the simulation, namely, "thickness", "density" and "roughness" were optimized by a non-linear least-squares curve-fitting technique. Data analysis was conducted with a software program of GXRR version 2.1.3.0 (Rigaku Co.). The average thickness and their uncertainties of the HfO_2 films were shown in the following tables.
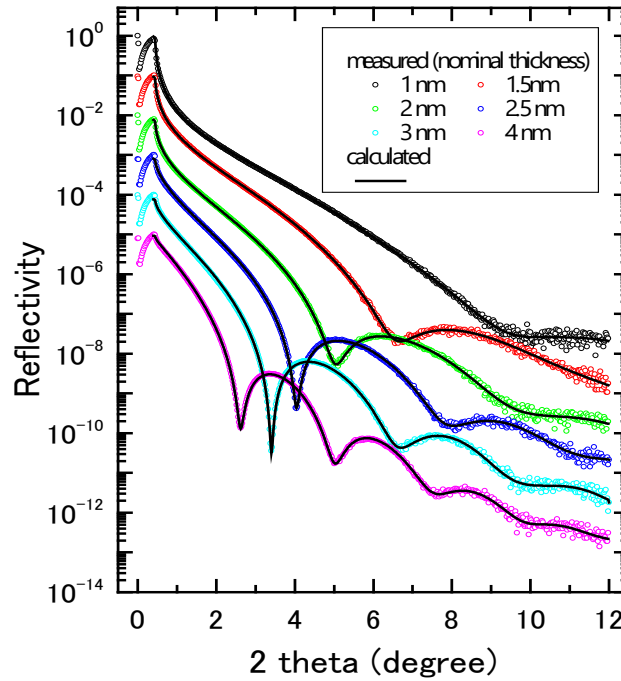
Figure B-2. XRR profiles of HfO_2/SiO_2/Si substrate obtained by NMIJ. The symbols and the solid lines in the figure indicate the measured and calculated results.

Table B-10. NMIJ data for the thickness measurement of HfO_2 thin films by XRR.

Reference Thickness (nm)	Measured Thickness (nm)	Expanded uncertainty at 95% confidence (nm)
	0.95	0.15
1.24	1.41	0.13
1.67	1.78	0.10
2.11	2.26	0.11
2.57	2.73	0.12
	3.61	0.08

Table B-11. Uncertainty of NMIJ data for the thickness measurement of HfO_2 thin films by XRR

Components	Sample No.					
	1	2	3	4	5	6
Repeatability (nm)	0.001	0.014	0.005	0.003	0.030	0.023
Analysis model (nm)	0.073	0.064	0.047	0.057	0.053	0.032
Fitting (nm)	0.007	-	0.006	0.001	0.010	0.007
Wavelength (nm)	0.001	0.001	0.001	0.001	0.001	0.001
Angle scan (nm)	-	-	-	0.001	0.001	0.001
Combined uncertainty (nm)	0.07	0.07	0.05	0.06	0.06	0.04
Expanded uncertainty $k=2$ (nm)	0.15	0.13	0.10	0.11	0.12	0.08

(4) PTB

The samples of the comparison have been measured with the X-ray diffractometer of type Empyrean of Panalytical. The system consists of a Cu tube 2.2 kV electrical input power, a parabolic mirror for converting the divergent X-ray beam into an almost parallel beam. Incident an exit angle is controlled by a two-axis goniometer with Heidenhain encoder. The reflected X-ray intensity is finally detected by solid state detector (type PIXcel) with a very large region of linearity, up to several million counts per second (cps) of throughput. The noise level of this detector is below 0.1 cps. The complete system is installed in a radiation protection cabinet and remotely control by a PC.

Table B-12. Thickness values derived from XRR measurements. For the sample with a nominal thickness of 1.0 nm of the HfO_2 layer, a reliable data evaluation was not possible.

Reference Thickness (nm)	Measured Thickness (nm)	Uncertainty (nm)
0.76	-	-
1.20	-	-
1.64	1.83	0.25
2.08	2.23	0.20
2.52	2.73	0.20
3.36	3.56	0.20

Methodology

With this setup, it is possible the carry out reflectometry measurements over almost eight to nine orders of magnitude of reflected intensity. Additionally the diffractometer is equipped with a Cartesian linear translation stage(x, y, and z) for positioning the sample with a precision of few microns.
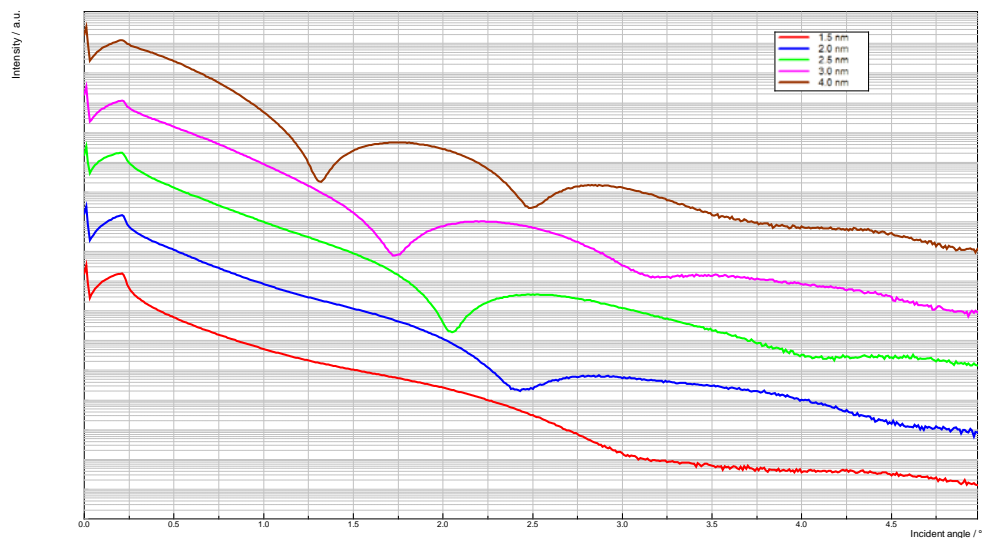
Figure B-3. PTB XRR measurement of sample set A. The measurements are ranging from 1.5 nm to 4.0 nm nominal thickness of the HfO_2 layer. The reflected x-ray intensity (arbitrary units) is plotted against the incident angle of the beam. The individual reflectograms have been shifted on the vertical axis to provide a better overview.

XRR is a so-called inverse method, i.e. the result of the measurement is not within the real space but in the reciprocal space. Hence, the refinement of the data (here: the thickness of the HfO_2 film) requires modeling of the measurement process. Only for the case of a very simple system consisting of only on a layer on a substrate a direct calculation of the thickness is possible. This option is not applicable for the samples used in this comparison.

For the simulation of XRR measurement data two physical models can be applied: first approaches by scattering theory and second by optical theory. One result of the first approach, which should be kept in mind during data refinement is, that the reflected X-ray intensity is proportional to the Fourier transform of the of the electron density profile perpendicular to the sample surface.[55]

The optical approach uses the Fresnel equations and the optical constants of the sample to calculate the transmitted and reflected X-ray intensities at the surface and interfaces of the multilayer stack. A recursive algorithm is used to calculate the complete intensity of the reflected beam.[56] Typically, simulation software is making use of the optical model, with some specific

---

[55] V. Holy, U. Pietsch and T.Baumbach: High-Resolution X-ray Scattering from Thin Films and Multilayers, Volume 149, Springer Tracts in modern Physics, Springer (1999)

[56] L.G. Paratt and C.F. Hempstedt. Anomalous Dispersion and Scattering of X-Rays. Phys. Rev. 94, 1593 (1954)

modifications. For this comparison the software delivered with the XRR instrument is used for data evaluation (X'Pert Reflectivity, Vers. 1.3a, 13.04.2011 of PANalytical).

For a reliable application of XRR simulation software it is still required to understand the impact of each specific simulation parameter onto the resulting reflectogram. Since XRR uses the interferometric superposition of different beam parts, reflected at the different interfaces of the multilayer stack.[57] Hence the slope of the reflectogram is superposed by an oscillation cause the interference of the different beam path. The position of the maxima (or minima) can be described in reciprocal space by the following equation:

$$2\pi = \Delta q_z\, d \tag{1}$$

where q_z is the reciprocal scattering vector q_z is calculated by

$$q_z = \frac{4\pi}{\lambda} sin\, \alpha. \tag{2}$$

α is the incident angle of the X-ray beam. The equations are depicting, that the variation of the film thickness d will result in a movement the maxima (or minima) along the horizontal axis.

All other parameter influencing the shape of the reflectogram (such as interface roughness σ, material density ρ) will have an impact along the vertical axis. Therefore, the location of the maximum (or minimum) is more important the reliability of the refinement of the layer thickness, than the minimization of the χ^2 value used during automatic fitting.

In consequence a semi-automatic method was used during the data evaluation for these measurements. First the thickness of the layer was adjusted, with a priority onto the HfO_2 film. For the assessment of the thickness value both the position of the minima and the maxima of simulated reflectogram were observed.

Regarding the additional simulation parameter, it should be considered, that

1. the density ρ of ultra-thin films is differing to the bulk value and typically smaller,

2. that roughness σ and density ρ are having nearly the same impact to the shape (on the vertical axis) of the reflectogram and

3. that these parameters are having a negligible impact on the position of minima and maxima regarding to the incident angle. Thus, these parameters have no crosstalk to the layer thickness d.

---

[57] Since the surface of the sample can be interpreted as an interface between any material and vacuum/air, in the following part of this text only the term interface is used. This includes also the surface of the sample.

Uncertainty estimation

A simple uncertainty estimation using Eqns. (1) and (2) is misleading. Calculating the uncertainty of the layer thickness using the equations as model equation will lead to a value of $u(d)$ in the order of some tens of picometer, if the uncertainties of the angle measurement and the wavelength are taken. For the instrument used for these measurements the relative uncertainties are approximately $u_r = 10^{-3}$. With this way of calculating the uncertainty estimation would not include the interface roughness and thus would lead to a small uncertainty value, not taking into account the interface of the multilayer stack.

For a reliable uncertainty estimation again, the simulation is used. Once the value of the layer thickness is derived, the value is varied as long as the position of the maxima and minima respectively is still in coincidence with the measured reflectogram (see XRR.PTB).
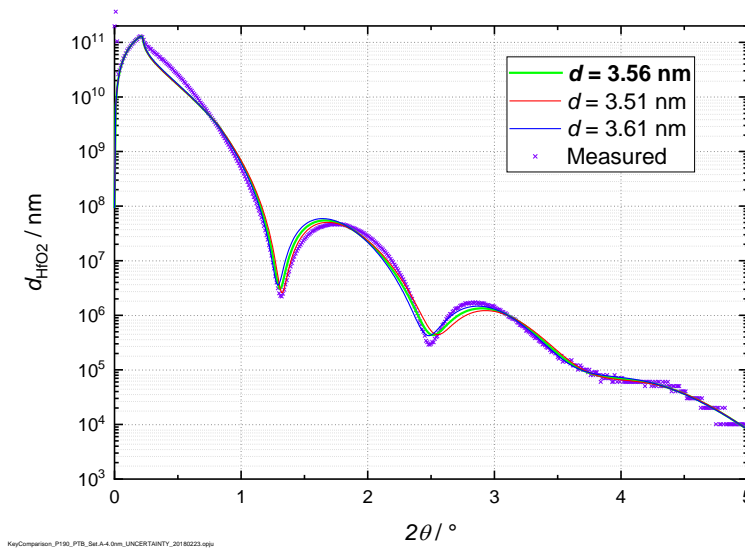
Figure B-4. The reflectogram of PTB XRR measurement results for the thickest sample and comparison with the simulated results.

Annex C. Experimental details of TEM data

(1) KRISS

The thicknesses of the HfO_2 films were determined from high-resolution (HR) TEM micrographs collected using a FEI-F30 microscopes operating at 300 kV. Film thickness of the samples were determined from the lattice constant of the Si(100) substrate as shown in Figure 5-5 (a). The HfO_2/SiO_2 interface was determined from the point with a half contrast of the average contrast of the SiO_2 layer and that of HfO_2 layer. As the same method, the film surface was determined from the point with a half contrast of the average contrast of the HfO_2 layer and that of the glue layer within the same width with that of SiO_2 layer as shown in Figure 5-5 (b). More than 10 TEM images at the different locations were derived and average values of those were reported as the results as shown in Table C-1.

Table C-1. Thicknesses of HfO_2 films by KRISS TEM.

Reference Thickness (nm)	Measured Thickness (nm)	Expanded uncertainty (nm)
0.76	1.25	0.21
1.20	1.60	0.20
1.64	2.11	0.21
2.08	2.57	0.22
2.52	3.03	0.21
3.36	3.76	0.20

The combined standard uncertainty u_c was calculated from the combination of the standard uncertainty in the measurement of film thickness (u_m), the standard uncertainty (u_r) in the measurement of line width of the periodic Si (110) lattice planes and the standard uncertainty (u_l) of the variation of the Si (110) lattice constant. The expanded uncertainty was determined at at 95% confidence level.

(2) NIST

A. Analytical method

Scanning transmission electron microscopy (STEM) was carried out using an FEI Titan 80-300 TEM/STEM equipped with a double-hexapole spherical aberration corrector. Specimens were

prepared via focused ion-beam milling using a standard in-situ lift-out protocol. High-angle annular dark-field (HAADF) images were collected using the following experimental parameters:

- Primary beam energy: 300 keV

- Probe current: ≈ 50 pA

- Probe forming aperture: 40 µm

- HAADF detector collection angles (inner – outer): 88 mrads -500 mrads

- Exposure time: 16 µs per pixel

- Image size: 1024x1024

- Pixel size: 0.02 nm

- Calibrated to Si<110> crystal lattice of substrate acquired simultaneously

<004> interplanar spacing measured in FFT for calibration to bulk value (136 pm)

B. Average thickness of HfO_2 layers

Pre-processing of acquired images

- Images cropped to exclude surface regions with FIB-deposited Pt layers

- Sub-image then binned to increase SNR

   2X horizontally, 4X vertically

   Resulting pixel size (0.04 nm x 0.08 nm)

- Each row of pixels in the binned image was aligned serially to the previous via cross-correlation to remove effects of specimen drift during data acquisition

Layer thickness measurement

- Extract intensity trace from single row of pixels in the image

- Determine center of the HfO_2 layer by finding the position of the maximum intensity value in the profile

- Estimate the peak intensity by calculating the mean value surrounding the maximum pixel

- Set the baseline intensity as the mean of the intensity in the SiO_x substrate region

- Determine the points in both the SiO_x/HfO_2 and HfO_2/Surface interfaces where the intensity equals 20 % and 80 % of the peak intensity value

   20 % and 80 % of peak determined

- Interface positions defined as the mid-point between the 20 % and 80 % intensity onset points

Repeat this process for each row of the image

- Results in 256 measurements in each image

C. Uncertainty

Multiple images were collected from each specimen and each row of intensity traces in each was measured separately. Error bars in plot and table below represent two times the standard deviation of all separate measurements.

Additional sources of error: Free surface of the HfO_2 layer displayed some roughness especially for the thinnest layers. In a projection image this will result in a diffuse intensity decay at this surface, increasing uncertainty in the interface position determination. In a projection image this will result in a diffuse intensity decay

A. Table of the measured thickness of the HfO₂ films

Table C-2. Thicknesses of HfO_2 films by NIST TEM.

Reference Thickness (nm)	Measured Thickness (nm)	+/- 95% confidence interval[*] (nm)
0.76	1.72	0.26
1.20	1.95	0.38
1.64	2.20	0.12
2.08	2.70	0.18
2.52	2.88	0.14
3.36	3.52	0.16

* Represents 2*StdDev of all rows in each image
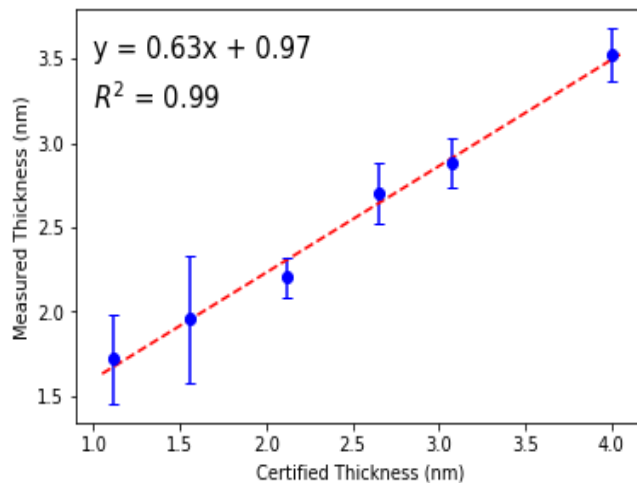
Figure C-1. Thicknesses of HfO_2 films by NIST TEM.

(3) NMIJ

Description of the measurement methods and instruments:

The measurement was carried out with a TEM system (JEOL JEM-3100F, V_{ACC} = 300 kV). Film thickness of the sample set-C was measured. The samples for TEM observations were prepared by argon ion milling technique. The TEM images were derived from at least 8 positions for every sample.

The interface positions were determined by the following procedure.

1. Intensity profile was derived by line integration as shown in Figure C-2.

2. The integrated intensity profile was smoothed by the 11-point moving average.

3. The moving-averaged profile was differentiated.

4. The maximum and minimum positions of the differentiated profile were defined as the interface positions.

5. The film thickness was evaluated with the lattice distance between Si (200) planes of 0.2715 nm as a reference.

(a)

(b)
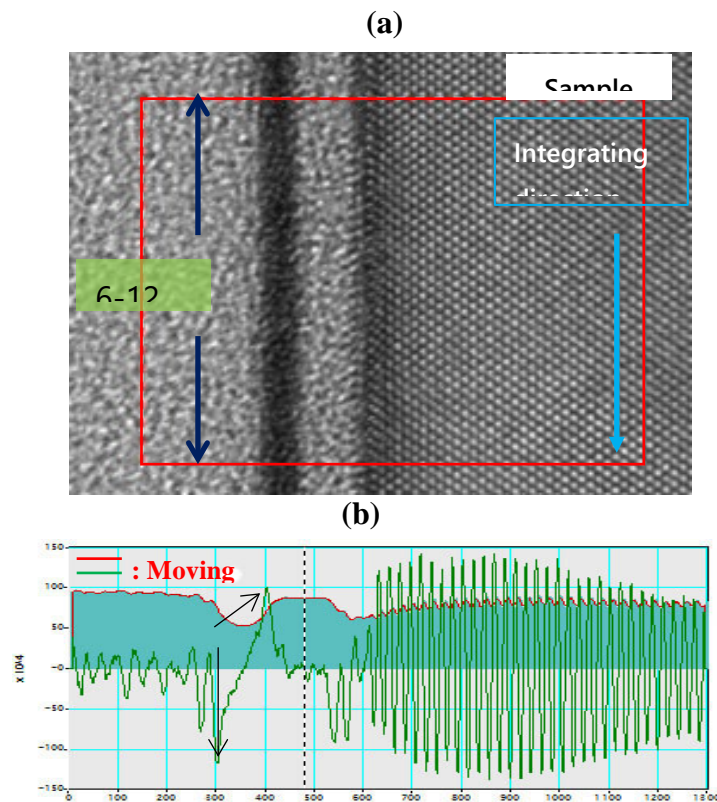
Figure C-2 (a) Typical TEM image. The nominal thicknesses of the HfO_2 film layer was 1.0 nm. (b) Intensity profile derived by the integration of the image contrast surrounded by a red box as shown in (a). The integration range was approximately 6 nm to 12 nm.
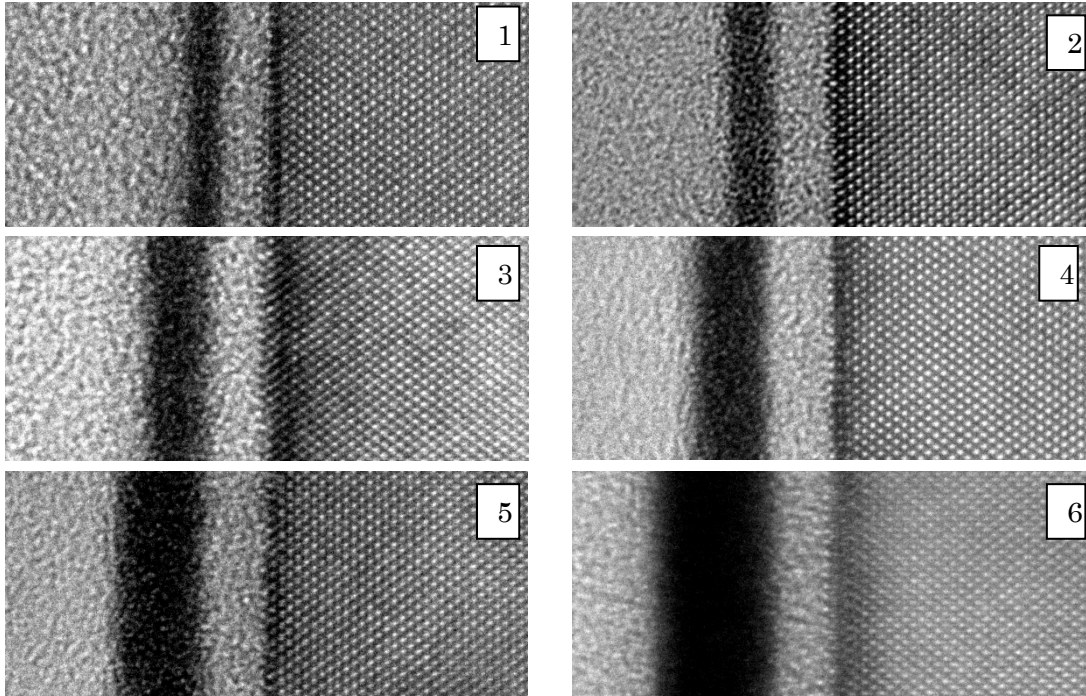
Figure C-3. Typical TEM images of the HfO$_2$/SiO$_2$/Si(100) samples which have the nominal thicknesses of the HfO$_2$ layers of (1) 1.0 nm, (2) 1.5 nm, (3) 2.0 nm, (4) 2.5 nm, (5) 3.0 nm and (6) 4.0 nm, respectively.

Uncertainty

Major factor of the uncertainty was the deviation of the measurement values among the sample position. Then the standard uncertainty was evaluated by the experimental standard deviation of the mean. Expanded uncertainty was calculated using coverage factor (k) of 2, which gives a level of confidence of approximately 95%.

Table C-3. NMIJ data for the measurement of HfO$_2$ thin films by TEM.

Sample No.	Thickness (nm)	Expanded uncertainty at 95% confidence (nm)
1	1.2	0.1
2	1.6	0.1
3	2.1	0.1
4	2.6	0.1
5	3.0	0.1
6	4.2	0.1

(4) INMETRO

The determination of thickness of HfO_2 films were performed using a set of electron microscopy techniques including a FEI Helios Nanolab 650 scanning electron microscopy (SEM) and focused ion beam (FIB) for sample preparation and a FEI Probe Corrected Titan 80-300 (working at 300kV) for high resolution transmission electron microscopy (HRTEM).

The electron transparent thin lamellas (ca. 20 nm thick) were obtained by FIB-SEM and the process started by depositing a Pt layer (~ 100 nm) using the electron beam at 2 keV and 0.84 nA to protect the surface of the samples. Afterwards, the gallium ion beam at 30 keV and 0.3 nA was used to deposit a Pt layer, approximately 2 μm thick, as the main protection layer. In order to mill the trenches on both sides of the lamellas, the gallium ion beam was set 7 nA. The lamellas were in-situ lifted-out and attached to a TEM copper grids also using Pt ion beam deposition. In next steps, the ion beam current was reduced from 1 nA down to 0.1 nA as the thickness of the lamella was reduced from 2 μm down to 200 nm. In the final steps, the samples were gently polished by reducing the ion beam accelerating voltage to 5 kV and then 2 kV at 70 pA.

For the TEM thickness analyses, three HRTEM images were collected from each sample at the same lamella in different positions. Before collection the images the Si substrate were used to align the sample along the (100) zone axis. Figure C-4 (a) shows a HRTEM image of the sample with the 4 nm HfO_2 film. In all images, the silicon atomic planes along the (111) crystalline direction were measured using FFT and used as length reference. The profile plot of each image was taken using an average process of about 1500 pixels (~15 nm) to reduce noise in the profile and to average the film roughness. The profile plots were then derived and their absolute values were taken. This process is shown in Figure C-4. Using this methodology the film interfaces are defined by peaks and the maximum value of the peaks (same as half contrast between the average contrasts of the two layers) and then used as the film interfaces locations. Five thickness values were taken from the three collected images for each sample.

Measurement uncertainties were determined according to the ISO Guide to the Expression of Uncertainty in Measurement (GUM). All sources of uncertainty considered in this measurement are described below. The following model was used for the calculation of thickness, d:

$$d = (d_m - h\sin(\beta))f\frac{\cos(\gamma)}{\cos(\beta)}$$

where d_m is the direct measured value of thickness, h is the approximate thickness (or depth) of the sample, $f = \frac{p}{p_m}$ is the calibration factor, p is the certified value for spacing between the (111) planes in silicon, p_m is the measured value for p, γ is the angle for the rotation of the sample about the normal axis and β is the angle for the sample tilt.
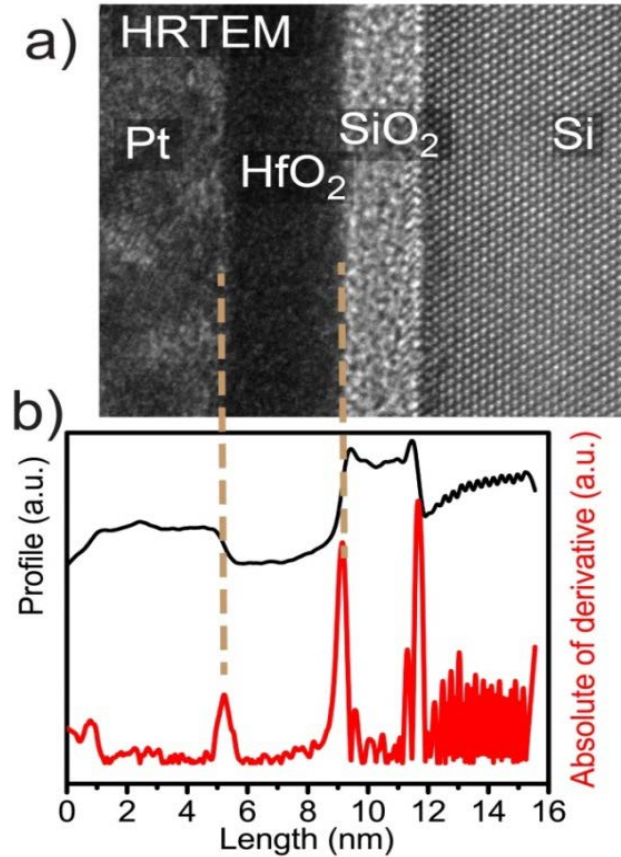

Figure C-4. Cross section of the 4 nm HfO₂ film. a) HRTEM image showing the sample layers including the Pt protecting layer. b) In black, on top, the contrast profile of the cross section is shown. In red, bellow, the absolute of the derivative from the profile is seen. The dashed yellow lines were drawn as guidance to the eyes to locate the interfaces of the HfO₂ film

where d_m is the direct measured value of thickness, h is the approximate thickness (or depth) of the sample, $f = \frac{p}{p_m}$ is the calibration factor, p is the certified value for spacing between the (111) planes in silicon, p_m is the measured value for p, γ is the angle for the rotation of the sample about the normal axis and β is the angle for the sample tilt.

Application of the law of propagation of uncertainties leads to:

$$u(d)^2 = \left(\frac{\partial d}{\partial d_m}\right)^2 u(d_m)^2 + \left(\frac{\partial d}{\partial h}\right)^2 u(h)^2 + \left(\frac{\partial d}{\partial p}\right)^2 u(p)^2 + \left(\frac{\partial d}{\partial p_m}\right)^2 u(p_m)^2 + \left(\frac{\partial d}{\partial \gamma}\right)^2 u(\gamma)^2$$
$$+ \left(\frac{\partial d}{\partial \beta}\right)^2 u(\beta)^2$$

Where:

- $u(d_m)$ is the uncertainty for the measured value of thickness, and is composed by the following sources:
    - 6 repeated indications of direct measurements, taken as a type A uncertainty
    - Image resolution, evaluated as a uniform distribution with ± 0.01 nm/pixel for 1 pixel
    - Position of the HfO$_2$ film interfaces, estimated as a uniform distribution. The range of this interval is defined by the width at half maximum (FWHM) of the peak that constitutes the indication of the interface in the derived profile plot.
- $u(h)$ is the uncertainty of the thickness (or depth) of the sample. The value of h was estimated as 20 nm $\pm$ 2 nm. This was considered as having uniform distribution.
- $u(p)$ is the uncertainty of the certified value for spacing between the (111) planes in silicon. The value of p was taken from CODATA as 0.313560115 nm with a standard uncertainty of 0.000000005 nm.
- $u(p_m)$ is the uncertainty for the measured values of p, and is composed by the following sources:
    - A type A uncertainty for 5 repeated indications
    - A uniform distribution uncertainty based on the process of taking the correct peak positions for the measurement. This was evaluated based on the relative uncertainty of 1.3 % taken from the measurements of the width at half maximum of the peaks on the reciprocal space of the silicon diffraction pattern.
- $u(\gamma)$ is the uncertainty for the angle of rotation of the sample about the normal axis. In this case, γ was considered to be zero degrees, with an uncertainty of $\pm 1°$. This uncertainty was taken as a uniform distribution.

- $u(\beta)$ is the uncertainty for the angle of the sample tilt. In this case, β was considered to be zero degrees, with an uncertainty of $\pm\,0.5°$. This uncertainty was taken as a uniform distribution.

The final uncertainty budget is presented in Table C-4 for each nominal thickness:

Table C-4. INMETRO data for the thickness measurement of HfO_2 films by TEM with input parameters, and the expanded uncertainty at 95%.

Parameter	Reference and Measured Thickness (nm)					
	0.76	1.20	1.64	2.08	2.52	3.36
$u(d_m)$, nm	0.116775	0.098616	0.111482	0.094119	0.119152	0.180877
$u(p)$, nm	5.14E-09	5.14E-09	5.14E-09	5.14E-09	5.14E-09	5.14E-09
$u(p_m)$, nm	0.004069	0.004069	0.004069	0.004069	0.004069	0.004069
$u(h)$, nm	1.154701	1.154701	1.154701	1.154701	1.154701	1.154701
$u(\gamma)$, °	0.010077	0.010077	0.010077	0.010077	0.010077	0.010077
$u(\beta)$, °	0.005038	0.005038	0.005038	0.005038	0.005038	0.005038
$u(d)$, nm	0.160	0.147	0.157	0.147	0.167	0.221
ν_{eff}	240	2170	428	252	612	12
k (95%)	1.97	1.96	1.97	1.97	1.96	2.18
Thickness (nm)	1.298	1.658	2.153	2.936	3.327	4.223
U of thickness (nm)	0.315	0.288	0.309	0.290	0.328	0.481

Annex D. Experimental details of ellipsometry data

(1) DFM

      The six HfO_2 films and four standard ellipsometry SiO_2 reference samples with the nominal thicknesses of 6, 70, 160 and 1000 nm have been measured in reflection mode using 70 degrees angle of incidence and wavelengths from 210 nm to 850 nm. The samples were measured in the same configuration without performing any alignment between the measurements. The SiO_2 reference samples were used for giving the best possible estimate of the refractive index for the 2 nm SiO_2 layer beneath the HfO_2 films. The six HfO_2 films are analyzed using a four-layer model (air/HfO_2/SiO_2/Si) with known optical properties. The thicknesses of the SiO_2 layers were fixed as 3.1 nm for all samples. These values are similar with the reported SiO_2 thickness from CENAM (~3.3 nm). The thickness is found by from the best fit between the model and the data using the Levenberg-Marquardt $\chi2$−optimization method.
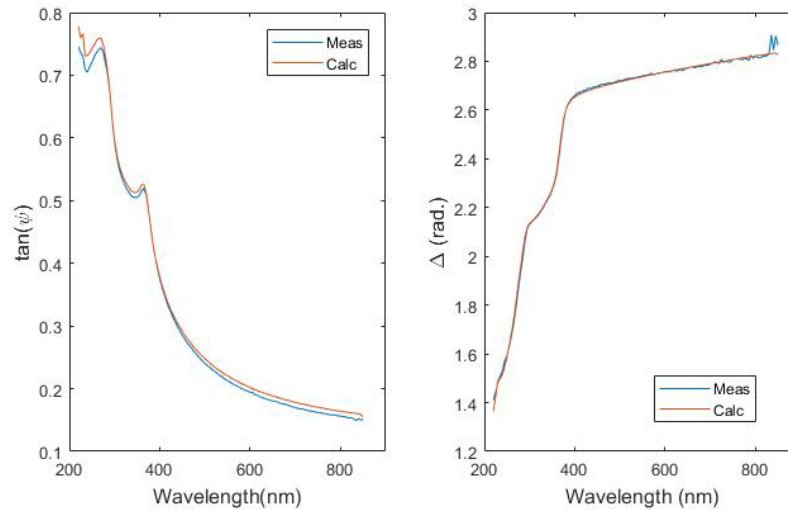
Figure D-1. The figure shows the measured and fitted data for Sample 5

Table D-1. Summary of DFM ellipsometry measurement

Sample	Thickness of HfO_2 layer (nm)	Expanded uncertainty (nm)
1	1.27	0.23
2	1.70	0.23
3	2.35	0.23
4	2.71	0.23
5	3.26	0.23
6	4,01	0.25

(2) NPL

Spectroscopic ellipsometry (SE) measurements were performed using a Woollam M-2000 DI spectroscopic ellipsometer. All samples were cleaned by sonicating in acetone for 10 min then transferred to isopropyl alcohol (IPA) without drying the acetone and sonicated for 10 min. The samples were then sonicated in ultra-high purity water and soaked overnight in IPA. They were then sonicated in fresh IPA and dried with an argon jet.

Spectra were acquired from three areas approximately 3 mm x 10 mm from each sample over a wavelength range of ~192 to ~1700 nm at angles of 65°, 70° and 75° from the surface normal. Repeat spectra were then acquired from each of these areas. The laboratory temperature during acquisition of data was 22.0 °C to 22.3 °C and the humidity 48%.

Average thickness of HfO$_2$ films

The manufacturer's (J. A. Woollam) software, CompleteEASE, was used create a model using the following materials files which were supplied with the instrument by the manufacturer.

HfO$_2$ - allowed to fit for thickness

SiO$_2$_JAW - set to 2.00 nm, the thickness stated in the protocol supplied with the samples

Si_JAW - substrate

The data was fitted to the model in the wavelength range 300 nm to 1000 nm which is within the range of the manufacturer's HfO$_2$ material file. No attempt was made to account for any contamination on the surface.

Uncertainty

It is difficult to determine uncertainty for the ellipsometry measurements. The error due to contamination on sample surface is probably ~1 nm. Errors in refractive index are unknown.

Table D-2. NPL data for the thickness measurement of HfO$_2$ films by spectroscopic ellipsometry and uncertainties.

Parameter	Reference and Measured Thickness (nm)					
	0.76	1.20	1.64	2.08	2.52	3.36
Estimated contamination	1 nm					
Thickness (nm)	1.85	2.38	2.82	3.31	3.76	4.55
U of thickness (nm)	> 1.00	> 1.00	> 1.00	> 1.00	> 1.00	> 1.00

(3) CENAM

A Uvisel Elipsometer model LT M200AGMS brand HORIBA Jobin Yvon was used, the samples were placed in the sample holder of the equipment without any preparation using the following parameters:

- Lamp: Xenon high pressure, 75 W.
- Incidence angle: 70°.
- Spot: 1200 μm
- $E_{spectral\ range}$: 1.5 - 5.5 eV.
- Increase: 0.0500 eV.
- Number of points: 81.
- Configuration: Modulator: 0°, Analyzer: +45°
- Acquisition: Reflection
- Mode: Standard.
- Dispersion Formula: SiO_2, Classical, HfO_2, New Amorphous, c-Si[58]

RESULTS

Calibration of the ellipsometer was performed using the provided references, Silicon, SiO_2 and HfO_2 films with 50 nm thickness, consisting of a series of mathematical parameters and adjustment, using simulation by a computer program based on the matrix method, using a Lorentz Tauc and New Amorphous dispersion formula.

Table D-3. Measured thickness and uncertainty of the HfO_2 films. The thickness of the SiO_2 layer is also shown.

Sample No.	Thickness of HfO_2 layer (nm)	Expanded uncertainty (nm)	Thickness of SiO_2 layer (nm)
1	1.65	0.21	2.4
2	1.80	0.30	3.3
3	2.25	0.50	3.7
4	2.90	0.35	3.3
5	3.10	0.42	3.2
6	4.20	0.53	3.2
SiO_2 reference			51.05
HfO_2 reference	48.2	2.37	

---

[58] G. E. Jellison, Jr. Optical functions of silicon determined by two-channel polarization modulation ellipsometry, Opt. Mater. 1, 41 (1992)

Estimation of uncertainty.

The estimation of uncertainty was carried out according to the ISO JCGM guide 100:2008, GUM 1995 with minor corrections "Evaluation of measurement data — Guide to the expression of uncertainty in measurement" Mainly, repeatability, reproducibility, resolution and the intrinsic of the measurement method were evaluated.

Annex E. Calculation of standard uncertainty in linear regression equation

(1) Coefficients of linear regression equation

The pairs of results obtained by two different methods for a series of sample (n) are (x_1, y_1), $(x_2, y_2), \cdots\cdots$, and (x_n, y_n), and the linear relation to satisfy the results is assumed to be an equation (Eq.E--1).

$$y = a_0 + a_1 x \qquad\qquad (Eq.E-1)$$

In this case, the intercept (a_0) and slope (a_1) are obtained by least square technique. For this, the sum of the squares of the y-axis difference ($y_i - (a_0 + a_1 x_i)$) is defined as Q.

$$Q = \sum_{i=1}^{n}\{y_i - (a_0 + a_1 x_i)\}^2 \qquad\qquad (Eq.E-2)$$

In order to apply the statistical procedure to minimize the Q value for the coefficients (a_0 and a_1), Eq.E-3 and Eq.E-4 are obtained by partial differentiation of Eq.E-2 for the coefficients a_0 and a_1, respectively.

$$\frac{\partial Q}{\partial a_0} = -2\sum_{i=1}^{n}\{y_i - (a_0 + a_1 x_i)\} = 0 \qquad\qquad (Eq.E-3)$$

$$\frac{\partial Q}{\partial a_1} = -2\sum_{i=1}^{n} x_i\{y_i - (a_0 + a_1 x_i)\} = 0 \qquad\qquad (Eq.E-4)$$

Eq.E-5 and Eq.E-6 are derived from Eq.E-3 and Eq.E-4,

$$\sum_{i=1}^{n} y_i = n a_0 + a_1 \sum_{i=1}^{n} x_i \qquad\qquad (Eq.E-5)$$

$$\sum_{i=1}^{n} x_i y_i = a_0 \sum_{i=1}^{n} x_i + a_1 \sum_{i=1}^{n} x_i^2 \qquad\qquad (Eq.E-6)$$

As a result of the Eq.E-5 and Eq.E-6, the intercept (a_0) and slope (a_1) can be determined from Eq.E-7 and Eq.E-8,

$$a_0 = \frac{1}{n}\left(\sum_{i=1}^{n} y_i - a_1 \sum_{i=1}^{n} x_i\right) \qquad\qquad (Eq.E-7)$$

$$a_1 = \frac{n\sum_{i=1}^{n} x_i y_i - \sum_{i=1}^{n} x_i \sum_{i=1}^{n} y_i}{n\sum_{i=1}^{n} x_i^2 - \left(\sum_{i=1}^{n} x_i\right)^2} = \frac{\sum_{i=1}^{n}(x_i - \bar{x})(y_i - \bar{y})}{\sum_{i=1}^{n}(x_i - \bar{x})^2} \qquad\qquad (Eq.E-8)$$

(2) Combined standard uncertainty of the linear regression coefficients

The fundamental reference document of uncertainty expression is *Guide to the expression of*

Uncertainty in Measurment (GUM).[59] As shown in the Eq.E-5 and Eq.E-6, GUM-Suppl.2[60] method is more convinient than GUM method because there are two measurands (in this case, a_0 and a_1) in the two model equations used for the calculation. Especially, this method is much simpler because the combinded standard uncertainties and the correlation coefficients of two measurands can be simultaneously obtained from model equations of linear regression.[61] As described in GUM-Suppl.2, several matrices should be used to obtain the combined standard uncertainty values by multivariate analysis of the following steps.

1) Negative functions of a matrix (F) for two measurands (the offset and slope)

Eq.E-5 and Eq.E-6 for the calculation of offset and slope can be a matrix form Eq.E-9,

$$\boldsymbol{F} = \begin{pmatrix} F_1 \\ F_2 \end{pmatrix} = \begin{pmatrix} na_0 + a_1 \sum_{i=1}^{n} x_i - \sum_{i=1}^{n} y_i \\ a_0 \sum_{i=1}^{n} x_i + a_1 \sum_{i=1}^{n} x_i - \sum_{i=1}^{n} x_i y_i \end{pmatrix} = \boldsymbol{0} = \begin{pmatrix} 0 \\ 0 \end{pmatrix} \qquad \text{(Eq.E-9)}$$

2) Determination of standard uncertainty of variance matrix of input quantity

In the equations to determine the intercept and slope, the number of the input variables are $2n$, that is, all of the pairs of results (x_1, y_1), (x_2, y_2), $\cdots$, and (x_n, y_n) measured by the two methods can be assumed to be input variables. In the general calculation process of the uncertainty for ordinary linear regression analysis, it is assumed that there is no uncertainty at the $x_1, x_2, \cdots$, and x_n values and the uncertainties at the $y_1, y_2, \cdots$, and y_n values are assumed to exist. Then the variables $x_1, x_2, \cdots$, and x_n are assumed to be constants because their uncertainties of variables do not need to be considered and the standard uncertainty of the input variables $y_1, y_2, \cdots$, and y_n is determined from the standard deviation of the linear regression equation Eq.E-10.

$$s = \sqrt{\frac{\sum_{i=1}^{n} \{y_i - (a_0 + a_1 x_i)\}^2}{n-2}} \qquad \text{(Eq.E-10)}$$

Moreover, the standard uncertainty of variance matrix ($\boldsymbol{U}_x$) of the input variables is defined to be Eq.E-11 because the input quantities $y_1, y_2, \cdots$, and y_n are independent in the regression equation,

---

59 "Uncertainty of measurement - Part 3: Guide to the expression of uncertainty in measurement (GUM:1995)", ISO/IEC Guide 98-3:2008, Opt. Mater. 1, 41 (1992)

60 "Extension to any number of output quantities," ISO/IEC Guide 98-3:2008/Suppl. 2:2011

61 "Probability and Statistics for Engineers and Scientists," Walpole Mayers, Mayers Ye, 9th Ed., p. 513, 2014, PEARSON, UK

$$U_x = \begin{pmatrix} s^2 & 0 & \cdots & 0 \\ 0 & s^2 & \cdots & 0 \\ \vdots & \vdots & \ddots & 0 \\ 0 & 0 & \cdots & s^2 \end{pmatrix} = s^2 \begin{pmatrix} 1 & 0 & \cdots & 0 \\ 0 & 1 & \cdots & 0 \\ \vdots & \vdots & \ddots & 0 \\ 0 & 0 & \cdots & 1 \end{pmatrix} \qquad \text{(Eq.E-11)}$$

3) Determination of partial differential coefficient matrix (F_x)of input quantity

For Eq.E-9, the partial differential matrix of the input quantity is calculated by Eq.E-12 and Eq.E-13,

$$F_x = \begin{pmatrix} \dfrac{\partial F_1}{\partial y_1} & \dfrac{\partial F_1}{\partial y_2} & \cdots & \dfrac{\partial F_1}{\partial y_n} \\ \dfrac{\partial F_2}{\partial y_1} & \dfrac{\partial F_2}{\partial y_2} & \cdots & \dfrac{\partial F_2}{\partial y_n} \end{pmatrix} \qquad \text{(Eq.E-12)}$$

$$F_x = \begin{pmatrix} -1 & -1 & \cdots & -1 \\ -x_1 & -x_2 & \cdots & -x_n \end{pmatrix} \qquad \text{(Eq.E-13)}$$

4) Determination of partial differential coefficient matrix of measurand

For Eq.E- 9, the partial differential matrix of the output quantity is calculated by Eq.E-14 and Eq.E-15,

$$F_y = \begin{pmatrix} \dfrac{\partial F_1}{\partial a_0} & \dfrac{\partial F_1}{\partial a_1} \\ \dfrac{\partial F_2}{\partial a_0} & \dfrac{\partial F_2}{\partial a_1} \end{pmatrix} \qquad \text{(Eq.E-14)}$$

$$F_y = \begin{pmatrix} n & \sum_{i=1}^{n} x_i \\ \sum_{i=1}^{n} x_i & \sum_{i=1}^{n} x_i^2 \end{pmatrix} \qquad \text{(Eq.E-15)}$$

5) Determination of combinded standard uncertanty of variance matrix (U_y) of measurand

In general, the variance matrix of the measurands is assigned by Eq.E-16,

$$U_y = \begin{pmatrix} u^2(a_0) & u(a_0, a_1) \\ u(a_0, a_1) & u^2(a_1) \end{pmatrix} \qquad \text{(Eq.16)}$$

Here, $u(a_0, a_1)$ and $u(a_0, a_1)$ are covariance uncertainties between $u(a_0)$ and $u(a_1)$. The sensitivity coefficient matrix (C) is given by Eq.E-17 for the determination of variance matrix of the measurands,

$$C = -F_y^{-1} F_x \qquad \text{(Eq.E-17)}$$

The variance matrix of the measurand is determined from Eq.E-18 by using the sensitivity coefficient matrix

$$U_y = CU_x C^T \qquad \text{(Eq.E-18)}$$

For the convenience, substitution of the variance matrix equation of measurand (Eq.E-18) by sensitivity coefficient matrix equation (Eq.E-14) results in Eq.E-19.

$$
\begin{aligned}
U_y &= -F_y^{-1}F_x U_x \left(-F_y^{-1}F_x\right)^T \\
&= F_y^{-1}F_x U_x F_x^T \left(F_y^{-1}\right)^T \\
&= F_y^{-1}F_x U_x F_x^T F_y^{-1} \\
&= F_y^{-1}\left(F_x U_x F_x^T\right)F_y^{-1} \qquad \text{(Eq.E-19)}
\end{aligned}
$$

The middle factor $(F_x U_x F_x^T)$ of Eq.E-19 is calculated in Eq.E-20,

$$F_x U_x F_x^T =$$

$$
\begin{pmatrix} -1 & -1 & \cdots & -1 \\ -x_1 & -x_2 & \cdots & -x_n \end{pmatrix}
\begin{pmatrix} s^2 & 0 & \cdots & 0 \\ 0 & s^2 & \cdots & 0 \\ \vdots & \vdots & \ddots & 0 \\ 0 & 0 & \cdots & s^2 \end{pmatrix}
\begin{pmatrix} -1 & -1 & \cdots & -1 \\ -x_1 & -x_2 & \cdots & -x_n \end{pmatrix}^T
$$

$$
= s^2 \begin{pmatrix} n & \sum_{i=1}^n x_i \\ \sum_{i=1}^n x_i & \sum_{i=1}^n x_i^2 \end{pmatrix} \qquad \text{(Eq.E-20)}
$$

If the middle factor $(F_x U_x F_x^T)$ of Eq.E-19 is substituted and the calculation is completed, the combined standard uncertainty (U_y) of variance matrix of the measurands can be determined by Eq.E-21 and Eq.E-22,

$$U_y = F_y^{-1}\left(F_x U_x F_x^T\right)F_y^{-1} = s^2 \begin{pmatrix} n & \sum_{i=1}^n x_i \\ \sum_{i=1}^n x_i & \sum_{i=1}^n x_i^2 \end{pmatrix}^{-1} \qquad \text{(Eq.E-21)}$$

$$U_y = \frac{s^2}{n\sum_{i=1}^n x_i^2 - \left(\sum_{i=1}^n x_i^2\right)^2} \begin{pmatrix} \sum_{i=1}^n x_i^2 & -\sum_{i=1}^n x_i \\ -\sum_{i=1}^n x_i & n \end{pmatrix} \qquad \text{(Eq.E-22)}$$

6) combined standard uncertainty of measurands (slope and offset)

The combined standard uncertainties of the slope $u(a_0)$ and intercept $u(a_1)$ are determined by Eq.E-23 and Eq.E-24 from Eq.E-16 and Eq.E-22

$$u(a_0) = \sqrt{\frac{s^2 \sum_{i=1}^n x_i^2}{n\sum_{i=1}^n x_i^2 - \left(\sum_{i=1}^n x_i\right)^2}} \qquad \text{(Eq.E-23)}$$

$$u(a_1) = \sqrt{\frac{ns^2}{n\sum_{i=1}^n x_i^2 - \left(\sum_{i=1}^n x_i\right)^2}} \qquad \text{(Eq.E-24)}$$

7) Calculation of the correlation coefficient ($r(a_0, a_1)$) for slope and intercept

The covariance uncertainty in the Eq.E-16, is expressed by Eq.E-25 from the relationship between the standard uncertainty of the slope $u(a_0)$ and intercept $u(a_1)$ and their correlation coefficient.

$$u(a_0, a_1) = u(a_0)u(a_1)r(a_0, a_1) \qquad \text{(Eq.E-25)}$$

Accodingly, the correlation coefficient $r(a_0, a_1)$ of the slope and intercept is determined by Eq.E-26

$$r(a_0, a_1) = \frac{u(a_0, a_1)}{u(a_0)u(a_1)} \qquad \text{(Eq.E-26)}$$

Annex F. Procedure for XPS Analysis of HfO₂ Films

(1) XPS analysis of HfO₂ films in P190

It is assumed that the samples have the following structure with uniform thicknesses, d_X:

Effective attenuation lengths (EALs) of electrons, L, are defined for a particular electron energy travelling through a particular material. Thus $L_{Hf4f,C}$ represents the EAL of Hf 4f electrons in the carbon layer. The ratio of attenuation lengths within a particular material can be calculated with small error. For Al Kα radiation equation F-1 and F-2 provide numerical values and associated uncertainties.

$$\beta = \frac{L_{Si2p,X}}{L_{Hf4f,X}} = 0.950 \pm 0.003 \qquad \text{(Eq.F-1)}$$

and

$$\gamma = \frac{L_{C1s,X}}{L_{Si2p,X}} = 0.885 \pm 0.006 \qquad \text{(Eq.F--2)}$$

The uncertainty is established from various databases and for materials ranging from carbon to gold. For Al Kα X-rays, $L_{Si2p,O} = 3.485$ nm, is an accurate result from CCQM studies P84 and K32.

(2) Carbon overlayer thickness

The carbon overlayer signal, I_C is related to thickness by:

$$I_C = I_C^\infty \left[1 - \exp\left(\frac{-d_C}{L_{C1s,C} \cos \theta} \right) \right] \qquad \text{(Eq.F-3)}$$

Where: I_C^∞ is the intensity of a carbon layer much thicker than the XPS information depth and θ is the electron emission angle relative to the surface normal. No reference materials exist for the thick carbon layer and therefore an estimate is required. This is achieved using the method outlined

in "Evaluation of a simple correction for the hydrocarbon contamination layer in quantitative surface analysis by XPS", G. Smith, J. Elec. Spec. 148, 21 (2005).

$$d_C = -L_{C1s,C} \cos\theta \ln\left(1 - \frac{I_C}{I_C^\infty}\right) \approx -L_{C1s,C} \cos\theta \ln(1 - X_C) \qquad \text{(Eq.F-4)}$$

Where X_C is the equivalent homogeneous fraction of carbon for the sample determined by XPS and including all detectable elements (hafnium, silicon and oxygen). This will be substituted into later equations to eliminate the uncertainty associated with $L_{C1s,C}$. It is important to note that X_C has a relative uncertainty of approximately 20%, largely due to uncertainties in the comparability of inelastic background subtraction procedures for different elements in different matrixes.

(3) **Hafnium oxide reference intensity**

For the thick hafnium oxide layer sample with a carbon overlayer, the Hf 4f intensity is given in Eq.F--5

$$I_{Hf} = I_{Hf}^\infty \exp\left(\frac{-d_{C,Hf}}{L_{Hf4f,C} \cos\theta}\right) \qquad \text{(Eq.F-5)}$$

Where I_{Hf}^∞ is the reference intensity of the hafnium oxide material. Combining with Eq.F-4 and then 2 and 1 results in Eq.F-6.

$$I_{Hf} = I_{Hf}^\infty \exp\left(\frac{L_{C1s,C} \cos\theta \ln(1 - X_C)}{L_{Hf4f,C} \cos\theta}\right) = I_{Hf}^\infty \exp\left(\beta\gamma \ln\left(1 - X_{C,Hf}\right)\right) \qquad \text{(Eq.F-6)}$$

Where $X_{C,Hf}$ is the equivalent homogeneous fraction of carbon on the hafnium oxide sample. Thus, Eq.F-7 relates the measured Hf4f intensity to the absolute reference intensity with approximately 5% relative error based on typical X_C values.

$$I_{Hf}^\infty = I_{Hf}\left(1 - X_{C,Hf}\right)^{-\beta\gamma} \qquad \text{(Eq.F-7)}$$

(4) Substrate reference intensity

For reasons of consistency and similarity to the samples being analysed, the silicon substrate reference intensity shall be determined from a silicon wafer with a similar oxide thickness to the

samples themselves and without a hafnium oxide overlayer. The substrate reference intensity is a combination of the silicon metal (M) and silicon oxide (O) layers. Eq.F-8 and 9 describe these.

$$I_M = I_M^\infty \exp\left(\frac{-d_{O,Si}}{L_{Si2p,O} \cos\theta}\right) \exp\left(\frac{-d_{C,Si}}{L_{Si2p,C} \cos\theta}\right) \qquad \text{(Eq.F-8)}$$

$$I_O = I_O^\infty \left[1 - \exp\left(\frac{-d_{O,Si}}{L_{Si2p,O} \cos\theta}\right)\right] \exp\left(\frac{-d_{C,Si}}{L_{Si2p,C} \cos\theta}\right) \qquad \text{(Eq.F-9)}$$

Where I_M^∞ is the reference intensity of silicon metal and I_O^∞ is the reference intensity of silicon oxide. CCQM studies P84 and K32 established the relationship given in Eq.F--10 which is appropriate for analysis based on Shirley background subtraction.

$$I_O^\infty = 0.9329 I_M^\infty \qquad \text{(Eq.F-10)}$$

The total silicon intensity, I_{Si}, is the sum of Eq.F-8 and 9 which, with Eq.F-4 and 10 can be written as Eq.F-11.

$$I_{Si} = I_M^\infty \left[0.9329 + 0.0671 \exp\left(\frac{-d_{O,Si}}{L_{Si2p,O} \cos\theta}\right)\right] \exp\left(\gamma \ln\left(1 - X_{C,Si}\right)\right) \qquad \text{(Eq.F-11)}$$

Where $X_{C,Si}$ is the equivalent homogeneous fraction of carbon on the silicon sample. The thickness of oxide on the silicon reference material, $d_{0,Si}$, can be accurately measured using the method in CCQM studies P84 and K32 from a fit to the peaks in the Si 2p region. Therefore the silicon metal reference intensity is provided by Eq.F-12 with approximately 2% error from X_C.

$$I_M^\infty = \frac{I_{Si}\left(1 - X_{C,Si}\right)^{-\gamma}}{\left[0.9329 + 0.0671 \exp\left(\frac{-d_{O,Si}}{L_{Si2p,O} \cos\theta}\right)\right]} \qquad \text{(Eq.F-12)}$$

(5) Reference intensities ratios, $R_{0,i}$

The silicon substrate intensity depends upon the oxide layer thickness, as described above. Therefore, each sample will have a reference intensity that is appropriate to the silicon oxide layer thickness of that sample. For each sample (i), the oxide thickness, $d_{0,i}$, should be measured using the method in CCQM studies P84 and K32. Neglecting the carbon overlayer on the sample, Eq.F-13 can be written for the silicon reference intensity of sample i.

$$I^{\infty}_{Si,i} = I^{\infty}_M \left[0.9329 + 0.0671 \exp\left(\frac{-d_{O,i}}{L_{Si2p,O} \cos\theta} \right) \right] \tag{Eq.F-13}$$

For each sample, i, the $R_{0,i}$ value is defined in Eq.F-14.

$$R_{0,i} = \frac{I^{\infty}_{Hf}}{I^{\infty}_{Si,i}} = \alpha \frac{I_{Hf} \left[0.9329 + 0.0671 \exp\left(\frac{-d_{O,Si}}{L_{Si2p,O} \cos\theta} \right) \right] (1 - X_{C,Si})^{\gamma}}{I_{Si} \left[0.9329 + 0.0671 \exp\left(\frac{-d_{O,i}}{L_{Si2p,O} \cos\theta} \right) \right] (1 - X_{C,Hf})^{\beta\gamma}} \tag{Eq.F-14}$$

In which α is a factor that accounts for any drift or change in instrument response between the reference samples and for variability in intensity due to mounting and positioning each sample. This factor is unity, ($\alpha = 1$) but is present as a reminder that these effects should be evaluated and the variability included in the uncertainty budget for R_0. In practice, the silicon oxide thickness of samples in the study is relatively constant and R_0 varies by less than 0.1%.

(5) Hafnium oxide thickness of samples, d$_{H,i}$

The intensity for the hafnium oxide layer is given by Eq.F-15.

$$I_{Hf,i} = a I^{\infty}_{Hf} \left[1 - \exp\left(\frac{-d_{H,i}}{L_{Hf4f,H} \cos\theta} \right) \right] \exp\left(\frac{-d_{C,i}}{L_{Hf4f,C} \cos\theta} \right) \tag{Eq.F-15}$$

The silicon substrate intensity is given by Eq.F--16.

$$I_{Si,i} = a I^{\infty}_{Si} \exp\left(\frac{-d_{H,i}}{L_{Si2p,H} \cos\theta} \right) \exp\left(\frac{-d_{C,i}}{L_{Si2p,C} \cos\theta} \right) \tag{Eq.F-16}$$

In which a is a factor that accounts for any drift or change in instrument response between analysing this sample and the reference samples. To eliminate this factor a ratio is taken, which is expressed in Eq.F-17.

$$\frac{I_{Hf,i}}{I_{Si,i}} = R_{0,i} \frac{\left[1 - \exp\left(\frac{-\beta d_{H,i}}{L_{Si2p,H} \cos\theta} \right) \right]}{\exp\left(\frac{-d_{H,i}}{L_{Si2p,H} \cos\theta} \right)} \exp\left(\frac{d_{C,i}}{L_{Si2p,C} \cos\theta} - \frac{d_{C,i}}{L_{Hf4f,C} \cos\theta} \right) \tag{Eq.F-17}$$

$$\frac{I_{Hf,i}}{I_{Si,i}} = R_{0,i} \frac{\left[1 - \exp\left(\frac{-\beta d_{H,i}}{L_{Si2p,H} \cos\theta}\right)\right]}{\exp\left(\frac{-d_{H,i}}{L_{Si2p,H} \cos\theta}\right)} (1 - X_{C,i})^{\gamma(1-\beta)}$$

The final result requires Eq.F-18 to be solved to find $d_{H,i}/L_{Si2p,H}$. The thickness, $d_{H,i}$, requires an accurate value for $L_{Si2p,H}$ which is established in comparison to other techniques.

(6) Review of sources of error and correlations

Error from use of an approximate equation

Use of the simple Eq.F-19 as suggested in the original protocol is possible, but introduces some error and a lack of clarity in physical quantities. The equation is attractive due to the ability to rearrange it to get a simple expression for $d_{H,i}$.

$$\frac{I_{Hf,i}}{I_{Si,i}} = R_0 \frac{\left[1 - \exp\left(\frac{-d_{H,i}}{L \cos\theta}\right)\right]}{\exp\left(\frac{-d_{H,i}}{L \cos\theta}\right)}$$

(Eq.F-19)

By comparison to Eq.F-18, it is clear that two effects are neglected:

1) The correction for differential attenuation of electrons through the carbon layer introduces an error of ~1%. For these systems ($X_C \approx 0.25$), Eq.F-20 provides a typical result and this is directly equivalent to a similar error in R_0.

$$(1 - X_{C,i})^{\gamma(1-\beta)} \approx 0.988$$

(Eq.F-20)

2) The value of L is ambiguous. For most of the films in this study, the Si 2p electron intensity becomes dominant in determining the thickness and therefore the $L_{Si2p,H}$ is the appropriate value of L. In this case the error amounts to approximately ±0.01 nm, with thin films being underestimated in thickness and thick films being overestimated.

Correlation between R_0 and $L_{Si2p,H}$

Analysis shows that, across the range of thicknesses used in the study, similar results may be obtained if the value of R_0 is changed by a factor f and the value of $L_{Si2p,H}$ changed by a factor approximately $f^{0.56}$. There will be a change of slope and intercept, but these are small: for a 10%

change in R_0 and 5% change in $L_{Si2p,H}$, the change in slope is of the order of 2% with an offset of ±0.05 nm.

Therefore, the value of $L_{Si2p,H}$ cannot be determined unless R_0 is first accurately measured. Because the kinetic energies of Si 2p and Hf 4f are different, the value of R_0 will include variations in instrument transmission and therefore a single value can only be obtained for instruments which have the same geometry and intensity scale calibration.

Annex G. Derivation of the thickness equation (Eq. 5.1) from the basic equations of XPS intensity for conformal multilayer films

1. Introduction

This appendix is about the equations used in the P-190 study to obtain the thickness of the hafnia layers using XPS data. The equation proposed to calculate the thickness of hafnia layers from XPS data

$$T_{HfO2} = L_{Si,HfO2} \cos\theta \ln\left(\frac{R_{exp}}{R_0} + 1\right) \tag{Eq.G-1}$$

which corresponds to Eq. 5.1 in the main document, is an approximation of Eq. (2) in Kim et al. paper [1] (Anal. Chem. 81, 2009)

$$T_{HfO2} = L_{Si,HfO2} \cos\theta \ln\left(\frac{R_{exp}}{R_0} + \exp\left\{\frac{T_{HfO2}}{\cos\theta}\left(\frac{1}{L_{Si,HfO2}} - \frac{1}{L_{Hf,HfO2}}\right)\right\}\right) \tag{Eq.G-2}$$

The purpose of this document is to discuss the derivation of Eq.G-2 from the XPS basic equations relating peak intensities with the density and structure of the sample, together with physical parameters such as photoelectric cross sections and effective attenuation lengths. This is successfully done and is presented in Section 3-4. Section 2 is dedicated to discuss the basic equations for photoemission signal appropriate to the structure of the samples employed in the study and the required assumptions involved in the derivation. It culminates with Eq.G-7; it is noted that the system is overdetermined. Sections 3-1 to 3-2 shows simple equations for getting the thickness of the hafnia overlayer without the need of approximating one EAL to another. Section A4 shows a numerical comparison of the thickness of the hafnia layers obtained from the various approaches.

2. Basic equations

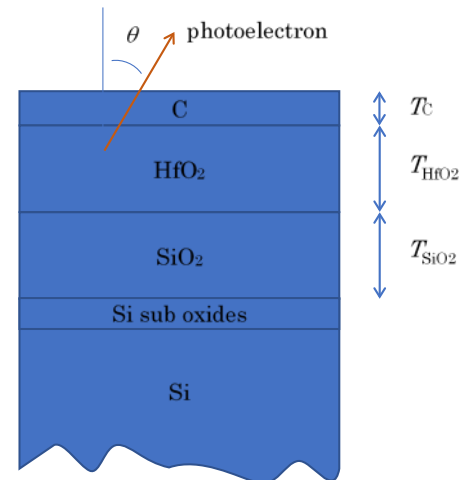The structure of the samples of the study is represented in the diagram in Fig. G-1.

Figure G-1. Diagram of the physical structure of the multilayer samples used in the study.

The equations applicable to this structure are the following:

$$I_{Si}^{exp}(\theta) = c(\theta)\rho_{Si}A_{Si}\frac{d\sigma_{Si}}{d\Omega}L_{Si,Si}\cos\theta\exp\left(-\frac{T_{SiSubOxi}}{L_{Si,SiSubOxi}\cos\theta}\right)\exp\left(-\frac{T_{SiO2}}{L_{Si,SiO2}\cos\theta}\right)\exp\left(-\frac{T_{HfO2}}{L_{Si,HfO2}\cos\theta}\right)\exp\left(-\frac{T_C}{L_{Si,C}\cos\theta}\right)$$

$$I_{SiSubOxi}^{exp}(\theta) = c(\theta)\rho_{Si}A_{Si}\frac{d\sigma_{Si}}{d\Omega}L_{Si,SiSubOxi}\cos\theta\exp\left(-\frac{T_{SiO2}}{L_{Si,SiO2}\cos\theta}\right)\exp\left(-\frac{T_{HfO2}}{L_{Si,HfO2}\cos\theta}\right)\exp\left(-\frac{T_C}{L_{Si,C}\cos\theta}\right)$$

$$I_{SiO2}^{exp}(\theta) = c(\theta)\rho_{Si4+}A_{Si4+}\frac{d\sigma_{Si4+}}{d\Omega}L_{Si4+,SiO2}\cos\theta\left[1-\exp\left(-\frac{T_{SiO2}}{L_{Si,4+SiO2}\sin\theta}\right)\right]\exp\left(-\frac{T_{HfO2}}{L_{Si4+,HfO2}\cos\theta}\right)\exp\left(-\frac{T_C}{L_{Si4+,C}\cos\theta}\right)$$

$$I_{Hf}^{exp}(\theta) = c(\theta)\rho_{Hf}A_{Hf}\frac{d\sigma_{Hf}}{d\Omega}L_{Hf,HfO2}\cos\theta\left[1-\exp\left(-\frac{T_{HfO2}}{L_{Hf,HfO2}\cos\theta}\right)\right]\exp\left(-\frac{T_C}{L_{Hf,C}\cos\theta}\right)$$

$$I_C^{exp}(\theta) = c(\theta)\rho_C A_C\frac{d\sigma_C}{d\Omega}L_{C,C}\cos\theta\left[1-\exp\left(-\frac{T_C}{L_{C,C}\cos\theta}\right)\right]$$

$$(Eq.G\text{-}3)$$

where I_S^{exp} is the peak intensity of species S, θ is the takeoff angle of the electron measured from the surface normal, ρ_S is the atomic density of species S, A_S is the transmission function at electron kinetic energy K_S, $d\sigma_S/d\Omega$ is the photoelectric cross section at photon energy $h\nu$, $\{T_S\}$ are the thicknesses of the layers, $\{L_{S,i}\}$ are the EALs associated to the electron from species S traveling through layer i. c is an overall constant, the same for all species, that depends on the characteristics of the XPS equipment such as the X-ray flux and the geometrical overlap between the spectrometer analysis volume, the X-ray beam and the sample surface [2].

Neglecting the carbon layer, that is, neglecting the influence of the presence of the adventitious carbon layer on the assessment of the thickness of the silica and hafnia layers, is a good approximation. This is because the carbon layer on the samples used on the study were, when the characterization was done, thin enough (about 1/2 nm).

Even a better approximation is to neglect the contribution of the suboxides (or just to consider them as part of the oxide layer or substrate). Figure G-2 shows that the signal associated to the suboxides is very small. We indeed quantified the thickness of the Si suboxide layers and found that they are of the order of half a monolayer for most cases (about 1 Å).
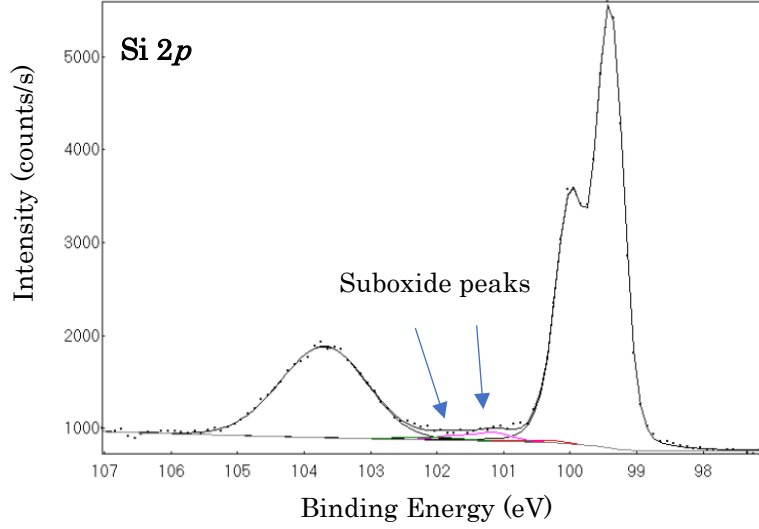
Figure G-2. High resolution Si 2*p* spectrum for Sample # 1 showing the Si suboxide peaks in color.

The resulting equations are the following:

1) $I_{Si}^{exp}(\theta) = c(\theta)\rho_{Si}A_{Si}\dfrac{d\sigma_{Si}}{d\Omega}L_{Si,Si}\cos\theta\exp\left(-\dfrac{T_{SiO2}}{L_{Si,SiO2}\cos\theta}\right)\exp\left(-\dfrac{T_{HfO2}}{L_{Si,HfO2}\cos\theta}\right)$

2) $I_{Si4+}^{exp}(\theta) = c(\theta)\rho_{Si4+}A_{Si}\dfrac{d\sigma_{Si}}{d\Omega}L_{Si,SiO2}\cos\theta\left[1-\exp\left(-\dfrac{T_{SiO2}}{L_{Si,SiO2}\cos\theta}\right)\right]\exp\left(-\dfrac{T_{HfO2}}{L_{Si,HfO2}\cos\theta}\right)$ (Eq.G-4)

3) $I_{Hf}^{exp}(\theta) = c(\theta)\rho_{Hf}A_{Hf}\dfrac{d\sigma_{Hf}}{d\Omega}L_{Hf,HfO2}\cos\theta\left[1-\exp\left(-\dfrac{T_{HfO2}}{L_{Hf,HfO2}\cos\theta}\right)\right]$

where the (very good) approximations $L_{Si4+,SiO2} \approx L_{Si,SiO2}$, $L_{Si4+,HfO2} \approx L_{Si,HfO2}$, $d\sigma_{Si4+}/d\Omega \approx d\sigma_{Si}/d\Omega$, and $A_{Si4+} \approx A_{Si}$ have been made.

Eq.G-4 is a system of three equations with three unknowns (c, T_{SiO2}, T_{HfO2}) which solution is straightforward. This approach assumes that we know the values for the transmission function of the spectrometer, the differential photoelectron cross sections, the densities and the effective attenuation lengths. These parameters can indeed be obtained from public tables and from information from the equipment vendor.

However, we might want to declare that these quantities are not precisely known and that we rather get extra experimental information. One way is to get data from homogeneous systems, as those shown in the following diagram:

Figure G-3. Diagram of the structure of the homogeneous samples used in the study.

The associated equations are the following:

1) $I_{\mathrm{Si}}^{\infty}(\theta) = c(\theta)\rho_{\mathrm{Si}}A_{\mathrm{Si}}\dfrac{d\sigma_{\mathrm{Si}}}{d\Omega}L_{\mathrm{Si,Si}}\cos\theta$

2) $I_{\mathrm{Si4+}}^{\infty}(\theta) = c(\theta)\rho_{\mathrm{Si4+}\infty}A_{\mathrm{Si}}\dfrac{d\sigma_{\mathrm{Si}}}{d\Omega}L_{\mathrm{Si,SiO2}\infty}\cos\theta$, (Eq.G-5)

3) $I_{\mathrm{Hf}}^{\infty}(\theta) = c(\theta)\rho_{\mathrm{Hf}\infty}A_{\mathrm{Hf}}\dfrac{d\sigma_{\mathrm{Hf}}}{d\Omega}L_{\mathrm{Hf,HfO2}\infty}\cos\theta$

where $\rho_{\mathrm{Si4+}\infty}$ is the density of silicon atoms in a thick SiO_2 layer, $\rho_{\mathrm{Hf}\infty}$ is the density of hafnium atoms in a thick HfO_2 layer, $T_{\mathrm{Si,SiO2}\infty}$ is the EAL of Si $2p$ electrons traveling through a thick SiO_2 layer, and $T_{\mathrm{Hf,HfO2}\infty}$ stands for the EAL of Hf $4f$ electrons traveling through a thick HfO_2 layer.

It is known, and it is also a result from this study, that the bulk density of thin and thick layers of hafnia might differ for as much as 20%. The same for the density of silica in thin and thick layers. Nevertheless, this derivation requires making the following approximations:

1) $\rho_{\mathrm{Si4+}\infty}T_{\mathrm{Si,SiO2}\infty} \approx \rho_{\mathrm{Si4}}T_{\mathrm{Si,SiO2}}$

2) $\rho_{\mathrm{Hf}\infty}T_{\mathrm{Hf,HfO2}\infty} \approx \rho_{\mathrm{Hf}}T_{\mathrm{Hf,HfO2}}$ (Eq.G-6)

This approximation is slightly less strong than assuming that the densities are the same. This is because, while the bulk density is larger than the thin film density ($\rho_{\mathrm{Hf}\infty} > \rho_{\mathrm{Hf}}$), the EAL in the bulk is slightly lower than the EAL in the thin film ($T_{\mathrm{Hf,HfO2}\infty} < T_{\mathrm{Hf,HfO2}}$). However, the decrease on the EAL does not compensate for the increase in the density.

By substituting Eq.G-5 into Eq.G-4 and using Eq.G-6 we get:

1) $I_{\mathrm{Si}}^{\exp}(\theta) = I_{\mathrm{Si}}^{\infty}(\theta) \exp\left(-\dfrac{T_{\mathrm{SiO2}}}{L_{\mathrm{Si,SiO2}} \cos\theta}\right) \exp\left(-\dfrac{T_{\mathrm{HfO2}}}{L_{\mathrm{Si,HfO2}} \cos\theta}\right)$

2) $I_{\mathrm{Si4+}}^{\exp}(\theta) = I_{\mathrm{Si4+}}^{\infty}(\theta) \left[1 - \exp\left(-\dfrac{T_{\mathrm{SiO2}}}{L_{\mathrm{Si,SiO2}} \cos\theta}\right)\right] \exp\left(-\dfrac{T_{\mathrm{HfO2}}}{L_{\mathrm{Si,HfO2}} \cos\theta}\right)$,

3) $I_{\mathrm{Hf}}^{\exp}(\theta) = I_{\mathrm{Hf}}^{\infty}(\theta) \left[1 - \exp\left(-\dfrac{T_{\mathrm{HfO2}}}{L_{\mathrm{Hf,HfO2}} \cos\theta}\right)\right]$

These equations can be written as follows:

1) $Q_{\mathrm{Si}}(\theta) = \exp\left(-\dfrac{T_{\mathrm{SiO2}}}{L_{\mathrm{Si,SiO2}} \cos\theta}\right) \exp\left(-\dfrac{T_{\mathrm{HfO2}}}{L_{\mathrm{Si,HfO2}} \cos\theta}\right)$

2) $Q_{\mathrm{Si4+}}(\theta) = \left[1 - \exp\left(-\dfrac{T_{\mathrm{SiO2}}}{L_{\mathrm{Si,SiO2}} \cos\theta}\right)\right] \exp\left(-\dfrac{T_{\mathrm{HfO2}}}{L_{\mathrm{Si,HfO2}} \cos\theta}\right)$ (Eq.G-7)

3) $Q_{\mathrm{Hf}}(\theta) = 1 - \exp\left(-\dfrac{T_{\mathrm{HfO2}}}{L_{\mathrm{Hf,HfO2}} \cos\theta}\right)$

where $Q_{\mathrm{Si}}(\theta) \equiv I_{\mathrm{Si}}^{\exp}(\theta)/I_{\mathrm{Si}}^{\infty}(\theta)$, $Q_{\mathrm{Si4+}}(\theta) \equiv I_{\mathrm{Si4+}}^{\exp}(\theta)/I_{\mathrm{Si4+}}^{\infty}(\theta)$, and $Q_{Hf}(\theta) \equiv I_{Hf}^{\exp}(\theta)/I_{Hf}^{\infty}(\theta)$.

If we assume that $L_{\mathrm{Si,SiO2}}$ and $L_{\mathrm{Hf,HfO2}}$ can reliably be obtained from tables, then Eq.G-7 is an over-determined system because there are three equations and only two unknowns ($T_{\mathrm{SiO2}}, T_{\mathrm{HfO2}}$). The over-determination of the system open the possibility of inconsistent solutions if not all the assumptions made to reach Eq.G-7 (i.e., Eq.G-6) are valid.

3. Different approaches for solving Eq.G-7

Solving the system represented by Eq.G-7 can be done in very different ways.

3-1. The most straightforward approach: start with Eq.G-7-3

The most straightforward is to solve for T_{HfO2} directly from Eq.G-7-3:

$$T_{\mathrm{HfO2}} = -L_{\mathrm{Hf,HfO2}} \cos\theta \ln\left(1 - Q_{Hf}(\theta)\right) \qquad \text{(Eq.G-8)}$$

and then substitute this value to get T_{SiO2} from either Eq.G-7-1 or Eq.G-7-2. If all the assumptions made to obtain Eq.G-7 are valid, then both solutions would coincide within the experimental error.

Substituting this result into Eq.G-7-1 gives:

$$T_{SiO2} = \frac{L_{Si,SiO2} \sin\theta}{Q_{Si}(\theta)} \exp\left(\frac{L_{Hf,HfO2} \ln\left(1 - Q_{Hf}(\theta)\right)}{L_{Si,HfO2}} \right)$$

3-2. Second most straightforward approach: combine Eq. G-7-1 and G-7-2

Since Eq.G-7-1 and Eq.G-7-2

1) $\quad Q_{Si}(\theta) = \exp\left(-\frac{T_{SiO2}}{L_{Si,SiO2} \cos\theta} \right) \exp\left(-\frac{T_{HfO2}}{L_{Si,HfO2} \cos\theta} \right)$

2) $\quad Q_{Si4+}(\theta) = \left[1 - \exp\left(-\frac{T_{SiO2}}{L_{Si,SiO2} \cos\theta} \right) \right] \exp\left(-\frac{T_{HfO2}}{L_{Si,HfO2} \cos\theta} \right)$

form a complete set (two equations with two unknowns), another approach is to solve them for T_{SiO2} and T_{HfO2}. We can do it by solving for the exponential involving T_{SiO2} in Eq.G-7-1 as follows:

$$\exp\left(-\frac{T_{SiO2}}{L_{Si,SiO2} \cos\theta} \right) = \frac{Q_{Si}(\theta)}{\exp\left(-\frac{T_{HfO2}}{L_{Si,HfO2} \cos\theta} \right)}$$

and then substitute it into Eq.G-7-2 to get

$$Q_{Si4+}(\theta) = \left[1 - \frac{Q_{Si}(\theta)}{\exp\left(-\frac{T_{HfO2}}{L_{Si,HfO2} \cos\theta} \right)} \right] \exp\left(-\frac{T_{HfO2}}{L_{Si,HfO2} \cos\theta} \right) \quad \text{or}$$

$$Q_{Si4+}(\theta) + Q_{Si}(\theta) = \exp\left(-\frac{T_{HfO2}}{L_{Si,HfO2} \cos\theta} \right), \quad \text{(Eq.G-9)}$$

This can be solved for T_{HfO2} to get:

$$T_{HfO2} = L_{Si4+,HfO2} \cos\theta \ln \frac{1}{Q_{Si4+}(\theta) + Q_{Si}(\theta)} \quad \text{(Eq.G-10)}$$

To solve for T_{SiO2}, this result can be substituted into Eq.G-7-1.

$$Q_{\text{Si}}(\theta) = \exp\left(-\frac{T_{\text{SiO2}}}{L_{\text{Si,SiO2}}\cos\theta}\right)\left(Q_{\text{Si4+}}(\theta) + Q_{\text{Si}}(\theta)\right)$$

and then solve for T_{SiO2}:

$$T_{\text{SiO2}} = -L_{\text{Si,SiO2}}\cos\theta\ln\frac{Q_{\text{Si}}(\theta)}{Q_{\text{Si4+}}(\theta) + Q_{\text{Si}}(\theta)}$$

3-3. Approach by normalizing by the Si equation (Eq.G-7-1)

Two equations can be obtained from the system represented by Eq.G-7 by dividing Eq.G-7-2 and Eq.G-7-3 by Eq.G-7-1:

$$2/1)\quad \frac{Q_{\text{Si4+}}(\theta)}{Q_{\text{Si}}(\theta)} = \frac{1 - \exp\left(-\dfrac{T_{\text{SiO2}}}{L_{\text{Si,SiO2}}\cos\theta}\right)}{\exp\left(-\dfrac{T_{\text{SiO2}}}{L_{\text{Si,SiO2}}\cos\theta}\right)}$$

$$3/1)\quad \frac{Q_{\text{Hf}}(\theta)}{Q_{\text{Si}}(\theta)} = \frac{1 - \exp\left(-\dfrac{T_{\text{HfO2}}}{L_{\text{Hf,HfO2}}\cos\theta}\right)}{\exp\left(-\dfrac{T_{\text{SiO2}}}{L_{\text{Si,SiO2}}\cos\theta}\right)\exp\left(-\dfrac{T_{\text{HfO2}}}{L_{\text{Si,HfO2}}\cos\theta}\right)}$$

This system can be solved numerically for $T_{\text{SiO2}}, T_{\text{HfO2}}$.

3-4. Another approach: getting Kim et al. equation

The purpose of this section is to derive Equation (2) in Kyung Joong Kim et al. paper [1] (Anal. Chem. 81, p. 8519, 2009), which is displayed above as Eq.G-1,

Eq. (2) in Kim et al. paper: $T_{\text{HfO2}} = L_{\text{Si,HfO2}}\cos\theta\ln\left(\dfrac{R_{\exp}}{R_0} + \exp\left\{\dfrac{T_{\text{HfO2}}}{\cos\theta}\left(\dfrac{1}{L_{\text{Si,HfO2}}} - \dfrac{1}{L_{\text{Hf,HfO2}}}\right)\right\}\right)$

from our Eq.G-7.

The first step is to combine Eq.G-7-1 and Eq.G-7-2 into one equation. The new system can be written as follows:

$$1,2)\quad Q_{SiO2}+Q_{Si}=\exp\left(-\frac{T_{HfO2}}{L_{Si,HfO2}\cos\theta}\right)$$

$$3)\quad \exp\left(-\frac{T_{HfO2}}{L_{Hf,HfO2}\cos\theta}\right)=1-Q_{Hf}$$

where the first equation results from combining Eq.G-7-1 with Eq.G-7-2 to get Eq.G-9 (see Section 3-2), and the second corresponds to writing Eq.G-7-3 in a slightly different way. As mentioned above, t_{HfO2} can be solved from either of these two equations, as shown in Eq.G-8 and Eq.G-10.

However, we can get many other equivalent equations by algebraical manipulation. To get Kim's equation, it is necessary to combine them in the following way:

The next step is to multiply them:

$$1,2)\times 3)\quad \left(Q_{SiO2}+Q_{Si}\right)\exp\left(-\frac{T_{HfO2}}{L_{Hf,HfO2}\cos\theta}\right)=\exp\left(-\frac{T_{HfO2}}{L_{Si,HfO2}\cos\theta}\right)(1-Q_{Hf})$$

and then to rearrange as follows:

$$1,2)\times 3)\quad 0=\left(Q_{SiO2}+Q_{Si}\right)\exp\left(-\frac{T_{HfO2}}{L_{Hf,HfO2}\cos\theta}\right)-\exp\left(-\frac{T_{HfO2}}{L_{Si,HfO2}\cos\theta}\right)(1-Q_{Hf}).$$

The third step is to add this expression to Eq. 1,2) to get

$$1,2)\times 3)+1,2)\quad Q_{SiO2}+Q_{Si}=\exp\left(-\frac{T_{HfO2}}{L_{Si,HfO2}\cos\theta}\right)+\left(Q_{SiO2}+Q_{Si}\right)\exp\left(-\frac{T_{HfO2}}{L_{Hf,HfO2}\cos\theta}\right)-\exp\left(-\frac{T_{HfO2}}{L_{Si,HfO2}\cos\theta}\right)(1-Q_{Hf})$$

This can be solved for T_{HfO2} to get:

$$T_{HfO2}=L_{Si,HfO2}\cos\theta\ln\left(\frac{Q_{Hf}}{Q_{SiO2}+Q_{Si}}+\exp\left\{\frac{T_{HfO2}}{\cos\theta}\left(\frac{1}{L_{Si,HfO2}}-\frac{1}{L_{Hf,HfO2}}\right)\right\}\right)$$

It can be easily shown that

$$\frac{Q_{Hf}}{Q_{SiO2}+Q_{Si}}=\frac{R_{exp}}{R_0}$$

Therefore, the previous equation can be written as

$$T_{HfO2}=L_{Si,HfO2}\cos\theta\ln\left(\frac{R_{exp}}{R_0}+\exp\left\{\frac{T_{HfO2}}{\cos\theta}\left(\frac{1}{L_{Si,HfO2}}-\frac{1}{L_{Hf,HfO2}}\right)\right\}\right)$$

which is precisely Kim's equation (Eq.G-1).

3-5. Deriving the equation used in the P-190 study

To get the equation used in this study, it is necessary to assume that $L_{\text{Hf,HfO2}} \approx L_{\text{Si,HfO2}}$ (as it is shown by numerical comparison in Section 4, this is an excellent approximation).

In this way, Kim's equation becomes:

$$T_{\text{HfO2}} = L_{\text{Si,HfO2}} \cos\theta \ln\left(\frac{R_{\text{exp}}}{R_0} + 1 \right)$$

which is Eq.G-1, i.e., the proposed equation used in P-190 (Eq. 5.1 of the main document).

4. Numerical comparison of the different approaches

The experimental results relevant to this study are shown in Table AI and the results from the analysis in Table AII.

Table G-1. Experimental results by CENAM-Cinvestav. The experimental values for $I_{\text{Hf}}^{\text{exp}}$, $I_{\text{Si}}^{\text{exp}}$, and $I_{\text{Si4+}}^{\text{exp}}$ are 6985.1, 1986.0, and 1338.5 eV s, respectively.

Sample	$I_{\text{Hf}}^{\text{exp}}$ (eV s)	$I_{\text{Si}}^{\text{exp}}$ (eV s)	$I_{\text{Si4+}}^{\text{exp}}$ (eV s)
1	1920.0	691.9	270.9
2	2070.2	384.4	172.1
3	3807.8	457.8	203.0
4	3156.7	247.1	162.6
5	3452.0	195.7	91.9
6	5020.8	150.9	72.5

Table G-2. Results from the various approaches described in Section 3. The values employed for $L_{\text{Si,SiO2}}$, $L_{\text{Si,HfO2}}$ and $L_{\text{Hf,HfO2}}$ are 35.1, 17.2, and 18.0 Å, respectively.

Approach	Sample 1 T_{SiO2}	Sample 1 T_{HfO2}	Sample 2 T_{SiO2}	Sample 2 T_{HfO2}	Sample 3 T_{SiO2}	Sample 3 T_{HfO2}	Sample 4 T_{SiO2}	Sample 4 T_{HfO2}	Sample 5 T_{SiO2}	Sample 5 T_{HfO2}	Sample 6 T_{SiO2}	Sample 6 T_{HfO2}
Sec. 3-1		5.7		6.3		14.1		10.8		12.2		22.7
Sec. 3-2	16.0	10.2	17.8	19.4	17.7	16.5	23.8	24.0	18.5	30.6	18.8	34.9
Sec. 3-3	16.0	7.1	17.8	11.4	17.7	15.5	23.8	18.2	18.5	23.8	18.8	32.4
Sec. 3-4		7.1		11.4		15.5		18.2		23.8		32.4
Sec. 3-5		6.9		11.2		15.2		17.9		23.6		32.1

There is full numerical coincidence between the approaches of Sections 3-3 and 3-4 even though they are different. For example, in contrast to Section 3-4, the approach in Section 3-3 involves the value of $L_{\text{Si,SiO2}}$.

The approximate approach of Section 3-5, which is that used for P-190, is also consistent with the approaches of Sections 3-3 and 3-4.

The outcome from approaches of Sections 3-1 and 3-2, even though the expressions are very simple, is very different from the rest of the approaches. The reason might be that the approximations, such as that described in Eq. G-6, directly affect the results. The other approaches (3-3, 3-4 and 3-5) involve ratios that might cancel out the errors of the approximations.

References

[1] K. J. Kim, J. S. Jang, J. H. Lee, Y. J. Jee, and C. S. Jun, "Determination of the absolute thickness of ultrathin Al_2O_3 overlayers on Si (100) substrate," *Anal. Chem.*, vol. 81, no. 20, pp. 8519–8522, 2009, doi: 10.1021/ac901463m.

[2] A. Herrera-Gomez *et al.*, "Instrument-related geometrical factors affecting the intensity in XPS and ARXPS experiments," *J. Electron Spectros. Relat. Phenomena*, vol. 184, no. 8–10, pp. 487–500, 2011, doi: 10.1016/j.elspec.2011.08.002.